The Biological and Pharmacological Allosteric Modulation of Inositol Monophosphatase

James William Noble

University of Sussex

Thesis submitted for the degree of

PhD in Biochemistry

August 2019

Abstract

The purpose of this project was to develop novel pharmacological tools against Inositol Monophosphatase (IMPase) and gain new insights into the Calbindin-IMPase interaction. IMPase is an enzyme that has been of significant therapeutic interest since the development of the inositol depletion hypothesis of lithium's efficacy in the treatment of bipolar disorder. More recent studies have implicated IMPase inhibition in the induction of autophagy and the clearance of peptides involved in the pathogenesis of neurodegenerative diseases. Despite this there is a lack of specific inhibitors and those that have been developed lack favorable physiochemical properties to explore specific IMPase inhibition *in vivo*. My aim was to find novel inhibiters and binding chemical fragments that could later be developed into potent specific inhibitors of IMPase that would allow for the specific evaluation of IMPase inhibition *in vivo*. To achieve this, two approaches were tried: first a crystallographic fragment soaking screen was used to identify novel binding sites and chemical matter. This resulted in the discovery of a novel fragment binding site at the homodimer interface and mutagenesis at this site inhibited IMPase activity, indicating that the site could be therapeutically relevant. The second approach was to screen a specially curated isothiazolone library based on the previously identified covalent inhibitor Ebselen. Here I identified a new class of isothiazolone inhibitors of IMPase.

The calcium binding protein Calbindin-D28k can allosterically modulate IMPase, this results in the increase in the catalytic activity of IMPase. I aimed to explore this interaction by fusing the proteins using a flexible amino acid linker. The resulting complexes had activity in excess of that of the wild type IMPase, confirming that Calbindin-D28k activated IMPase. Low resolution structural analysis using small angle X-ray scattering (SAXS) revealed a V-shaped IMPase-calbindin complex which was in contrast to the more linear shape predicted by computational docking models. Here we also obtained the first crystal structure of Calbindin-D28k. This crystal structure gave the first direct visualization of the calcium binding sites of the protein and is a better model of Calbindin-D28k in solution than the previous NMR structure.

DECLARATION

The thesis conforms to an 'article format' in which the middle chapters consist of discrete articles written in a style that is appropriate for publication in peer-reviewed journals in the field. The first and final chapters present synthetic overviews and discussions of the field and the research undertaken.

Chapter 2 is published in the Acta Crystallographica Section D as:
James W. Noble, Rehab Almalki, S. Mark Roe, Armin Wagner, Ramona Duman and John R. Atack. The X-ray Structure Of Human Calbindin-D28K: An Improved Model. Acta Cryst. (2018). D74, 1008–1014
doi.org/10.1107/S2059798318011610

The author contributions are as follows: James W Noble was responsible for initial conception and all aspects of, data analysis, writing of the manuscript and most data collection. Rehab Almalki was a final year project student supervised by S. Mark Roe and myself, she helped with protein crystallization. S. Mark Roe had scientific input in all areas of the project. Armin Wagner and Ramona Duman are the beamline scientist from the I23 beamline and collected the data on this beamline. John R. Atack, supervision.

Chapter 3 is written in the style of an article appropriate for submission to a journal.

James W. Noble and John R. Atack. Exploration of the Calbindin-IMPase Interaction Using Fusion Proteins

The author contributions are as follows: James W Noble was responsible and all aspects of, data analysis, writing of the manuscript and data collection. John R. Atack, initial conception of the research.

Chapter 4 is written in the style of an article appropriate for submission to a journal.

James W Noble, Iain J Day, S. Mark Roe, Gary J Tresadern and John R Atack. Exploration of a Novel Fragment Binding Site at the Homodimer Interface of Inositol Monophosphatase.

The author contributions are as follows: James W Noble was responsible and all aspects of, data analysis, writing of the manuscript and data collection. Iain J Day was responsible performing NMR expriments. S. Mark Roe was responsible support with crystallographic data analysis. Gary J Tresadern was responsible selection of some fragments to screen. John R. attack was responsible conception of the research.

Chapter 5 is written in the style of an article appropriate for submission to a journal.

James W Noble, Gary J Tresadern and John R Atack. Isothiazolinone Inhibition of Inositol Monophosphatase

The author contributions are as follows: James W Noble was responsible and all aspects of, data analysis, writing of the manuscript and data collection. Gary J Tresadern was responsible selection of Isothiazolinone compounds to screen. John R. Atack was responsible initial conception of the research.

WORK NOT SUBMITTED ELSEWHERE FOR EXAMINATION

I hereby declare that this thesis has not been and will not be, submitted in whole or in part to another University for the award of any other degree.

Signature: JNoble

Table of contents

Acknowledgments

Firstly I would like to thank my fiends and family who have supported me over the 4 years. With particular thanks to Peter Gregory, Adrian Smith, Chris Hazel, James Mawdsley and Luke Readman all of whom I've lived with, and have supported me during my PhD studies.

I would like to thank everyone at the Sussex Drug Discovery Centre, for making it a nice working environment over the last 4 years. Particularly I would like to thank Lucas Kraft, Chloe Kolossus (sunbeam), Gareth Williams, Sarah Walker, Karen Scruby and Raj Gill; their conversations have made the laboratory a lovely place to work and their academic and administrative support has been invaluable.

A very big thanks to Mark Roe who has had to deal with all of my questions as I taught myself biomolecular crystallography, and for his help in all aspects of this project.

Many thanks to both my supervisor and co-supervisor for securing the funding and support, my industrial collaborator Gary J Tresadern, and thanks to BBSRC who funded the project.

Abbreviations

CNS	Central nervous system
DAG	Diacylglycero
EF	EF-hand
FPLC	Fast protein liquid chromatography
GPCR	G-protein coupled receptors
HPLC	high-performance liquid chromatography
HRV	Human rhinovirus
IMPase	Inositol monophosphatase
IP1	D-myo-inositol 1-monophosphate
IP3	Inositol 1,4,5-triphosphate
IPP	Inositol-1,4 bisphosphate 1-phosphatase
MHC	major histocompatibility complex
NIH	national institute of health
NMR	Nuclear Magnetic Resonance
PAINS	Pan assay interference compounds
PanDDA	Pan-Dataset Density Analysis
PI	Phosphatidyl inositol
PIP2	phosphatidylinositol 4,5-bisphosphate
PLC	Phospholipase C
PMCA	Plasma membrane calcium ATPase
PROTAC	Proteolysis-targeting chimera
RMSZ	Root mean square Z-score
SAD	Single anomalous dispersion

SAXS	Small angle X-ray scattering
SEC	Size exclusion chromatography
SERCA	Sarco- or endoplasmic reticulum calcium ATPase's
STD	Saturation Transfer Difference
TCR	T-cell receptor
T_m	Melting temperature

Chapter 1

INTRODUCTION

Introduction

1.1 Phosphatidylinositol signaling cascade

The Phosphatidylinositol (PI) cascade is one of the most ubiquitous cell signaling pathways in intracellular signaling. It involves the creation of the phosphorylated sugar molecule Inositol 1,4,5-triphosphate (IP3). IP3 is produced by the hydrolytic decapitation of the hydrophilic head of phosphatidylinositol 4,5-bisphosphate (PIP2). PIP2 is a phospholipid found in the inner leaflet of the cell membrane. The hydrolysis of PIP2 is catalyzed by Phospholipase C (PLC) activated downstream of G-protein coupled receptors (GPCR) which is the most common route of PLC activation. There are multiple isoforms of PLC. PLC-γ is activated by protein-tyrosine kinases due to this PLC isoform containing a Src Homology 2 domain. When PIP2 is hydrolyzed two signaling molecules are produced: IP3 and diacylglycerol (DAG). DAG remains in the cell membrane and activates protein kinase C (PKC). In contrast, IP3 is highly soluble and can diffuse through the cytosol where it binds to receptors inducing the release of calcium from intracellular sources, in particular, the endoplasmic reticulum (Figure 1) *(*Majerus, 1992*;* Streb *et al.,* 1983; Furuichi *et al.,* 1989; Newton, 1995). IP3 is recycled back to free inositol by a series of dephosphorylation steps catalyzed by enzymes such as Inositol-1,4 bisphosphate 1-phosphatase (IPP) and inositol monophosphatase (IMPase). Free inositol is then utilised in the re-synthesis of PIP2 (Gani *et al*., 1993; Harwood, 2005).

Calcium levels in the cell cytosol are maintained at low levels (cytoplasmic levels are approximately 100nM whilst extracellular concentrations are much higher at

approximately 1mM) by the action of calcium pumps. There are two families of calcium ATPases; plasma membrane calcium ATPases (PMCA 1-4) that pump calcium out of the cell and sarco- or endoplasmic reticulum calcium ATPases (SERCA 1-3) that pump calcium into intracellular stores. Calcium is an important signaling molecule and an increase in cytosolic levels causes activation of target proteins such as phosphatases and kinases. Many functions are regulated by increases in cytosolic calcium concentration, these include but are not limited to the cell cycle, granule secretion (exocytosis), cell contraction, apoptosis, cell adhesion, migration and transcription (Berridge, 1993).

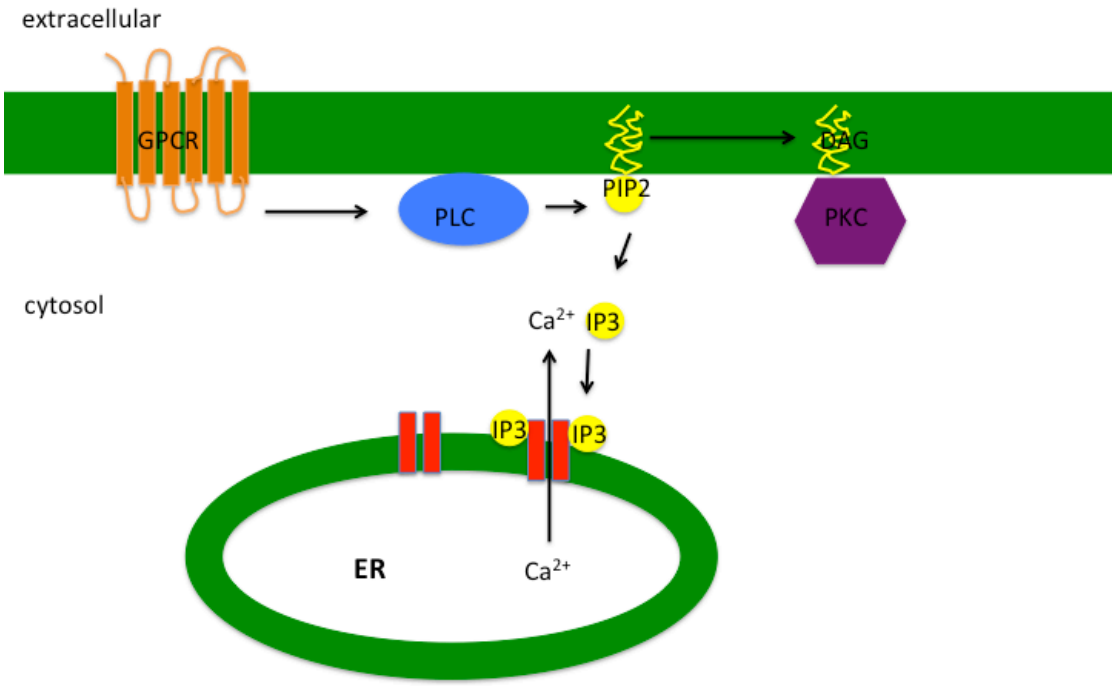

Figure 1. An illustration of the PI signaling cascade. GPCR activation causes the hydrolysis PIP2 by PLC, IP3 defuses through the cytosol and triggers the release of calcium by binding to receptors on the surface of intracellular calcium stores such as the ER. DAG remains in the inner leaflet of the cell membrane after the hydrolysis of PIP2 and activates PKC. PKC is also regulated by calcium.

1.2 IMPase: Structure and function

IMPase is a highly conserved enzyme found across groups at the highest taxonomic ranks. It is a metallo-phosphodiesterase enzyme that requires 2 or 3 magnesium ions for its catalytic activity and is inhibited by ions such as calcium. IMPase is a soluble cytosolic protein that assembles into a homodimer with a large dimer interface. It exhibits an αβαβα structural topology with two active sites per homodimer (Figure 2) (Bone, Springer, and Atack., 1992). The resulting protein is

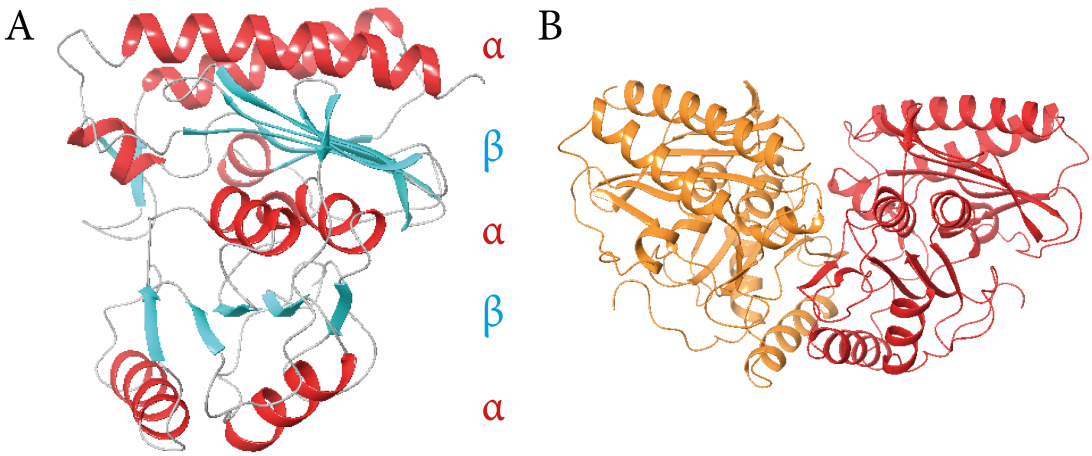

Figure 2. A) A ribbon illustration of IMPase with only one chain of the dimer shown. The secondary structural topology is shown with α-helices in red and β-sheets in turquoise. B) The IMPase homodimer. The individual chains are depicted in different colours: one red and one orange. It can be seen that both chains have a similar polarity but the monomers are not parallel as they have a slight rotation relative to one another. Reference for figure

extremely stable with a high melting temperature (T_m), for example, *H. sapiens* IMPase possesses a T_m of 79°C (Kraft *et al.,* 2018).

Mammalian IMPase exists in 2 isoforms, IMPase1 and IMPase2, encoded by the *impa1* and *impa2* genes respectively. IMPase1 consists of a 277 amino acid primary structure whilst IMPase2 contains an extra 11 amino acids on the N-terminus. These extra residues do not form any secondary structural elements and have been suggested to be a signal peptide element. Excluding the extra N-terminal region of IMPase2, the proteins share 54% sequence identity. Structurally the proteins are

homologous, having the same structural topology, with all cations and ligands in the active site positioned at the same locations (Arai *et al*., 2007). There is, however, a significant difference in the activity of the IMPase isoforms. IMPase2 has lower activity than IMPase1 and is also less sensitive to inhibition by lithium (Ohnishi *et al.,* 2014). Both isoforms are expressed in the brain with lower expression of IMPase2 except in the visual cortex and the mid-hind brain when compared to IMPase1. Outside of the central nervous system (CNS) IMPase2 is expressed at much higher levels than IMPase1 and in some cases exclusively (Ohnishi *et al*., 2007).

IMPase belongs to a large superfamily of structurally related phosphomonoesterases that are inhibited by lithium. IMPase displays broad substrate specificity and can hydrolyze many other phosphate monoesters such as those in β–glycerophosphate, adenosine-2'-monophosphate and *p*-nitrophenyl phosphate as well as other inositol monophosphate isoforms, inositol 4-monophosphate and *meso* inositol 5-phosphate (Ganzhorn and Chanal, 1990; Leech *et al.*, 1993; Cole and Gani, 1994; Fauroux and Freeman, 2009; Ackermann *et al*., 1987). In the following section I will focus on Myo-inositol 1-monophosphate (IP1) as a substrate for IMPase.

1.2.1 Mechanism of action of IMPase

IMPase requires magnesium for its catalytic activity at concentrations of between 0.5 – 5mM *in vitro.* Concentrations of magnesium above 5mM result in an inhibitory effect on IMPase activity, suggesting that the release of magnesium from the active site may be a part of the catalytic cycle of IMPase (Hallcher and Sherman, 1980). There is inconclusive evidence regarding how many magnesium ions are involved in the catalytic mechanism, and indeed, the mechanism of catalysis itself. There are

three magnesium binding sites in the active site of IMPase; two high affinity and one low affinity magnesium binding site. There are two suggested catalytic mechanisms for IMPase based on the magnesium binding properties; a 3-metal mechanism and a 2-metal mechanism (Pollack *et al.,* 1994; Lu *et al*., 2012; Gill *et al.,* 2005). Both mechanisms function through nucleophilic attack in a similar way to the mechanism of fructose 1,6-bisphosphate (Johnson *et al*., 2001). Glu70 and Thr95 coordinate the first Mg magnesium and the second magnesium ion is bound to three aspartate residues (Asp90, 93 and 220). These make up the 2 highest affinity magnesium binding sites. Glu70 coordinates the third magnesium ion and this makes the only coordinating interaction between the ion and the protein, forming the weakest magnesium binding site. Both proposed mechanisms use the activation of a nucleophilic water molecule to catalyse the hydrolysis of the IP1 substrate (Singh *et al*., 2012).

1.3 IMPase therapeutic interest

IMPase has been of therapeutic interest since it was hypothesised to be the putative target of lithium therapy in the treatment of bipolar in the 1980s (Berridge, Downes, and Hanley, 1982). More recently, it has been demonstrated that the inhibition of IMPase can stimulate autophagy and attempts are ongoing to determine if this can be exploited therapeutically in neurodegenerative diseases (Sarkar *et al*., 2005).

1.3.1 Bipolar Disorder and the inositol depletion hypothesis

Bipolar disorder is a psychotic disorder that is characterized by periods of depression and mania. People with bipolar disorder are often diagnosed with depression in the first instance; this is because the characteristic that distinguishes

bipolar disorder from major depression is the occurrence of mania, which can occur infrequently. Initially referred to as manic depression, bipolar disorder belongs to a class of psychiatric disorders known as affective disorders (mood disorders). The depressive episodes of bipolar disorder are characterized by a low mood, a feeling of low self-worth and patients may stop washing and feel lethargic. Depressive episodes can lead to suicidal thoughts and self-harm. These symptoms occur at a higher frequency in bipolar disorder than in major depression alone.

Mania is the distinguishing characteristic that separates bipolar disorder from major depression. Manic episodes are characterized by an elevated mood that may be described as euphoric. Whilst in a manic phase, patients may require less sleep, often make poorly thought out decisions with little regard to the consequences and be irritable. Mania in severe cases can be accompanied by psychosis (American Psychiatric Association, 2013). People experiencing mania often do not seek medical intervention and may not report it, leading to a misdiagnosis of major depression (Hirschfeld, Lewis, and Vornik, 2003).

Lithium has been used in the management of bipolar disorder for almost 100 years (Cade, 1949; Hammond, 1871) and remains one of the most widely used and effective treatments (Shorter 2009). Lithium is one of the few drugs for which there is evidence of its use resulting in a reduction in suicidal thoughts (Lewitzka *et al*., 2015). Lithium, a small cation, results in a wide polypharmacology that has made it difficult to determine an exact mechanism of its therapeutic action. Many hypotheses exist with varying amounts of evidence for each. In the 1970's studies

demonstrated that lithium treatment reduces inositol levels in the brains of mammals (Allison and Stewart, 1971). This decrease in inositol levels was mirrored by an increase of IP1. It was later shown that lithium inhibits the activity of inositol monophosphatase (Allison *et al*., 1976; Sherman *et al*., 1985). These observations led to the formation of the inositol depletion hypothesis of lithium's efficacy for the treatment of bipolar disorder (Berridge, Downes, and Hanley, 1982). This hypothesis suggests that the reduction in free inositol levels, observed following treatment with lithium, is a direct result of the inhibition of IMPase and leads to the attenuation of IP signalling. PIP2 is not able be re-synthesized due to a lack of free inositol. This inositol depletion affect is confounded in the brain due to the slow rate at which inositol enters the CNS, compared to the periphery. Inhibition of IMPase by lithium also inhibits the *de novo* synthesis of inositol from glucose 6-phosphate, as the last step requires IMPase (Figure 3) (Barkai, 1981; Calker and Belmaker, 2000).

No specific inhibitor of IMPase has been found that is effective *in vivo*. The development of a specific inhibitor of IMPase would allow for the direct evaluation of the inositol depletion hypothesis.

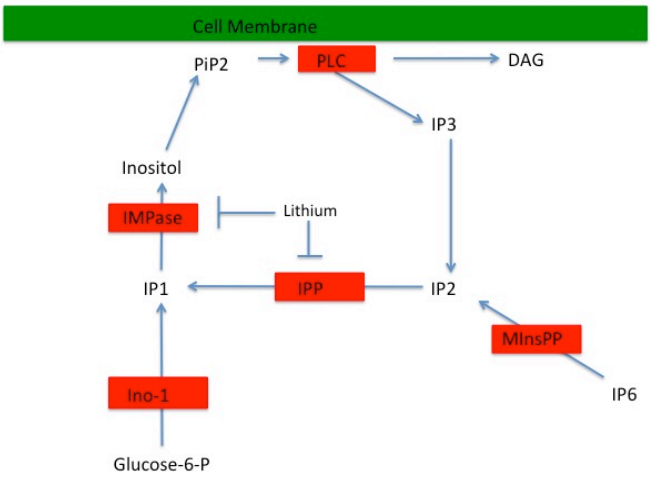

Figure 3. Inhibition of IMPase results in the attenuation of both *de novo* synthesis of inositol from glucose-6-phosphate via Inositol synthase (Ino-1) and the recycling of inositol from the Phosphatidylinositol signaling cascade and other inositol isoforms. IMPase is ideally placed as a target for the attenuation of inositol signaling as its inhibition prevents inositol production from multiple pathways. Multiple inositol polyphosphate phosphatase (MInsPP).

1.3.2 Autophagy, Neurodegeneration and IMPase inhibition

Autophagy is the process by which a cell removes, disassembles and recycles damaged or unwanted cellular components such as organelle and protein aggregates. The process begins with the formation of a membrane in which cellular waste resides in the lumen. This autophagosome then fuses with lysosomes (a membrane bound organelle that contains hydrolytic enzymes) to form a autolysosome in which the constituent biomolecules within are broken down (Klionsky and Emr, 2000). Many neurodegenerative diseases are characterized by the formation of protein aggregates in the brain. These proteins such as tau, α-synuclein and huntingtin are all substrates of the autophagic system (Ross and Poirier, 2004). Therefore, stimulating autophagy and the removal of pathogenic protein aggregates could be a useful therapeutic approach for treating neurodegenerative diseases such as Parkinson's and Huntington's disease. Intracellular levels of both inositol and IP3 negatively regulate autophagy (Criollo *et al*., 2007). A range of drugs that reduce intracellular levels of inositol have been shown to induce and upregulate autophagy. These include lithium, L690-330, valproic acid and carbamazepine (Fleming *et al.,* 2011; Williams *et al.,* 2002). With the addition of inositol, the autophagy-inducing action of these drugs can be reversed. Specific inhibition of IMPase by L690-330 resulted in the reduction of pathogenic peptides and protected against cell death *in vitro* (Sarkar *et al.*, 2005; Motoi *et al*., 2014). Down regulation of autophagy has been linked to a wide spectrum of neurodegenerative diseases, therefore, the stimulation of autophagy by

the inhibition of IMPase may provide a therapeutic strategy for the treatment of neurodegenerative diseases (Shintani and Klionsky, 2004).

1.4 IMPase Inhibitors

1.4.1 Lithium

Lithium inhibits IMPase via an uncompetitive mechanism. IMPase requires magnesium for its activity. Lithium causes displacement of a magnesium ion in the active site of IMPase and inhibits the release of the phosphate from the enzyme product complex. Purified IMPase is inhibited by lithium with a half maximal inhibition (IC50) seen at a concentration of approximately 0.8mM (Gani *et al.,* 1993; Hallcher and Sherman, 1980). The inhibitory mechanism of lithium requires the presence of the substrate in order to generate the inhibited lithium-IMPase-product complex. Therefore, the higher the substrate concentration, the greater the degree of enzyme inhibition seen (Leech *et al.*, 1993).

1.4.1 L-690,330

In the 1990s, the pharmaceutical company Merck produced a series of inhibitors based on the substrate of IMPase. Design of drugs based on the substrate or transition state analogue is a common strategy in drug discovery. These 'substrate mimetics' are typically competitive reversible inhibitors that function by competing with the substrate for the proteins active site. Merck's approach was to synthesis methylenebisphosphonic acid derivatives of IP1 that were non-hydrolysable (Baker *et al.,* 1990). The resulting compound 'L-690,330' was a potent inhibitor of IMPase (IC_{50} 0.2μM) (Figure 4) (Atack *et al.*, 1993).

The active site of IMPase is larger than that required to accommodate the IP1 substrate. L-690,330 contains an additional phosphate compared to the IP1

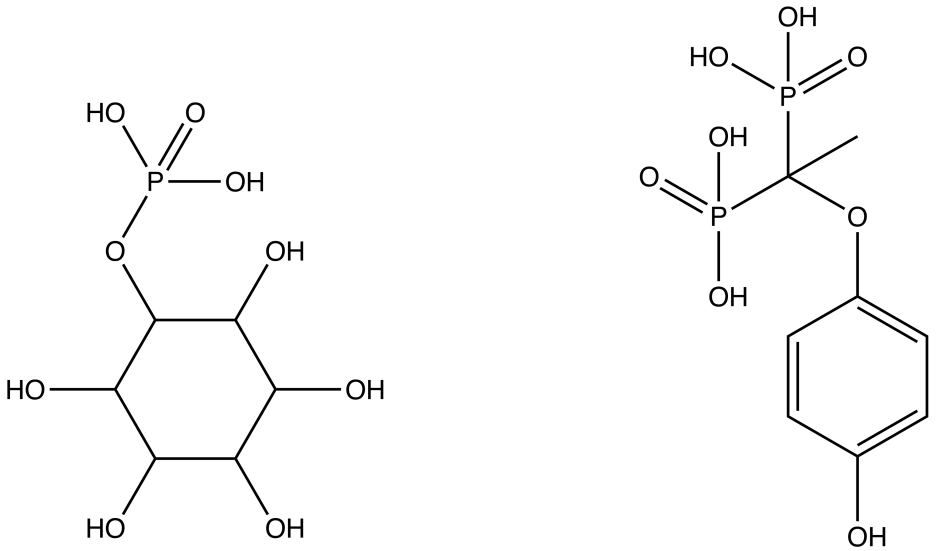

IP1 L-690,330

Figure 4. The structure of IP1, the substrate of IMPase, and L-690,330 the substrate mimetic produced by the pharmaceutical company Merck.

substrate. This extra phosphate forms further interactions with residues Trp219 and Asp220. IP1 is a very soluble, highly polar substrate and the active site of IMPase reflects these properties as does as the substrate mimetic L-690,330. Hydrophilic drug molecules lack cell and CNS penetration. IMPase is a cytosolic protein that has its therapeutic region in the CNS for the treatment of bipolar disorder. Therefore L-690,330 lacks the physicochemical properties necessary for it to be a good inhibitor *in vivo* and consequently is not of therapeutic use. Attempts were made to produce a tetrapivaloyloxymethyl ester prodrug that would be less charged and therefore more cell permeable. The prodrug would then be metabolised inside the cell to the active compound L-690,330, however these compounds later failed in *in vivo* studies due to solubility issues (Atack *et al.,* 1994).

1.4.2 Ebselen

A screen of the national institute of health (NIH) clinical collection revealed ebselen to be an inhibitor of IMPase (Singh *et al.*, 2013). The NIH clinical collection is a fragment library made up of drugs that have failed clinical trials for their initial intended therapeutic use but have a good safety profile. As there is human safety data already available for these compounds, they can be developed cheaper and faster than novel compounds. This process is known as drug repurposing and has become more popular in recent years. Ebselen is a synthetic organoselenium drug that was initially developed as an antioxidant drug that mimics glutathione peroxidase. The initial therapeutic application was to use ebselen's anti-inflammatory, anti-oxidant and cytoprotective properties to provide a neuroprotective effect in stroke patients (Schewe, 1995; Yamaguchi *et al.,* 1998). Clinical trials determined that ebselen was a safe drug, despite the fact that ebselen contains selenium which has known toxicity issues (REF). Studies that examined the metabolism of ebselen determined that it is metabolised into three products and negligible free selenium is released (REF).

Ebselen inhibits IMPase non-competitively and non-reversibly (REF). Ebselen contains an isoselenazolone ring that has similar activity to an isothiazolone. Isothiazolones contain a sulphur instead of selenium. Isothiazolone containing compounds are often identified as "hits" in compound screens in drug discovery. Isothiazolones and isoselenazolones are reactive, having the ability to covalently bind to cysteine residues of target proteins. Therefore, isothiazolones and isoselenazolones are classed as pan assay interference compounds (PAINS) (Baell

and Nissink, 2018). In this thesis I will be exploring the isothiazolone reactive group in an attempt to identify novel IMPase inhibitors (Figure 5).

Ebselen has an IC_{50} of approximately 1.5μM with respect to IMPase (Singh *et al.,* 2013). Ebselen exhibited IMPase inhibition *ex vivo* and mimics lithium in behavioural experiments tests in mice displaying symptoms of mania (ref). Due to the reactivity of the isoselenazolone ring in ebselen and its small size, ebselen possesses intrinsic polypharmacology. The translation of any potential therapeutic efficacy of ebselen to inhibition of a single target protein is therefore difficult.

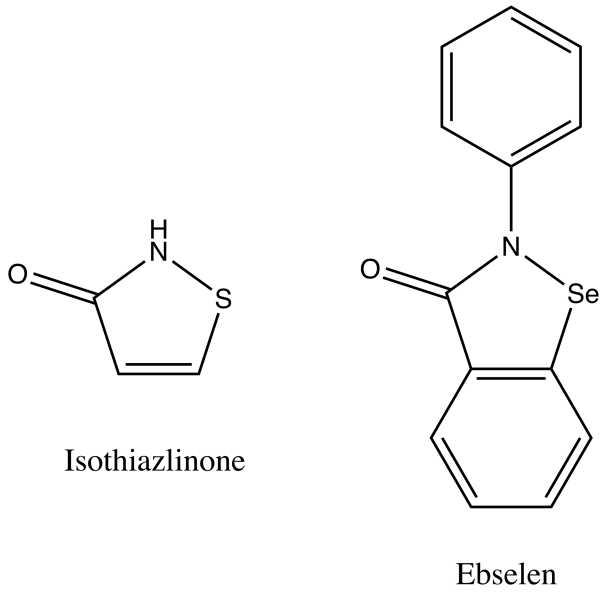

Figure 5. The isothiazolone reactive group and the IMPase inhibitor Ebselen

1.5 The Calbindin-IMPase Interaction

In 2002 it was reported that calbindin-D28k binds to and activates IMPase (Berggard, Szczepankiewicz, *et al.,* 2002). The interaction was identified by affinity chromatography using calbindin-D28k immobilized on magnetic beads and phage-

display peptides from a random 12 long polypeptides library. This approach was used to attempt to explore the calcium sensing function of calbindin-D28k. One peptide with homology to IMPase was highly retained in the column. Calbindin-D28k was found to increase IMPase activity by up to 250-fold, surprisingly in conditions that were unfavourable for IMPase activity. The interaction and activating effect of calbindin-D28k on IMPase occur in both the absence and presence of calcium, suggesting that calbindin-D28k is not acting as a calcium sensor in this interaction. The interaction between IMPase and calbindin-D28k has a dissociation constant (K_d) of 0.9 μM. *In silico* modelling of the interaction indicated that Lys59 and Lys61 of IMPase along with Asp24 and Asp26 of calbindin-D28k were critical residues involved in this interaction. Mutagenesis of these resides confirmed that they (all of them?) are critical for the activating effect of calbindin-D28k on IMPase (Figure 6) (Levi *et al.,* 2013). Using this information, small competitive peptide interaction inhibitors were designed that were able to attenuate the activating effect of calbindin-D28k on IMPase.

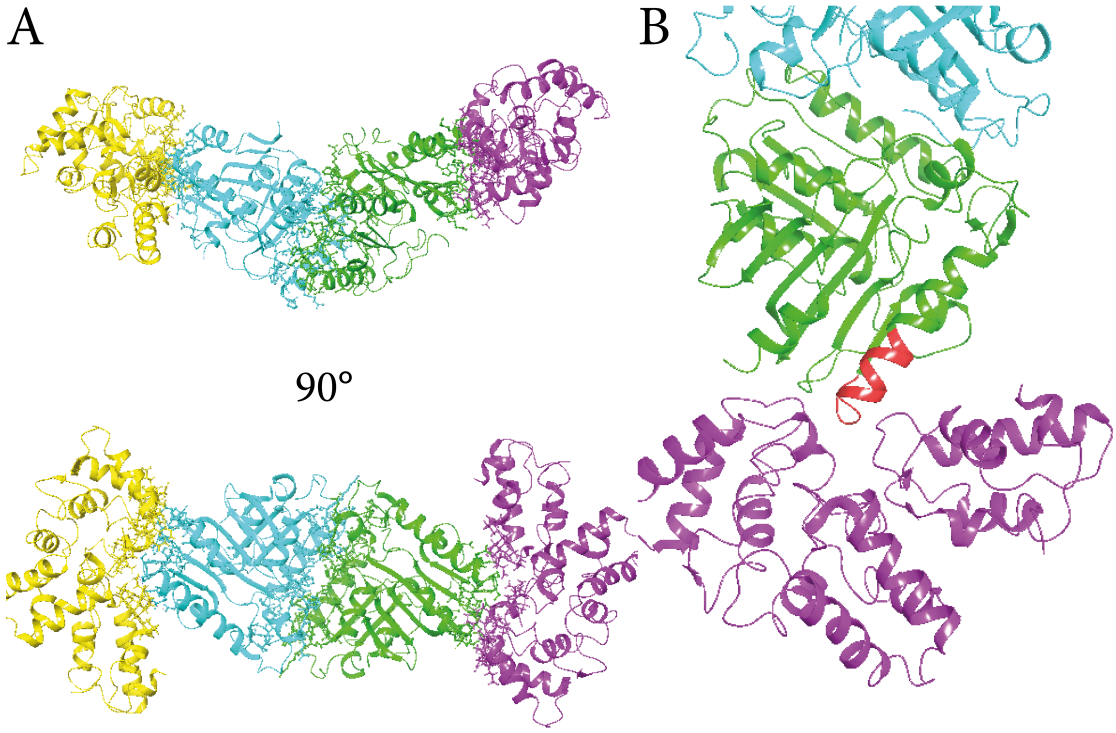

Figure 6. A) The *in silico* docking model of the Calbindin-IMPase complex. IMPase in green and blue and Calbindin-D28k in yellow and lavender. B) The peptide fragment of IMPase that was identified as the calbindin-D28K ligand is coloured red.

1.5.1 Calbindin-D28k structure and function

Calbindin-D28k is a calcium buffering protein that is present in high concentrations in the CNS and absorptive epithelia. In absorptive epithelia, calbindin-D28k expression is under the control of a vitamin D dependent expression system, whilst in the CNS calbindin-D28k expression is vitamin D independent (Clemens *et al.,* 1989; Arnold and Heintz, 1997). Calcium signalling is central in cell biology and therefore its cellular concentration is tightly regulated. Calbindin-D28k is a calcium buffering protein but it also acts as a calcium sensing protein (Schmidt, 2012). Calbindin-D28k undergoes small conformational changes upon calcium binding that initiate the binding of target proteins to Calbindin-D28k. Calbindin-D28k is a 30kDa

protein composed of 6 EF-hand motifs with a primary structure of 261 amino acids (Kojetin *et al.,* 2006). EF-hand motifs possess helix–loop–helix topology and are common structural domains found in calcium-binding proteins. Loop structures in these motifs form the calcium binding sites in calcium-binding proteins. Each of the EF-hand motifs is held together in a single globular fold (Figure 7) via hydrophobic interactions between each motif. This structure is maintained in both the calcium loaded and apo forms. Calbindin-D28k has four calcium binding sites in the loops of EF-hand 1, 3, 4 and 5 (Akerfeldt *et al.,* 1996). DOESN'T THIS SECTION NEED TO BE BEFORE THE SECTION ABOVE???

1.6 Introduction to Biomolecular Crystallography

Biomolecular crystallography is a technique that enables scientists to obtain close to atomic resolution structure of biological macromolecules. In order for a structure to be resolved, the molecule of interest must be arranged in a regular lattice to form

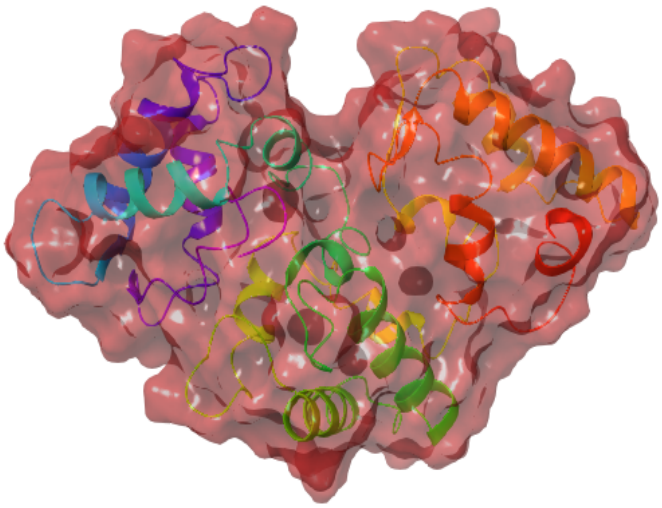

Figure 7. A ribbon representation of a nuclear magnetic resonance (NMR)model of calcium bound Calbindin-D28k, with its calculated surface shown in red. It can be observed that the protein forms a single domain protein and has a kidney bean-shaped structure.

a crystal. This is frequently the rate-limiting step in structural determination by bimolecular crystallography. The determination of a crystal structure begins with the collection of diffraction data. Crystals are exposed to a beam of X-rays (neutrons or electrons can also be used) and diffraction data collected. This data is then scaled and merged and phases of data are estimated by imposition of a previously identified model or are obtained experimentally. The model generated is then refined against the data to produce a final structure.

1.6.1 Protein crystallisation

In order to obtain an X-ray crystal structure of a protein the first step is to crystallise the protein of interest. Currently, there is no precise method of predicting which conditions are required for a protein to form a crystal. Therefore, a trial and error approach is often used, screening multiple conditions in order to identify those most suitable for crystallisation. Crystallisation experiments require a sample of highly purified protein at high concentrations (frequently in excess of 1 mg/ml). Precipitants are then added to the protein solution and water removed by diffusion over time to create a supersaturated sample. In conditions favourable to crystallisation, crystals will eventually grow from the metastable supersaturated solution. In conditions unsuitable for crystallisation the protein will precipitate, or phase separation may occur. It is often the case that the first crystal obtained from a screen may not diffract well or may be too small. In such circumstances, it is necessary to optimize the crystallisation conditions. Changing pH or precipitant concentration may enable an experimentally viable crystal to be obtained that will diffract well.

The most common method of growing crystals (and the method used

experimentally in this dissertation) is a technique known as vapour diffusion. Protein solution is mixed with a precipitant solution at defined ratios and kept in close proximity to a reservoir of the precipitant solution in a closed system. Water from the protein drop then diffuses from the protein drop into the precipitant reservoir, resulting in a progressive increase in the precipitant and protein concentration within the drop (McPherson and Gavira, 2014).

After crystals are acquired, they are harvested on specially designed loops and cryo-cooled in liquid nitrogen. The crystal cooling serves multiple purposes, depending on future experimental requirements. Advantages of crystal cooling include; a reduction of the effects of radiation damage, reduction in crystal movement during data collection and to help prevent the crystal from drying out. Unlike small molecule crystals, protein crystals contain a high percentage of solvent and consequently, water. The formation of ice crystals within the solvent filled pores of a protein crystal can disrupt the crystal lattice, distorting its diffractive properties. Therefore, it is necessary to protect crystals with cryoprotectants. These include glycerol, polyethylene glycols or high salt (Bergfors, 1999).

1.6.2 Properties of protein crystals

Protein crystals are formed via weak intermolecular interactions between each individual globular protein molecule. These intermolecular interactions are sparse relative to the size of the protein molecule, leading to a low contact to volume ratio. This results in protein crystals that are often soft and fragile. As proteins have an irregular surface, large solvent filled pores are present in between individual molecules. The solvent molecules are mostly disordered and therefore do not contribute to the diffraction pattern.

The fundamental property exploited in a diffraction experiment is the internal symmetry of the crystal. The regular, periodic arrangement of protein molecules within the crystal is necessary to produce the discrete X-ray diffraction that permits determination of a structure. There are limited conformations in which a protein molecule can be arranged into a crystal lattice. The translation periodicity and internal symmetry requirements allow for 65 possible arrangements for a chiral protein molecule in 3-dimensional space. The internal symmetry of a crystal is an important feature to consider when collecting diffraction data from a crystal, as more degrees of data will need to be acquired from crystals with lower order symmetry (Chernov, 2003).

1.6.3 Basics of X-ray diffraction

Unlike individual atoms, irradiation of a crystal from specific angles will yield positive diffraction data often referred to as reflections. This property of crystal diffraction is expressed by the Bragg equation $2\,\mathrm{dsin}\,\theta = n\lambda$ (Bragg and Bragg, 1913). Bragg's law outlines the conditions when constructive and destructive scattering occurs. Coherent constructive interference only occurs when a beam of X-rays (of identical wavelength and phase) falling on adjacent lattice planes, that the extra length travelled between the adjacent lattice planes needs to be an integer of the wavelength of the irradiating x-ray. The position and distance between the diffraction reflections are directly related to the crystal symmetry and unit cell dimensions (the smallest unit of the crystal whereby the crystal could be rebuilt by simple translation). The information that allows resolution of the the atomic structure is the intensity of the reflections. This value is directly related to the underlying molecular transform in reciprocal space of the molecular electron

density and is linked to the real space electron density via a Fourier transformation. Due to the experimental parameters the phase information is lost, as only intensity data is collected. Therefore, to solve the structure this phase information must be obtained via supplementary experimentation. This includes multiple/single isomorphous replacement, multiple/single wavelength anomalous dispersion or molecular replacement (Taylor, 2003).

1.6.4 Basics of structural determination

Electron density obtained from Fourier transformation of the reciprocal space data is presented as a contoured electron density map. A model is built into the electron density map using standard amino acid bond lengths and geometries. This model is then refined against the electron density map. During each cycle of refinement, adjustments are made to the phases that reduce the difference in the calculated and observed diffraction patterns. Adjustments are also made to the coordinates of the model using maximum likelihood or dynamics simulations. Repeated cycles of refinement and model building are employed in order to obtain the final structure. To ensure the refinement process does not bias the map 5-10% of the collected data is set aside and not refined against. This is then used to monitor any biasing of the map.

1.6.5 Crystallisation of protein ligand-complexes

There are two major methods for crystallising protein-ligand complexes. These are co-crystallisation and soaking. The soaking method exploits the solvent filled pores that are characteristic of protein crystals. The crystal pores allow small molecules to diffuse through the crystal and bind to the protein *in situ.* However, there are

some limitations to this method. Large molecules may not be able to diffuse through the crystallographic pores and conformational changes induced by ligand binding may be inhibited by crystallographic packing restraints or may disrupt the crystal making it unviable. The co-crystallisation method incorporates the ligand of interest into the protein crystallisation mix. If successful, the protein will crystallise with the ligand bound. Proteins are often crystallised with ligands when crystallisation is aided by the stabilisation of the protein in a single conformation due to ligand binding. However, some ligands may also precipitate out in the crystallisation mix or crystallise independently of the protein (Hassell *et al,.* 2007).

1.7 Introduction to Small angle X-Ray Scattering

Small angle X-ray scattering (SAXS) is a biophysical technique that can be employed to study the size, shape, and dynamics of molecules in solution. The wavelength of X-rays are smaller than that of the protein molecules studied. Therefore, X-ray scattering can give rise to inference effects that lead to an angular dependence of X-rays scattering, revealing structural information about the sample. SAXS experiments are frequently performed at synchrotrons on purpose-built beamlines. Typically, a sample concentration of between 0.5 and 10mg/ml is used. In this dissertation Size exclusion chromatography - Small angle X-ray scattering (SEC-SAXS) is utilised. This method employs High Performance Liquid Chromatography (HPLC) where the sample flows through a size exclusion column before entering the X-ray beam. In contrast to X-ray crystallography, in SEC-SAXS the molecules in solution are arranged randomly in different orientations. The data collected is therefore spherically averaged, creating a low-resolution model of the molecule studied. Scattering data is collected on a detector and a radial integration is

performed to produce a one-dimensional SAXS profile. The scattering profile is the scattering intensity plotted against a function of the angular dependants known as q ($q=4\pi\sin\theta/\lambda$). This value can be converted to real space with an indirect Fourier transformation. Significant scattering from the solvent is observed in a SAXS experiment and must be subtracted from the scattering profile in order to gain accurate insight into the molecule of interest. The intensity of the data collected is dependent on the interparticle interactions within the solution. To obtain data on the size and shape of a single particle, there must be no interparticle interactions and a mono-disperse/non-aggregated sample is required (Svergun and Koch, 2003). Expected scattering profiles can be calculated computationally for any given molecular shape. This process is widely used to compare SAXS data to models obtained in NMR, crystallography and other techniques. This same process can go in the other direction to obtain a low-resolution (bead model) structure from the SAXS data collected (Franke and Svergun, 2009).

1.7.1 Analysis of SAXS graphs

There are established plots that are used in the analysis of SAXS data and the three most essential of these are the Guinier plot, Kratky plot and Distance distribution function (REF). The Guinier plot is used to determine the Radius of gyration (R_g) of the molecule being studied. The R_g is an estimation of the size of the molecule being studied. It is the root mean square distance of all the distances to the centre of mass of the scattering molecule. The angular dependence of scattering intensity close to that of the incident beam should give a linear slope equal to $R_g^2/3$. This is known as the Guinier region and is obtained from the Guinier plot (REF). The Kratky plot is employed to examine the flexibility of a protein but also gives some information on

the type of protein being studied, for example if the protein is multidomain or single globular (Figure 8A) (REF). The Distance distribution function often referred to as the P(r) plot is the indirect fourier transform from the scattering function (I vs Q), and therefore represents the real space representation. Where the distance distribution function meets the x-axis (rÅ) this is equal to the maximum dimensions (D-max) of the scattering molecule. The shape of the distance distribution function also reveals aspects of the shape of the molecule being studied (figure 8B) (REF).

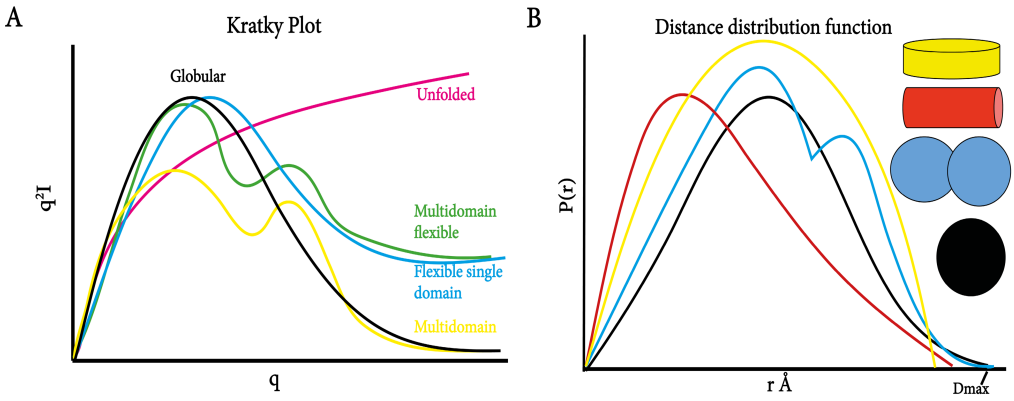

Figure 4. A) The different shaped curves produced by different types of protein on a Kratky plot. B) The distance distribution function that would be expected from different shape proteins. Ref for figure

1.8 Introduction to Assays and Inhibitors

1.8.1 Malachite green Assay

Inositol Monophosphatase produces free phosphate from IP1. The enzymatic assay used in this thesis measures the concentration of free phosphate using malachite green reagent (BIOMOL®GREEN). Free phosphate forms a complex with malachite green and absorbs light at wavelength of λ= 620-640 nm. The absorbance at this wavelength is directly related to the phosphate concentration. Therefore, the absorbance can then be measured and IMPase activity quantified with respect to phosphate production. This assay is an endpoint assay, therefore, IMPase activity is

stopped prior to the measurement (Itaya and Ui, 1966; D'Angelo, Crutchfield, and Vandiviere, 2001; O'Toole *et al.,* 2007).

1.8.2 Thermal shift Assay

Thermal shift is a biophysical assay that monitors the melting temperature (Tm), the temperature at which the protein loses it globular fold, of the target protein. Most proteins have a hydrophobic core, and this is the major driving force of protein folding. The hydrophobic core is not solvent exposed. In this assay the sample is slowly heated causing the protein to unfold (denature) and the hydrophobic residues become exposed. The denaturation of the protein can be monitored with the use of a fluorescent dye that binds to the exposed hydrophobic residues. The melting temperature of a protein can fluctuate if it is bound to a ligand. The binding of a ligand frequently stabilizes the fold of a protein, thereby increasing the melting temperature of a protein. However, some ligands can stabilise the fold but have the opposite effect on melting temperature. This fluctuation of the melting temperature of the target protein can be used to monitor ligand binding (Pantoliano *et al.,* 2001).

1.8.3 Saturation Transfer Difference (STD) Nuclear Magnetic Resonance (NMR)

Saturation Transfer Difference Nuclear Magnetic Resonance (STD-NMR) is a popular technique in drug discovery projects and can be used for both screening and ligand binding conformation. STD-NMR is a technique that measures the signal from the ligand rather than from the protein. In an STD-NMR experiment, the protein signal is selectively saturated, and this saturation can transfer from the protein to a binding ligand through the nuclear Overhauser effect. Hydrogen from the ligand needs to be ≤5Å to the protein for transference to take place. A difference spectrum

is produced by subtracting a saturated spectra from the off-saturation spectra. If a ligand binds to the protein there will be a difference between the ligand signals in the saturated spectra compares to the off-saturation spectra, producing peaks in the difference spectra (Mayer and Meyer, 2001; Viegas *et al.*, 2011).

1.8.4 Overview of inhibitors

Inhibitors are molecules that bind to and decrease the activity of a target protein such as an enzyme or ion channel. There are a variety of different types of inhibitors that have different biochemical properties and may be useful for different types of protein targets. In the following section I will focus on enzyme inhibition.

1.8.4.1 Competitive Inhibitors

Competitive inhibitors in relation to enzymes refer to inhibitors that bind to the active site of the enzymes. As the inhibitor and substrate bind to the same site, they are in competition with each other for that binding site. Competitive inhibitors often have similar chemical properties to the substrate they are competing with. This is a reflection of the fact that they are binding to the same site on the protein and usually make the same or similar interaction. The majority of competitive inhibitors are reversible with non-covalent interactions made between the protein and inhibitor. As reversible competitive inhibitors are in competition with the substrate, the higher the substrate concentration the higher the concentration of inhibitor required to inhibit the enzyme. Irreversible competitive inhibitors stop the enzyme binding and catalysing any additional substrate and frequently form a covalent bond with the target protein. Irreversible competitive inhibitors have different properties to reversible competitive inhibitors, such as taking longer to reach full inhibition

and higher substrate concentration resulting in more time required to reach maximal inhibition (REFS).

1.8.4.2 Non-competitive inhibitors

In contrast to competitive inhibitors, non-competitive inhibitors bind to a site outside of the active site and are therefore not in competition with any substrate. Non-competitive inhibitors function either through binding to physiological regulatory (allosteric) binding sites, binding to the enzyme substrate complex or covalently binding and inhibiting the dynamics of the protein. Similar to competitive inhibitors, non-competitive inhibitors may also be reversible or irreversible (REF).

1.8.4.4 *In situ* degradation

A relatively novel method of inhibiting proteins is by exploitation of the ubiquitin proteasome pathway. Proteolysis-targeting chimeras (PROTACs) are synthetic chemicals that link the target protein to an E3 ligase causing the ubiquitination of the target protein. This ubiquitination identifies the protein as a target of the proteasome; a large protein complex that hydrolyses surplus or damaged proteins. PROTACs have an E3 ligase ligand at one end and a target protein ligand at the opposite end, linked together by a flexible chemical linker to produce a single molecule. The majority of proteins do not have an active site or a channel. These include scaffold proteins, cytoskeletal proteins and transcription factors and therefore do not possess an active site that can be blocked. In this situation, traditional inhibitors can be ineffective and therefore the use of a PROTAC may be more successful (Toure and Crews, 2016; Ottis and Crews, 2017).

1.9 Overview of the Drug Discovery Process

The drug discovery process is a resource intensive and time intensive process that has a low success rate. To launch a new drug to the market takes typically 10-18 years, with the associated costs in excess of a billion pounds (DiMasi, Hansen, and Grabowski, 2003). The experimental stages of the drug discovery process can be split into three overarching categories:

1. Molecule discovery
2. Preclinical development
3. Clinical development

Each stage is made up of multiple steps. Fundamentally the drug discovery process is a periodic stepwise path with clear aims.

The molecule discovery stage typically takes between 2-5 years and is made up of four steps. The first and second steps are target identification and validation. Target identification consists of identification of a drug target usually by the discovery of a protein or gene involved in a particular disease. The target is then validated using typical approachs such as studies of knockout models of the target protein. The third and fourth stages are lead identification and optimization. The initial chemical matter is usually found by screening thousands of chemicals for inhibition activity or protein binding. Once the initial chemical matter is identified it is then optimized by medicinal chemistry efforts, in order to increase affinity and potency (REF).

After a potent compound has been developed it is then progressed into the preclinical development phase. This phase aims to meet all of the requirements for

the compound to be tested in humans. There are four main subcategories of the preclinical development phase. These are preliminary toxicological testing, pharmacokinetic testing, pharmacological testing and feasibility studies for large scale production of the compound. This stage frequently takes between 1 to 3 years and involves testing the compound in *in vitro* assays and on non-human animals. The aim is to attempt to minimise any safety risks in human clinical trials and test compound efficacy in disease models. Compounds at this stage may still be optimized in an effort to improve the pharmacokinetic properties. However, compounds with obvious toxicity or pharmacological hazards are dropped at this stage (REF).

After a compound has successfully been shown to be safe in non-human animals, it progresses into the clinical development phase. This is composed of three clinical trial phases known as Phases 1, 2 and 3. The phases are performed sequentially, and the compound must pass the previous phase before moving onto the next. A phase 1 clinical trial examines the tolerability and potential side effects of the compound, as well as the *in vivo* pharmacokinetics. The fundamental purpose of Phase 1 is to monitor the safety of the compound and calculate safe dosage regimes. Phase 2 clinical trials are small scale patient trials to assess the initial efficacy of the compound and determine effective dosage regimes. Phase 2 will also build on the safety evidence obtained in phase 1 trials by evaluating long term toxicology. Phase 3 are large-scale controlled clinical trials. At this stage the compound will also be a compared to alternative drugs, if available. The clinical development stage is the most expensive stage of drug development and usually takes between 5 to 7 years to complete. In order for a compound to be approved it has to have advantages

above those other drugs already on the market, such as being cheaper to manufacture or having better efficacy. Alternatively the compound may address an unmet clinical need. If the compound is approved for the market, there is a process of continual surveillance of patients. This is often referred to as phase 4. The purpose of this is to to monitor any side effects or long-term toxicity issues and identify drug interactions that have not or could not be identified during the drug development process (REF).

1.10 Aims and Project structure

The aims of this project were to explore the calbindin-IMPase interaction and to use this information to aid in the development of a range of novel chemical matter for development into potential IMPase inhibitors. Four lines of investigation were tackled in the following chapters; the first two examining the calbindin-IMPase interaction and the final two aiming to identify novel inhibitors and chemical matter. This project is divided into two sections. The first section consists of the biological allosteric modulation of IMPase, and second section covers pharmacological allosteric modulation of IMPase (Figure 9).

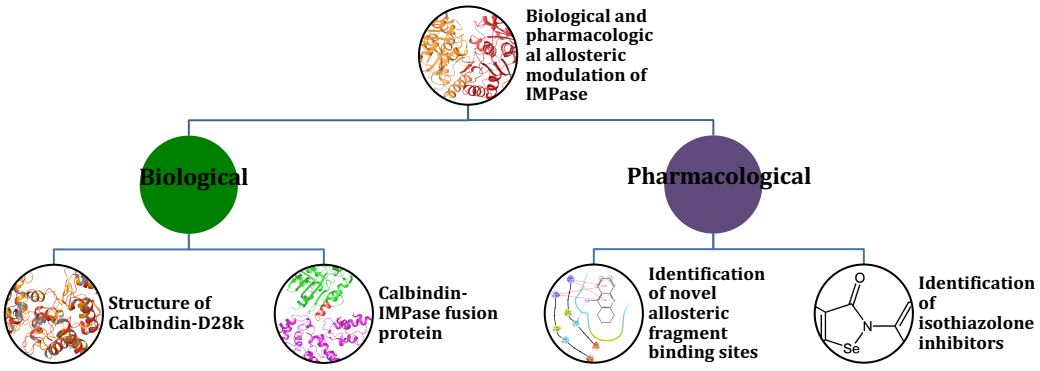

Figure 5. The structure of this thesis is illustrated in a tree diagram. The project is divided into two sections: Biological and Pharmacological.

1.10.1 Biological data

The biological section of this thesis explores the structure of the IMPase binding partner calbindin-D28k. Currently, only an NMR model of the rat calbindin-D28k has been solved (ref). Despite published attempts to secure a crystal structure, a structure has failed to be produced, as a phasing solution could not be found (ref). After purifying human calbindin-D28k, SAXS data indicated that there were differences between the NMR models of calbindin-D28k compared to the SAXS data

(ref). The NMR model does not allow direct visualization of calcium binding sites. This is an important structural feature as a central function of calbindin-D28k is as a calcium buffering and sensing protein. Therefore, an important project aim was to produce a crystal structure of calbindin-D28k. To gain an understanding of the calbindin-IMPase interaction it would be important to have the most accurate model of both binding partners.

A second aim of the biological data section of the project was to create a fusion protein using a flexible amino acid linker. The use of fusion proteins to study protein complexes is well established and has yielded both NMR and crystal structures (ref). Fusion of the proteins should stabilize the complex and this is particularly useful when protein interactions are of a low affinity. The fused complex is postulated to have increased catalytic activity compared to IMPase alone. (ref or is this your theory?). These studies would confirm that the activating effect of calbindin-D28k on IMPase is at a one to one concentration ratio (ref??).

1.10.2 Pharmacological data

Despite the identification of IMPase in the 1970s as a potential target of lithium (ref), the development of the pharmacology of IMPase has remained sluggish. IMPase has proven intractable to traditional drug discovery approaches. The inhibitors that have been identified to date (lithium, ebselen and L-690,330) all have issues with polypharmacology or undesirable physiochemical properties. Both lithium and ebselen have a polypharmacological profile; lithium because it is a small ion and ebselen because it is small and reactive. L-690,330 is very polar and therefore lacks cell and CNS penetration. In the pharmacological branch of the project, I aim firstly to identify novel binding sites outside the active site that may be of potential

therapeutic benefit. This will be attempted by the use of a crystallographic fragment soaking screen. Furthermore, I aim to explore potential novel binding sites using site-directed mutagenesis. Lastly, due to the relatively recent discovery of the inhibition of IMPase by ebselen, I aim to screen reactive compound inhibitors in order to identify novel chemical matter for future medicinal chemistry efforts.

1.10.3 Chapter Aims

1.10.3.1 Chapter 2: The X-ray structure of human calbindin-D28K: an improved model.

To express, crystalise and structurally resolve the IMPase binding partner Calbindin-D28k. This is the first structure produced of the human isoform and allows direct visualization of the calcium binding sites of Calbindin-D28k. Understanding the structure function relationship of Calbindin-D28k could give insights that will allow further understanding of the Calbindin-IMPase interaction.

1.10.3.2 Chapter 3: Fusion Protein Exploration of the Calbindin-IMPase Interaction.

To develop fusion proteins that mimic the Calbindin-IMPase interaction and use these in structural analysis in order to evaluate a previously published *in silico* docking model, and gain insights into the biophysical properties of the Calbindin-IMPase protein complex.

1.10.3.3 Chapter 4: Exploration of A Novel Fragment Binding Site at the Homodimer Interface of IMPase.

To use crystallographic screening to identify novel fragment binding sites of IMPase. To further evaluate the identified fragment binding sites using site-directed mutagenesis and crystallography.

1.10.3.4 Chapter 5: Isothiazolinone Inhibition of IMPase.

To expand the range of isothiazolinone inhibitors identified by creating a screening library based on the previously identified inhibitor ebselen. Any hits identified by the screen will then have compound properties and mechanism of action explored by the use of biochemical and biophysical assays.

Chapter2
Paper1

The X-ray Structure of Human Calbindin-D28K: An Improved Model

The X-ray Structure of Human Calbindin-D28K: An Improved Model

J. W. Noble[1,*], R. Almalki[2], S. M. Roe[2], A. Wagner[3], R. Duman[3], J. R. Atack[4]

[1] University Of Sussex, Sussex Drug Discovery Centre, Brighton, BN1 9QG, UK. [2]University Of Sussex, School Of Life Science, Brighton, BN1 9QG, UK. [3]Diamond Light Source, Harwell Science and Innovation Campus, Chilton, Didcot OX11 0DE, England. [4]Cardiff University, Medicines Discovery Institute, Cardiff, CF10 3AT, UK. *Corresponding author

Abstract:

Calbindin-D28K is a widely expressed calcium buffering cytoplasmic protein and is involved in many physiological processes. It has been shown to interact with other proteins, suggesting a role as a calcium sensor. Many of the targets of Calbindin-D28K are of therapeutic interest, for example, IMPase, the putative target of lithium therapy in bipolar disorder. Presented here is the first crystal structure of human Calbindin-D28K (6FIE). There are significant deviations in the tertiary structure when compared to the NMR structure of rat Calbindin-D28K (2G9B), despite 98% sequence identity. SAXS indicates the crystal structure better predicts the properties of Calbindin-D23K in solution compared to the NMR structure. We present here the first direct visualization of the calcium binding properties of Calbindin-D28K. Four of the six EF-hands (EF) that make up the proteins secondary structure contain a calcium-binding site. Two distinct conformations of the N-terminal EF1 calcium-binding site were identified using long-wavelength calcium-SAD. This flexible region has previously been recognized as a protein-protein

interaction interface. SAXS data collected both in the presence and absence of calcium indicates that there are no large structural differences in the globular structure of Calbindin-D28K between the calcium loaded and un-loaded protein.

Introduction:

Calbindin-D28K is a major calcium buffering cytoplasmic protein expressed at particularly high levels in the central nervous system and absorptive epithelium (gut and kidney)(Schmidt 2012). Calcium signaling is tightly regulated and is involved in a myriad of physiological processes and consequently calcium deregulation is a key factor in the pathogenesis of many diseases, such as Alzheimer's disease (Bojarski, Herms, and Kuznicki 2008; Kook et al. 2014). Calbindin-D28K was first identified in the intestine, colon, kidney and uterus of *gallus gallus domesticus* (chicken) (Wasserman, Corradino, and Taylor 1969), where it is involved in the transcellular movement of calcium across the absorptive epithelium such as those found distal convoluted tubules of the kidney (Lambers et al. 2006). Calbindin-D28K is also highly expressed in the central nervous system (CNS), where it contributes up to 1.5% of total soluble protein (Christakos, Gabrielides, and Rhoten 1989; Berggard, Szczepankiewicz, et al. 2002). In chicken kidney cells the expression of Calbindin-D28K is vitamin-D dependent and this is true for other absorptive cells (Clemens et al. 1989), this is not the case however in the CNS (Arnold and Heintz 1997). Calbindin-D28K has been reported to regulate the depolarization-stimulated release of insulin from pancreatic β-cells through the regulation of the cytoplasmic calcium concentration (Sooy et al. 1999). It is well documented in the literature that Calbindin-D28K has neuroprotective properties in the CNS (Yenari et al. 2001; Yuan et al. 2013; Sun et al. 2011), and recently it has

been demonstrated that its depletion in an Alzheimer's disease mouse model accelerates neuronal loss, apoptosis and mitochondrial dysfunction (Kook et al. 2014).

It has been shown that Calbindin-D28K interacts with a variety of proteins of therapeutic interest (Schmidt 2012). Calbindin-D28K binds and increases the catalytic activity of IMPase, the putative target of lithium therapy in bipolar disorder (Berggard, Szczepankiewicz, et al. 2002). IMPase has a key role in the homeostasis of the IP3 signaling cascade by replenishing free *myo*-inositol and inhibition of this enzyme by lithium has given rise to the Inositol depletion hypothesis of lithium's efficacy in the treatment of bipolar disorder (Harwood 2005). More recently IMPase inhibition has been shown to increase autophagy and the clearance of peptides involved in the pathogenesis of both Huntington's and Parkinson's diseases (Sarkar et al. 2005), indicating that the inhibition of the Calbindin-IMPase interaction maybe of therapeutic benefit in these diseases. The Calbindin-IMPase interaction has been modeled *in-silico* and the information used to develop a series of novel peptide inhibitors (Levi et al. 2013). Calbindin-D28K also exhibits anti-apoptotic activity by binding to and inhibiting caspase-3 (Bobay et al. 2012; Bellido et al. 2000). Understanding the structural basis of these interactions would offer possible new therapeutic approaches to tackling these diseases.

Calbindin-D28K belongs to a superfamily of calcium binding proteins that includes calmodulin and troponin C. All of these proteins have a high α-helical content and share EF-hand structures that constitute the calcium binding domains. Calbindin-D28K has a primary structure of 261 amino acids (Mr ~30kDa) and is encoded by the CALB1 gene. In 2006 a NMR structure of the *Rattus norvegicus* Calbindin-D28K

calcium-loaded protein revealed for the first time the tertiary fold of the protein, Calbindin-D28K is mainly α-helical and these make up six EF-hand motifs that are held together in a single globular fold via hydrophobic interactions (Kojetin et al. 2006). EF-hand motifs have a helix-loop-helix topology and are a common structural characteristic in calcium binding proteins. As in most calcium-binding proteins, the calcium ion is coordinated in the loop region between the two helices of the EF-hand, for Calbindin-D28K a calcium ion is coordinated in four out of the six EF-hand motifs. EF hands 1, 3, 4 and 5 bind calcium with high affinity (Akerfeldt et al. 1996; Venters et al. 2003). It has been shown that Calbindin-D28K undergoes structural changes upon calcium binding, indicative of a calcium sensing protein (Berggard, Miron, et al. 2002). However, both the APO and the calcium-loaded protein have exposed hydrophobic residues on the surface indicating that Calbindin-D28K interacts with other proteins in both states (Berggård et al. 2000). The high-resolution crystal structure of human Calbindin-D28K reported here confirms these secondary structural findings but also reveals some significant differences when compared to the NMR structure of rat Calbindin-D28K. The human Calbindin-D28K structure presented here allows for the first direct visualization of calcium ions bound by the protein.

Method

Cloning and expression

The *E.coli* codon-optimized Human CALB1 gene was synthesized and cloned into pET-15b using Nco1 and BamH1 restriction sites (Genscript). A polyhistidine tag followed by a human rhinovirus (HRV) 3C protease cleavage sequence was included

in the synthetic construct directly 5' of the Calbindin-D28K start codon. The recombinant plasmid was then transformed into *E.coli* Rosetta 2 DE3 cells (Novagen) and plated on LB agar containing 50μg/ml ampicillin. A 100 ml preculture was grown in LB broth (50ug/ml ampicillin) overnight at 310K with shaking at 200rpm. 10ml of the preculture was used to inoculate the main 1L cultures which were grown at 310K with 200rpm shaking to an OD_{600} ~ 0.6. The cultures were incubated on ice for 2 hours before Isopropyl β-D-1-thiogalactopyranoside

(IPTG) induction (0.4mM) and incubation overnight at 298K with shaking at 180 rpm.

Purification

Cells were harvested and spun at ~ 9500g for 20mins and the pellet resuspended in sonication buffer (150mM NaCl, 1mM MgCl, 20mM Tris pH 8.0 and protease inhibitor cocktail (cOmplete™, EDTA-free, Roche)). Cell lysis was achieved by sonication for 5 mins with 5s intervals and DNA removed by the addition of non-specific endonuclease (Benzonase® Nuclease, sigma) and incubation on ice for 10mins. The lysate was clarified at ~30,000g for 20mins and the supernatant retained. His-tagged recombinant protein was purified by cobalt affinity chromatography (Talon® metal affinity resin), the clarified lysate supernatant was incubated with 10ml of binding buffer equilibrated resin for 1hour at 277K (20mM tris pH 8.0, 150mM NaCl and 10mM imidazole). The flow-though was removed and the resin was washed sequentially with 7 column volumes of binding buffer. The bound proteins were then eluted with binding buffer containing 250mM imidazole. The his-tag was removed by incubation with rhinovirus (HRV) 3C protease overnight at 277K. The cleaved protein was further purified by size exclusion

chromatography on a Superdex G75 in 5mM tris pH 8.0 1mM $CaCl_2$, yielding ~ 25-30mg of Calbindin-D28K per litre of culture.

Crystallization

The Calbindin-D28K crystals that initially yielded the Ca-SAD phases where replicated from previously reported crystallization conditions (crystal condition 1: ~60mg ml^{-1} protein, 1mM CaCl, 5mM Tris pH 8.0 added to in a ratio of 1:1, 0.5M ammonium acetate, 0.1M Bis-Tris pH 6.5, 24% PEG 3350) (Zhang et al. 2008). The crystal structure reported here was obtained from the JCSG+ crystallographic screen from Molecular Dimensions (crystal condition 2: 0.1M Potassium thiocyanate and 30% w/v PEG 2000 MME) (Newman et al. 2005). Recombinant Calbindin-D28K was concentrated to ~40mg/ml in 1mM $CaCl_2$, 5mM Tris pH 8.0. Crystallization was performed in MRC 2 well crystallization plates (Swissci) with a reservoir volume of 50µl and a drop volume of 0.2µl containing a 1:1 ratio of precipitant mix to protein. The crystallization plates were incubated at 293K and Calbindin-D28K crystals grew within a week.

Data Collection and Processing

X-ray diffraction data was collected from Calbindin-D28K crystals grown under condition 1 at the long-wavelength macromolecular crystallography beamline I23 at the Diamond Light Source (Wagner et al. 2016). The Ca-SAD phasing experiment was performed at a wavelength of 3.02Å, close to the Ca K absorption edge (λ = 3.07 Å) at a temperature of ~50K. In total 8000 images from two 400° sweeps were collected with 0.1s exposure time using the inverse beam method. Data was processed with the DIALS/AIMLESS packages (Evans and Murshudov 2013; Winter et al. 2018). The anomalous substructure of five calcium atoms could be determined

with SHELXD (Sheldrick 2008). While three of the calcium atoms had close to full occupancy, the remaining two calcium atoms had estimated occupancies of around 50% each. After density modification, over 90% of the structure could be built into the resulting experimental electron density map. However, although the structure was solvable it could not be refined owing to ambiguous N-terminal electron density. Therefore, X-ray diffraction data was also collected from a Calbindin-D28K crystal grown under condition 2 at the Diamond Light Source I03 beamline. Data was collected at 100K with 30% glycerol as cryoprotectant. 1040 images were collected with an omega oscillation of 0.10° and an exposure time of 0.1s per image at a wavelength of 0.976A. Diffraction intensity data was indexed, integrated and scaled using the autoPROC toolbox (Table 1) (Vonrhein et al. 2011). Molecular replacement with the Ca-SAD model yielded a phasing solution using PHASER (McCoy et al. 2007). After cycles of model building and refinement using BUCCANEER and the CCP4 suite of programs (Cowtan 2012; Murshudov et al. 2011; Emsley et al. 2010), the final model building was completed in COOT and refined with BUSTER version 2.10.2.

SEC-SAXS

SEC-SAXS was performed at the Diamond Light Source B21 beamline. Calbindin-D28K samples were dialyzed for 12h at 277K against 1L of sample dialysis buffer (20mM Tris pH7.8, 150mM NaCl, ±3mM $CaCl_2$) prior to experiment. A 45µl sample of 11.5mg/ml Calcium loaded Calbindin-D28K or 12.2mg/ml of un-loaded Calbindin-D28k was injected onto a Shodex KW-402 size exclusion column pre-equilibrated in dialysis buffer and run at a flow rate of 0.16 ml/min. Intensity (I(q)) data was collected as the eluate passed through the X-ray beam and plotted against $q = 4\pi\sin\theta/\lambda$. The system operated with an exposure time of 3s at 12.4

keV (1Å) using a Pilatus 2M detector located at a distance of 4m. Data was analysed using the ATSAS and Scatter suite (Franke et al. 2017; Franke and Svergun 2009; Kozin and Svergun 2001). The FoXS web server was used to compute the theoretical scattering profile from NMR and crystal structures of Calbindin-D28K for comparison with the experimental data (Schneidman-Duhovny et al. 2013, 2016). No changes were made to the Calbindin-D28K protein models used. However, the solvent molecules were removed from the structures. They were used as deposited. 6FIE has extra three residues at the N-terminal due to the cleavage of the his-tag at the 3C protease cleavage sequence. The SAXS data and analysis is deposited in the Small Angle Scattering Biological Data Bank (Valentini et al. 2015) (accession codes: SASDDL6 for calcium loaded Calbindin-D28K and SASDDM6 for un-loaded).

Results

Calbindin-D28K Crystal structure

Refinement statistics for the Calbindin-D28K crystal structure (PDB code: 6FIE) (crystal condition 2) determined to a resolution of 1.51Å are presented in table 1.

Table 1 Crystallographic statistics and merging statistics produced by autoPROC for PDB entry 6fie (crystal condition 2) and AIMLESS for the calcium SAD data set (crystallization condition 1). Values in parentheses are for the highest shell.

Data set	PDB entry 6fie	Calcium SAD
Beamline	I03, DLS	I23, DLS
Unit-cell parameters		
a (Å)	84.62	88.09
b (Å)	104.22	100.17
c (Å)	29.61	30.69
α (°)	90	90
β (°)	90	90
γ (°)	90	90
Space group	$P2_12_12$	$P2_12_12$
Wavelength (Å)	0.976	3.02
Resolution range (Å)	29.61–1.51 (1.54–1.51)	50.9–1.98 (2.03–1.98)
No. of observations	151983 (7621)	119199 (3772)
No. of unique observations	41505 (2048)	15168 (848)
Completeness (%)	99.1 (99.8)	99.7 (60.2)
Multiplicity	3.7 (3.7)	7.9 (4.4)
Anomalous completeness (%)	91.6 (93.2)	73.8 (57.0)
Anomalous multiplicity	2.0 (2.0)	4.1 (2.3)
R_{merge} (%)	0.041 (0.852)	0.090 (0.970)
$R_{p.i.m.}(I)$ (%)	0.024 (0.506)	0.030 (0.330)
$CC_{1/2}$	0.998 (0.365)	0.997 (0.743)
$\langle I/\sigma(I)\rangle$	14.4 (1.4)	13.8 (1.8)
Refinement	*BUSTER* v.2.10.2	
Resolution range (Å)	21.90–1.51	
R_{cryst}	0.202	
R_{free}	0.236	
No. of protein atoms	4127	
No. of ligand atoms	4	
No. of solvent atoms	180	
Mean B factor (Å^2)	37	
R.m.s.d., bond lengths (Å)	0.01	
R.m.s.d., bond angles (°)	1.02	

The disorder in the first Ca2+ binding site is reflected in the weaker side-chain electron density in the N-terminal EF-hands accounting for the relatively high RMSZ score for this structure compared to other x-ray structures determined at similar resolution. The Ca-SAD structure determined from crystal condition 1 allowed the direct visualization of the calcium atoms (Supplementary Figure 1). This revealed

for the first time that there are two conformations with the calcium ions are located 4.7Å apart in the N-terminal EF-hand 1 (Figure 10). Only one of these calcium-binding conformations was visible in the electron density for both crystal conditions. Due to the increased noise in this region the calcium coordinating waters were not modeled around the disordered EF-hand 1. Zhang et al (Condition 1) determined a space group to be C2 for this condition. However, this repeated crystal had a space group of $P2_12_12$.

Calcium Binding

At 1mM Ca^{2+} concentration Calbindin-D28K binds 4 calcium ions at each of the EF1,

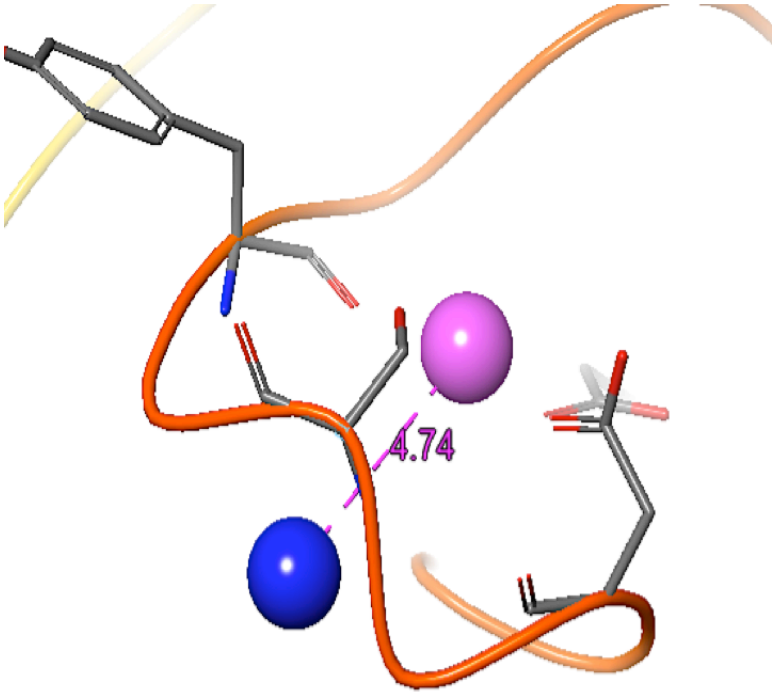

Figure 10 The two Ca atoms in EF1 from the substructure coordinates. The distance between the peaks is shown. There was an estimated occupancy of 50% for each calcium. The Ca atom in pink is that refined in PDB entry 6fie.

EF3, EF4 and EF5 motifs with pentagonal bipyramidal coordination geometry (Figure 11). The coordinating residues starting from the N-terminal binding residues of the calcium binding loops are aligned in Table 2. Five amino acid

residues, a backbone interaction and a water molecule complete the coordination of calcium in the EF1, EF4 and EF5 motifs. In contrast, the EF3 motif utilizes an interaction at Glu119 (position 9) instead of a water molecule to complete the coordination of calcium. At position 12 all four calcium binding loops possess a conserved Glu side-chain that acts as a bidentate coordinating residue. There are also non-calcium-binding conserved residues within the EF loops; there is a conserved glycine at position 6 and either a leucine or isoleucine at position 8. There were no detectable differences in the SAXS scattering curves for calcium loaded Calbindin-D28K and the calcium un-loaded protein (Supplementary Figure 2), indicating that the protein retains the same "kidney bean" shape post calcium-binding.

Table 2 The aligned calcium-binding loops from calbindin-D28K starting from the first calcium-binding residue. Calcium-binding residues are highlighted in bold. A backbone carbonyl group binds the calcium at position 7.

	Amino-acid position starting from the first calcium-binding residue												
EF-hand	1	2	3	4	5	6	7	8	9	10	11	12	Water
EF1	**Asp**	Ala	**Asp**	Gly	**Ser**	Gly	**Tyr**	Leu	Glu	Gly	Lys	**Glu**	**Y**
EF3	**Asp**	Thr	**Asp**	His	**Ser**	Gly	**Phe**	Ile	**Glu**	Thr	Glu	**Glu**	N
EF4	**Asp**	Ser	**Asn**	Asn	**Asp**	Gly	**Lys**	Leu	Glu	Leu	Thr	**Glu**	**Y**
EF5	**Asp**	Gln	**Asp**	Gly	**Asn**	Gly	**Tyr**	Ile	Asp	Glu	Asn	**Glu**	**Y**

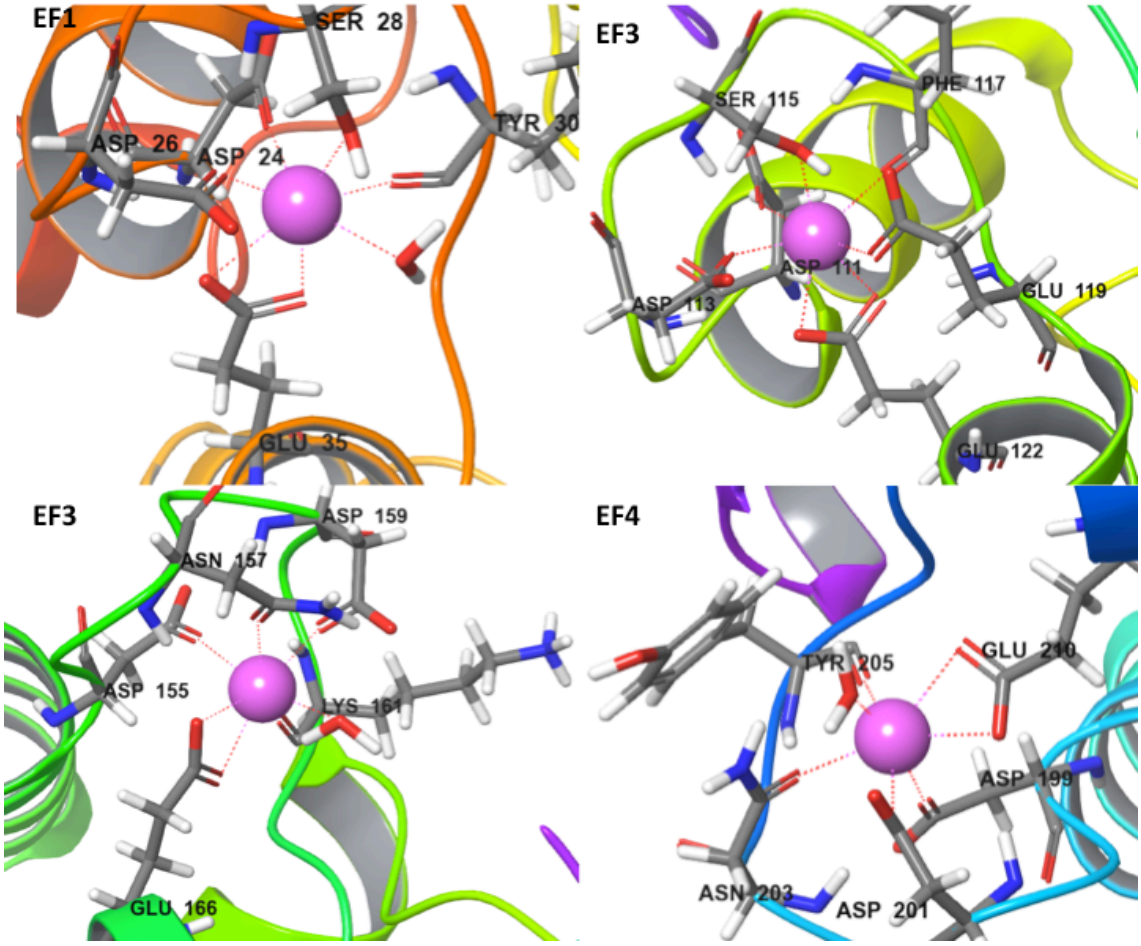

Figure 6 The four EF-hand calcium-binding loops of calbindin-D28K. Calcium-binding amino acids, water molecules and calcium ions are shown, while the rest of the structure is illustrated by a cartoon representation. Each calcium ion is coordinated with a pentagonal bipyramidal coordination geometry, the bonds for which are represented by a dotted line. The EF1 calcium is coordinated by Asp24, Asp26, Ser28, Tyr30, Glu35 and water, the EF3 calcium by Asp111, Asp113, Ser115, Phe117, Glu119 and Glu122, the EF4 calcium by Asp155, Asn157, Asp159, Lys161, Glu166 and water, and the EF5 calcium by Asp199, Asp201, Asn203, Tyr205, Glu210 and water.

Structural comparison

Calculated scattering curves for 6FIE and all ten models of 2G9B were compared with the X-ray scattering curve of Calbindin-D28K in solution. Interestingly, the crystal structure curve fitted the SAXS curve better than the NMR models with a lower Chi value of 1.19 versus a range of 1.98-2.43 for the NMR models (figure 12A).

FatCat pairwise alignment calculated an RMSD of 3.2Å between the crystal structure and the old NMR structure (figure 12B) (Ye and Godzik 2003). The distance between pairs of Cα atoms in EF1 and EF6 of the Calbindin models indicates that the NMR model is more compact when compared to the crystal structure. For instance, the distance between Lys 34 Cα and Lys 224 Cα is 35.59Å and 27.79Å for 6FIE and 2G9B (model 2) respectively (figure 12C).

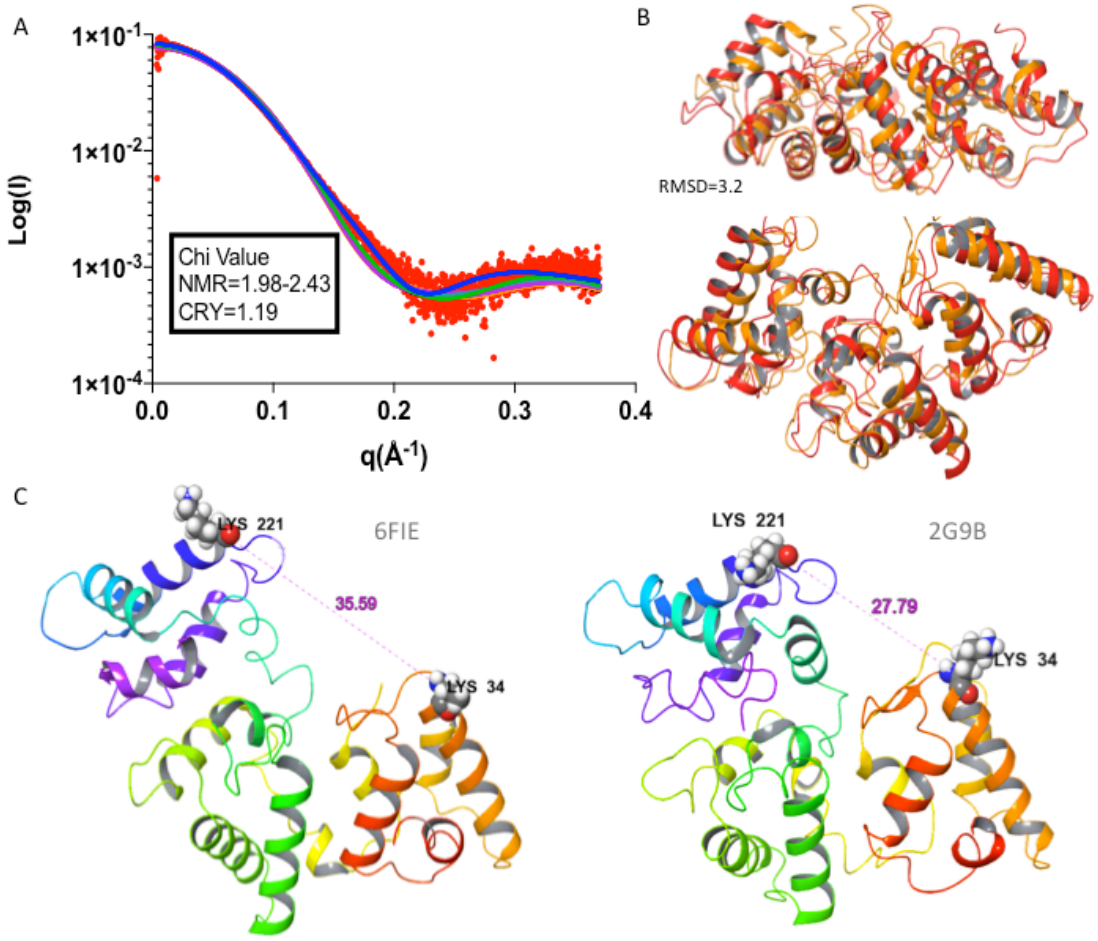

Figure 7 (a) Log10 SAXS intensity versus scattering vector q. The plotted range represents the positive-only data within the specified q-range (red). The calculated FoXS scattering curve of PDB entry 6fie (blue) and calculated FoXS scattering curves for the first five models of PDB entry 2g9b (green, turquoise, pink, orange and black). (b) FATCAT pairwise alignment and superimposition (PDB entry 6fie, red; PDB entry 2g9b, orange); there is a 90 rotation between the two images. (c) Measurement of the distance between the C atoms of Lys34 and Lys221; the distance is shown in A°

Discussion

Calbindin-D28K is a widely expressed calcium binding protein possessing a multiplicity of physiological functions. The expression is particularly high in the central nervous system, and absorptive epithelial tissues where it buffers and facilitates the movement of calcium (Clemens et al. 1989; Schmidt 2012; Wasserman, Corradino, and Taylor 1969). Recent work has hinted at a possible protective role of Calbindin-D28K in inhibiting apoptosis and necrosis and slowing the pathogenesis of neurodegenerative diseases such as Alzheimer's disease (Yuan et al. 2013; Yenari et al. 2001; Sun et al. 2011; Kook et al. 2014; Bellido et al. 2000). Not only does Calbindin-D28K act as a buffer for calcium ions but it has also been shown to interact with multiple protein targets to modulate their function or catalytic activity (Shamir et al. 2005; Berggard, Szczepankiewicz, et al. 2002; Lutz et al. 2003). Here we report the first X-ray structure of Calbindin-D28K allowing for the first time a detailed high-resolution analysis of its calcium binding properties. The human Calbindin-D28K X-ray structure also displays significant structural differences when compared with the previously published NMR structure of rat Calbindin-D28K molecule. The Human and Rat isoforms have a sequence intensity of 98%. GLN44, ASP225, THR232 and CYS257 in human Calbindin-D28K are changed to LEU44, GLU225, SER232 and SER257 in the Rat isoform. These residues are solvent exposed and seem not to explain the structural difference seen between the two structures. Human Calbindin-D28K consists of six EF-hand motifs arranged in three pairs that maintain a globular structure stabilized by hydrophobic interactions (Kojetin et al. 2006). Four EF-hands bind calcium at a concentration ~1mM in the crystallization buffer, a concentration significantly higher than the usually nanomolar physiological (cytosolic) concentration. This would imply that

the structure presented here represents a calcium-saturated form of the protein with respect to physiological conditions (Berridge 1997). There are differences in the calcium binding residues between the individual calcium binding loops, despite these differences in primary structure macroscopic studies have indicated that Calbindin-D28K binds calcium in a non-sequential, parallel manner (Berggard, Miron, et al. 2002). However other spectroscopic studies have indicated the opposite, that calcium binding is not simultaneous (Venters et al. 2003), the differences in the calcium binding mechanisms observed in the crystal structure support this. EF3 is the only calcium-binding loop not to use water in the pentagonal bipyramidal coordination of the calcium ion; glutamate 119 at position 9 fulfills this role instead. Interestingly both EF1 and EF4 also have glutamate at position 9 of the loop but these are not involved in calcium coordination. Compared to the existing NMR model of Calbindin-D28K the X-ray structure is less compact with the intramolecular distances increased by several angstroms across the molecule. This less condensed model was validated by SAXS as the scattering curve of the protein in solution was better predicted by the crystal structure. This is surprising as it is often assumed that crystal structures would to be more compact than solution NMR structures, owing to crystal packing restraints. The high overall RMSD score of 3.2Å also reflects significant structural differences between the X-ray structure and the NMR model. There are substantial differences in side chain conformations both across the molecule and within the calcium binding loops. Calcium binding at the N-terminal EF-hand (EF1) motif (where the electron density is more disordered) appears to be more flexible that at the other calcium binding loops. The Ca-SAD experiment indicated that there are two distinct calcium positions in the N-terminal EF-hand with the calcium ions bound 4.7Å apart in Zhang's (2008) crystal form

(crystal condition 1). Although the Ca-SAD data did yield a phasing solution, the dual calcium–binding geometry precluded full structure refinement. Consequently, new crystal growth conditions potentially favoring a single conformation were explored, yielding crystal condition 2 in which residues are visible at the N-terminal. Nevertheless, the N-terminal flexibility still manifests as structural disorder with higher temperature factors values in this region. It was not possible to build the two conformations into the electron density and only one calcium-binding site is visible in the final structure. The flexibility of this region could be important in facilitating interactions with other proteins. Site-directed mutagenesis studies have previously revealed that inositol monophosphatase (IMPase) binds to the aspartate residues 24 & 26 in this flexible calcium-binding loop (EF1) of Calbindin-D28K (Levi et al. 2013). Here we demonstrate that aspartate 24 & 26 are involved in calcium binding, It has been demonstrated previously that the potentiation of IMPase catalytic activity by Calbindin-D28K occurs irrespective calcium being present (Berggard, Szczepankiewicz, et al. 2002). The peptide binding fragment of Ran-binding protein M has also been shown to induce large chemical shifts in the NMR spectrum of Calbindin-D28K in the flexible N-terminal region (Lutz et al. 2003). Docking simulations predict binding of IMPase at that the grooved structure between the N and C terminal EF-hand bundles of Calbindin-D28K where the X-ray structure differs the most from the NMR model.

The SAXS scattering curves of calcium-loaded and un-loaded Calbindin-D28K are essentially identical indicating similar globular structures for both states and no increase in flexibility. Because SAXS is a low-resolution technique that can only be

used to monitor large conformation changes, these findings do not preclude significant changes at the intramolecular scale.

Conclusion

We present here the first X-ray structure of Calbindin-D28K at near-atomic resolution. Elucidation of the calcium coordination geometry in the EF-hand loops is consistent with previous reports that the protein has four calcium binding sites. Ca-SAD at long wavelength demonstrated that the N-terminal EF-hands are particularly flexible and possesses two calcium-binding conformations. Residues that have previously been shown to be involved in protein-protein interactions are demonstrated to also coordinate calcium, potentially bestowing a calcium sensor function on Calbindin-D28K. Calbindin-D28K maintains the same globular shape both in the calcium-loaded and un-loaded form. There is also no significant increase in the flexibility of the Calbindin-D28K protein in the un-loaded form. Intriguingly 6FIE is a better model of Calbindin-D28K in solution, as the X-ray scattering curve produced by the protein is better predicted by the crystal structure than the previously published NMR model (2G9B). We surmise that the high-resolution X-ray structure of Calbindin-D28K presented here be used as the model of choice for future experimentation and *in silico* modeling.

Chapter 3
Paper2

Exploration of the Calbindin-IMPase Interaction using Fusion Proteins

Exploration of the Calbindin-IMPase Interaction using Fusion Proteins

James W. Noble and John R. Atack

Abstract

Calbindin-D28k is a calcium buffering protein that is highly expressed in the mammalian CNS. It has been reported that calbindin-D28k binds to and increases the activity of IMPase (ref). IMPase is an enzyme that is involved in the homeostasis of the IP3 signalling cascade by catalysing the final dephosphorylation of inositol. IMPase has been implicated in the therapeutic mechanism of lithium treatment of bipolar disorder, which forms the basis of the inositol depletion hypothesis (ref). Previously reported activity assays have shown that calbindin-D28k can increase IMPase activity by up to 250 hundred-fold in conditions that are unfavourable for IMPase activity (ref). *In silico* modelling and mutagenesis studies were later performed to uncover further data regarding this interaction (ref).

Here we aim to explore the shape and properties of the calbindin-IMPase complex. We aim to confirm that calbindin-D28k increases IMPase activity at a one to one concentration ratio. We have created several fusion proteins of calbindin-D28k and IMPase, connected by a flexible amino acid linker that fuses the termini of the proteins together. A variety of different linker lengths and orientations were tested. The resulting fusion proteins have demonstrated relative activities of between 200% to 400% when compared to IMPase alone. The physical properties (flexibility, shape and size) and low-resolution models of these fusion proteins were then compared to the previously published *in silico* models using SAXS. Differences in the shape of the complex were observed between the low-resolution fusion protein

models and the *in silico* model. The fusion proteins form a V-shaped, longer and less compact complex, in contrast to the linear in silico model. The fusion protein presented here is a useful tool to further explore this protein-protein interaction.

Introduction

The calbindin-IMPase interaction was initially identified by affinity chromatography, using immobilized calbindin-D28k and phage-displayed peptides to explore the calcium sensing function of calbindin-D28k (Berggard *et al.,* 2002). This interaction is of particular interest due to of the therapeutic significance of IMPase in the treatment of bipolar disorder. In the 1970's, a study demonstrated that lithium treatment reduces inositol levels in the brains of mammals by inhibition of IMPase (ref). This formed the basis of the inositol depletion hypothesis of lithium's efficacy in the treatment of bipolar disorder (Berridge, Downes, and Hanley, 1982; Allison *et al.*, 1976; Hallcher and Sherman, 1980). More recently it has been shown that inhibition of IMPase leads to an increase in autophagy *in vitro* and it has been proposed that this could be used therapeutically in the treatment of neurodegenerative disorders in which protein aggregation plays a role in disease pathogenesis (Criollo *et al.,* 2007; Sarkar *et al.,* 2005). IMPase is a homodimeric phosphodiesterase enzyme which is involved in the phosphatidylinositol signalling cascade. This cascade is initiated by the activation of GPCRs causing the production of IP3 and DAG via the activation of PLC. IP3 induces the release of calcium from intracellular stores and DAG activates PKC. IMPase performs the final dephosphorylation of inositol, recycling this back to free inositol (Majerus 1992; Streb *et al.*, 1983; Furuichi *et al.,* 1989; Newton, 1995). IMPase is extremely

thermally stable displaying a Tm of 79°C and each monomer possesses an αβαβα topology (Kraft *et al.*, 2018; Bone, Springer, and Atack, 1992).

Calbindin-D28k was initially identified as a calcium buffering protein in the absorptive epithelia of *gallus gallus domesticus* (Wasserman, Corradino, and Taylor , 1969). Calbindin-D28k is highly expressed in the human central nervous system (CNS), and binds to several other proteins indicating a role as a calcium sensor. Binding partner proteins include: Ran-binding-protein-M, caspase-3, ATPases and cyclic nucleotide phosphodiesterases (Bellido *et al.,* 2000; Lutz *et al.*, 2003; Morgan *et al.*, 1986; Reisner, Christakos, and Vanaman, 1992). Calbindin-D28k is composed of six EF-hand domains that exhibit a typical helix-loop-helix topology. Four out of the six EF- hands that constitute calbindin-D28k coordinate a calcium ion in the central loop (EF1, EF3, EF4 and EF5). The six domains form one globular structure with significant flexibility in the N-terminal region (Kojetin *et al.,* 2006; Noble *et al.,* 2018).

The calbindin-IMPase interaction has been shown to increase the activity of IMPase by up to 250 fold (ref). Calbindin-D28k increases the activity of IMPase both when bound to calcium and in the apo form with a K_d of 0.9 μM (Berggard, Szczepankiewicz, *et al.,* 2002). The calbindin-IMPase interaction has been demonstrated *in situ* in the spines and dendrites of cerebellar Purkinje neurons (Schmidt, Schwaller, and Eilers, 2005). Mutagenesis studies, based on an *in silico* model of the protein complex, demonstrated that Asp24 and Asp26 of calbindin-D28k are critical for the activation of IMPase in biochemical assays. This data was then utilised to design peptide inhibitors of the interaction between IMPase and calbindin-D28k (Levi *et al.,* 2013). The interest in this interaction is of current interest because of the therapeutic potential of IMPase. An understanding of how

calbindin-D28k facilitates the increase in IMPase activity could reveal novel methods for inhibiting IMPase. This could be either by inhibition of the protein-protein interaction directly or by discovering more about the structural integrity of IMPase that could then be exploited pharmacologically.

Here we use Gly-rich flexible amino acid linkers to connect the termini of calbindin-D28k and IMPase. The aim is to produce a stable protein complex that can be used for further structural and biochemical analysis. The use of flexible amino acid linkers has been used previously to study the interactions of proteins. Linking proteins together can help stabilise protein-protein interactions by increasing the local concentration of the binding partner. This technique is often employed to study proteins that have relatively weak affinities or transient interaction. Hence, stabilising the complex allows the interaction to be studied more easily (Reddy Chichili, Kumar, and Sivaraman, 2013). The creation of a fusion protein with increased catalytic activity will confirm existing evidence for the protein interaction between calbindin-D28k and IMPase. Here we also employ SAXS to gain insights into the shape and flexibility of the protein complex.

Methods

Fusion Constructs and Protein Expression

Two sets of fusion proteins were developed. The FP group where calbindin-D28k is fused to the C terminal of IMPase and the Cal-FP group where IMPase is fused to the C terminal calbindin-D28k (Figure 13). The Gly-rich linkers were constituted of repeats of an 11 amino acid polypeptide linker (GGGSASGGGSG). This linker was designed based on previously reported studies (Reddy Chichili, Kumar, and Sivaraman, 2013). Protein expression was performed in a pET-15b vector at the

Nco1 and BamH1 sites in *E. coli* Rosetta 2 (DE3) cells (Novagen). A poly-histidine tag followed by a rhinovirus (HRV) 3C protease cleavage sequence was incorporated into the coding sequence of the N-terminus of fusion proteins. The synthetic constructs were produced by GenScript. Transformed cells were plated on LB agar containing 50 mg ml^{-1} ampicillin for selection. Colonies were harvested and grown in B broth (50 ug mL^{-1} ampicillin) to an OD_{600} of 0.6 in 1 L cultures at 310 K, with shaking at 200 rpm. The cultures were then incubated on ice for 2 h before induction with 0.4 mM IPTG and incubation overnight at 293 K with shaking at 180 rpm.

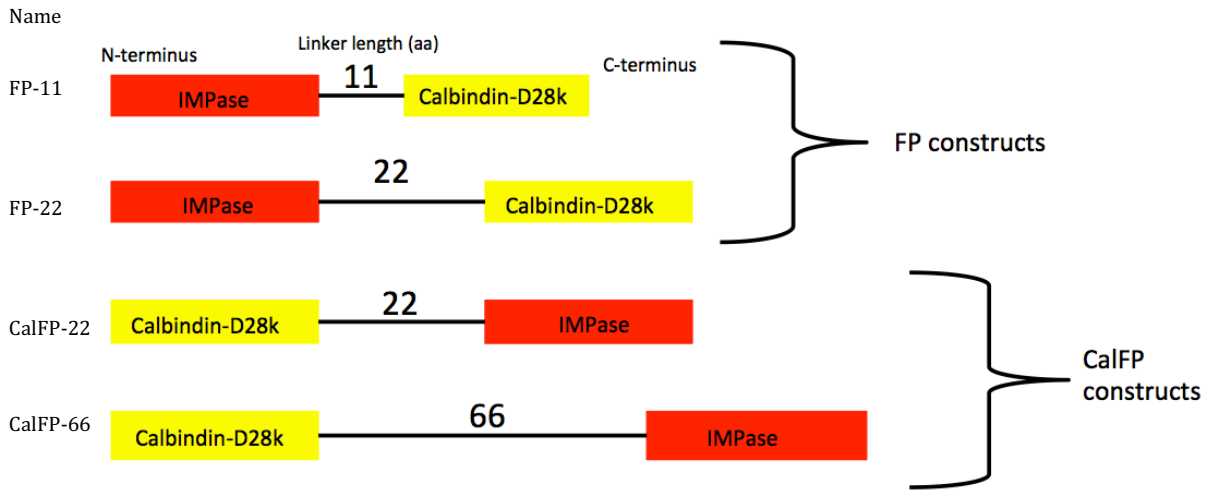

Figure 13. Fusion protein constructs. Two different fusion directionalities were tested. Nomenclature used was FP (fusion protein) when IMPase was present at the N-terminus and CalFP when Calbindin-D28k was present at the N-terminus. Three different linker lengths were employed. The names of each construct are stated.

Purification

The cells were pelleted by centrifugation at 9500 g for 20min. The cell pellets were resuspended in a buffer of 150 mM NaCl, 1 mM MgCl, 20 mM Tris pH 7.8 and protease inhibitor cocktail (cOmplete™, EDTA-free, Roche). The sample was sonicated for 5 min with 5-second intervals (5 sec on, 5 sec off) on ice. To ensure removal of DNA, 1 µL of non-specific endonuclease (Benzonase® Nuclease, sigma)

was added and the sample incubated on ice for a further 10 min. The lysate was clarified at 30,00 g for 20 min. The supernatant was mixed with cobalt affinity resin (Talon metal-affinity resin) and incubated for 1 h at 277 K in buffer. The resin was then pelleted by centrifugation at 9500 g for 20 min. Pellets were resuspended in a buffer of 150 mM NaCl, 10 mM imidazole and 20 mM Tris pH 7.8. The flow-through was discarded and the resin was washed 7 times with buffer. The fusion proteins were eluted using 5 washes of 250 mM imidazole. HRV C3 protease was added to cleave the His-Tag at a protease-to-target protein ratio of 1:100 (w/w) and incubated overnight at 277 K. The cleaved protein was purified by size exclusion chromatography on a Superdex G200 in 150 mM NaCl and 20 mM Tris pH 7.8. Typically, > 8 mg of protein was obtained from each 1 L of culture.

Purification of calbindin-D28k was performed as Noble *et al.,* 2018 and IMPase purification was performed as Kraft *et al.,* 2018.

SDS-page

1 µL of 1 mg/ml protein was mixed with 6 µL of water and 2.5 µL of NuPAGE™ LDS Sample Buffer. The samples were placed in a dry bath at 95 °C for 5 min and then loaded onto a NuPAGE Novex 4-12% bis-tris gel. The gel was run at 180 V for 40 min in NuPAGE™ MES SDS Running Buffer. A Mark12™ Unstained Standard was used as the standard protein ladder. (Thermo Fisher, Ladder: LC5677, Gel: NP0322BOX, Sample buffer: NP0007, running buffer: NP0002). Coomassie blue was used for gel staining (InstantBlue^{tm}, Expedeon).

Activity Assay

A colorimetric phosphate quantification assay was used as an endpoint activity assay. 15 nM of IMPase or fusion protein and 500 nM of calbindin-D28k were used as the assay protein concentrations in a final volume of 12 µL. 3 µL of substrate was added to produce a final concentration of 0.125 mM Inositol 1-phosphate in a final reaction volume of 15 µL. Reactions were incubated at 37 °C for 35 min, with 80 % humidity to prevent evaporation. Assay buffer was composed of 20 mM Tris (pH7.8), 150 mM NaCl and 3 mM MgCl. The addition of 30 µL of BIOMOL® green (Enzo) reagent was used to stop the reaction. Plates were incubated at room temperature for 30 min to allow the colour to fully develop. The assay was performed in Clear 384 well BRANDplates® pureGrade™ F-bottom plates (BRAND). Absorbance was measured at λ= 630 nm using a PHERAstar FS plate reader from BMG Labtech.

SAXS

SEC-SAXS was performed at the B21 beamline (Diamond Light Source UK). Fusion proteins were dialyzed overnight using Pur-A-Lyzer™ mini dialysis kit (Sigma-Aldrich PURN60030-1KT) in a buffer consisting of 20 mM Tris (pH7.8), 150 mM NaCl and 3 mM MgCl, at 277K. Using an HPLC system, 45 µL of the protein samples were loaded onto a Shodex KW-403 column at the concentrations of 12, 10, 10 and 15.1 mg/ml for FP, CAL-FP-66, CAL-FP-22 and FP-22 respectively. X-ray intensity data was collected as the eluent moved from the column to the beam at a flow rate of 0.16 ml/min. The intensity was plotted against its angular dependants q ($q=4\pi\sin\theta/\lambda$). The system operated with an exposure time of 3 s at 12.4 keV (1Å) using a PILATUS 2M detector located at a distance of 4 m (Eiger M4 detector was

used for FP-22). Data were analysed using the SCÅTTER and ATSAS program suites (Franke *et al.,* 2017; Franke and Svergun, 2009; Kozin and Svergun, 2001). The FoXS web server was employed to compute the theoretical scattering profile using a computational docking model of the calbindin-IMPase interaction (Levi *et al.,* 2013) for comparison with the experimental data (Schneidman-Duhovny *et al.,* 2013, 2016). The SAXS data, analysis and models have been deposited in the Small Angle Scattering Biological Data Bank (Valentini *et al.,* 2015); accession codes: TBC).

Results

Production of Fusion Proteins and assessment of catalytic activity

All 4 of the fusion proteins as well as calbindin-D28k and IMPase were successfully purified to a high level of purity. FP-11 demonstrated increased relative activity of 200 %, when compared to WT IMPase. FP-22, Cal-FP-22 and Cal-FP-66 demonstrated increased relative activity of approximately 400 % when compared to WT IMPase. IMPase and calbindin-D28k together demonstrated a relative activity of 600 %, compared to WT IMPase alone (Figure 14).

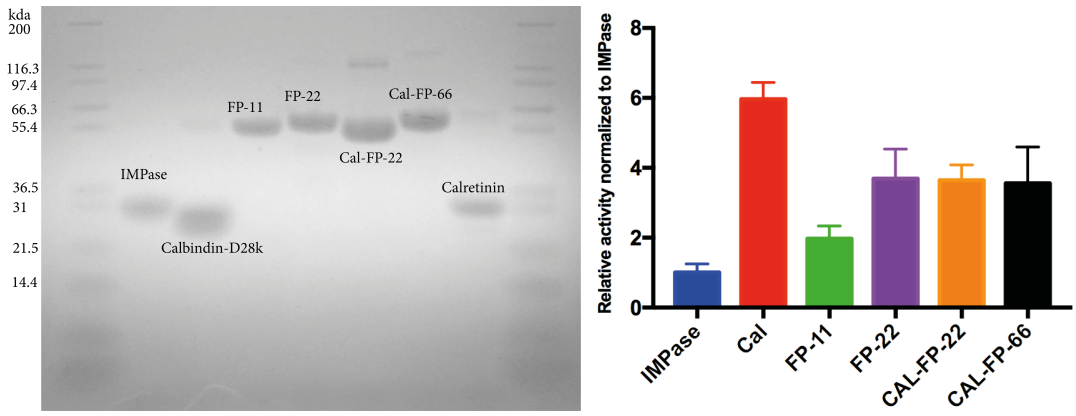

Figure 8. SDS PAGE gel of proteins after size exclusion chromatography and bar graph of the results from the activity assay with the standard deviation plotted. Cal sample contains both IMPase and Calbindin-D28k. You need the % sign on the axis for graph on the right. At the moment the graph and the text above don't match up well

Structural Analysis of Fusion Proteins (SAXS)

The Dmax of the proteins increases with increasing linker length, with values of 162, 176, 175 and 218Å obtained for FP-11, FP-22, Cal-FP-22 and Cal-FP-66 respectively. The radius of gyration (Rg) also increased with linker length. The shortest, FP-11, displayed a Rg of 46Å and the longest, Cal-FP-66, displayed a Rg of 57Å. The Porod slope for all four fusion proteins was q^4 indicating that the proteins were not diffuse and unfolded but possess a more globular structure. The Kratky plot, normalized to Rg, demonstrates that as linker length increases the protein becomes more flexible. The multiple peaks indicate a multi-domain characteristic of the fusion proteins. At high q the graph approaches the baseline indicating a folded but partially flexible structure and this flexibility increases slightly with increasing linker length (Figure 15B). The Distance distribution function shows multiple peaks indicating the multi-

domain characteristic of the fusion proteins and demonstrates the increase in Dmax where the distribution meets the X-axis (figure 15C).

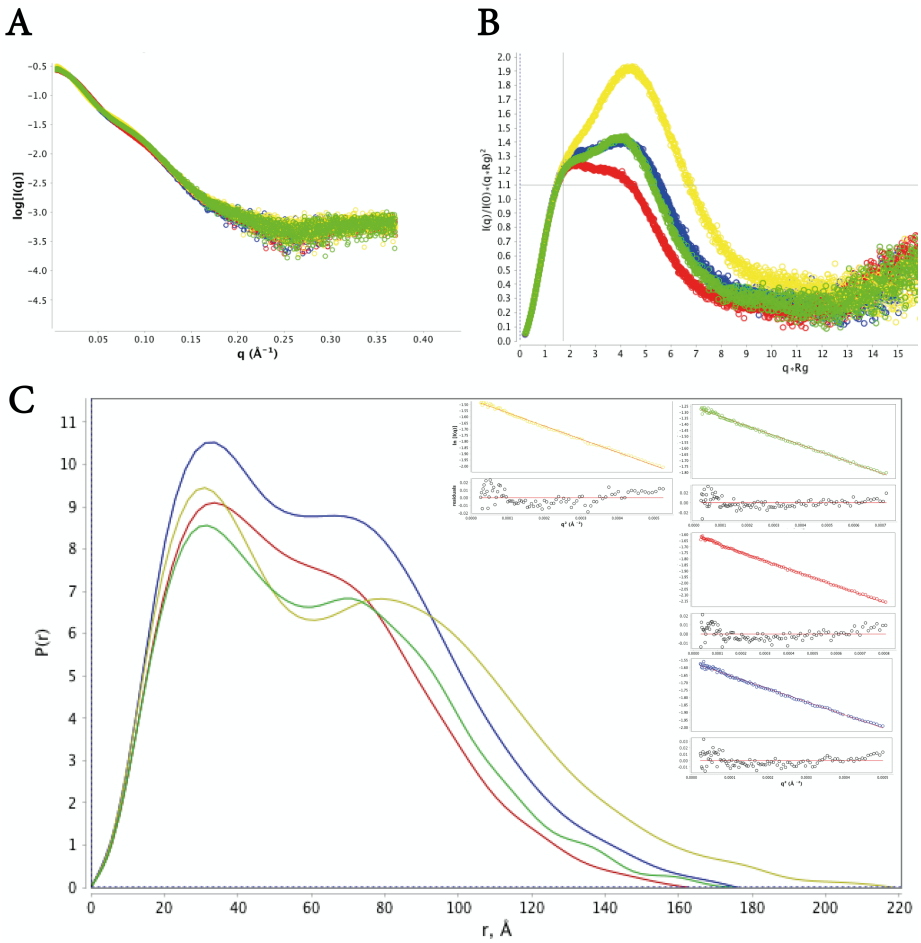

Figure 9. A) Log10 SAXS intensity versus scattering vector, *q*. Plotted range represents the positive only data within the specified *q*-range. B) Dimensionless Kratky plot. Crosshair marks the Guinier-Kratky point (1.7, 1.1). C) Pair-distance, P(r), distribution function. Maximum dimension, *dmax*, is the largest non-negative value that supports a smooth distribution function. The Guinier fitting for all data sets are also shown. In all plots Red = FP-11, Blue = FP-22, Green = Cal-FP-22 Yellow = Cal-FP-66

Ab initio envelope construction from SAXS data reveals a V-shaped structure of the fusion proteins, compared to the in-silico docking model that displays a more linear confirmation. The experimental intensities deviate significantly from the calculated model intensities. This deviation is significant at both high q to low q regions of the experimental intensities, reflecting differences in the shape and size of the fusion proteins (Figure 16).

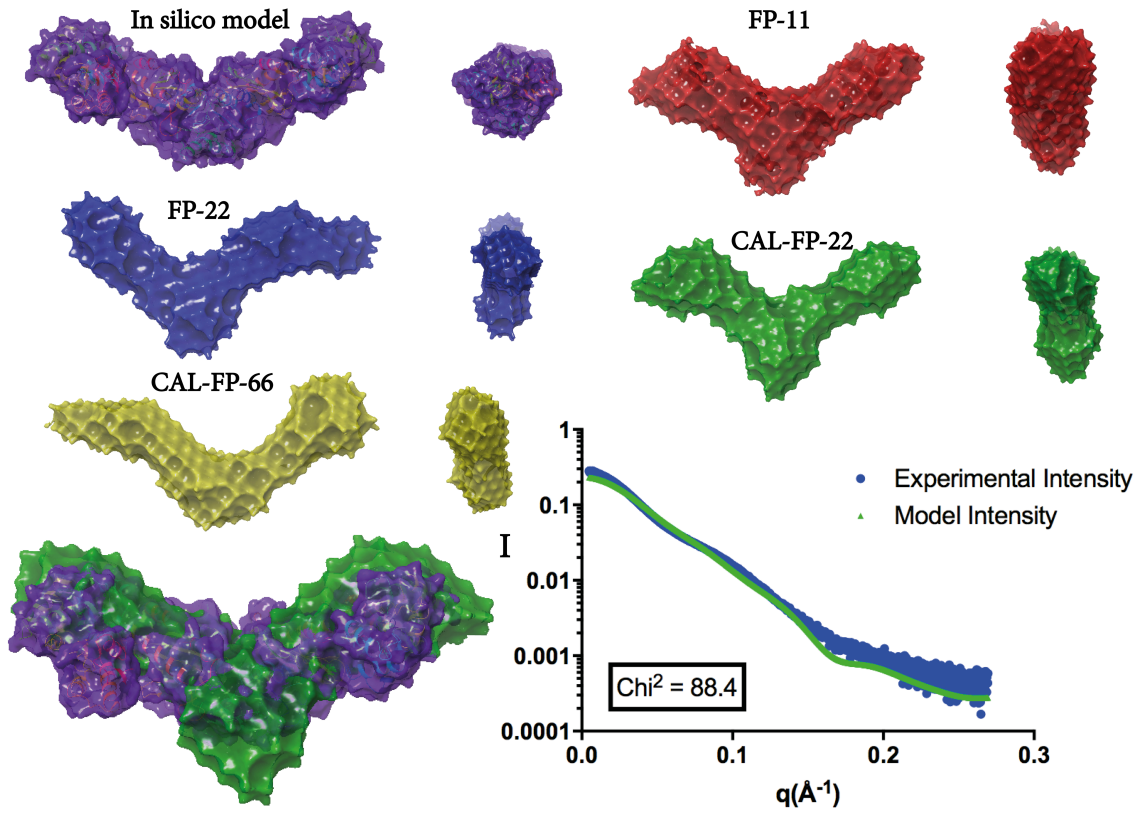

Figure 10. *Ab initio* envelope construction from the SAXS data of individual fusion proteins. Bottom right) A superimposition of the *in-silico* model and Cal-FP-22 fusion protein envelope. Bottom left) Log10 SAXS intensity versus scattering vector q (Blue), The calculated foXS scattering curve of the *in-silico* model (Green).

Discussion

The use of flexible linkers to stabilise protein-protein interactions has long been used to gain insights about the structure and function of protein complexes (Reddy Chichili, Kumar, and Sivaraman, 2013). This method is used to stabilize transient, lower affinity protein interactions, for example, TCR-peptide-MHC molecule complexes (Hennecke and Wiley, 2002; Yin *et al.,* 2011; Reddy Chichili, Kumar, and Sivaraman, 2013). Here we used this method to study the interaction between the calcium binding protein calbindin-D28k and the enzyme IMPase, a putative therapeutic target of lithium in bipolar disorder. This interaction has a relatively low affinity (0.9 μM) (Berggard, Szczepankiewicz, *et al.,* 2002) when compared to other

protein-protein interactions that often exhibit affinities in the low nanomolar and picomolar range with large protein interfaces. We reasoned that the production of fusion proteins of IMPase and calbindin-D28k, exploiting the use of linkers, would result in a more stable complex and allow for easier study of the interactions between these proteins.

IMPase has remained of significant therapeutic interest since the development of the inositol depletion hypothesis, and more recently in the induction of autophagy (Allison and Stewart, 1971; Harwood, 2005; Sarkar *et al.,* 2005). IMPase is an extremely stable protein and is able to withstand high temperatures in excess of 80°C (Kraft *et al.*, 2018). Despite the interest in IMPase as a therapeutic target, the discovery of specific inhibitors that are effective *in vivo* has remained elusive. The finding that calbindin-D28k can allosterically increase the catalytic activity (Vmax) of IMPase indicates that the enzyme could have significant structural plasticity. Understanding this interaction and how it results in an increase in catalytic activity of IMPase may reveal novel therapeutic approaches to IMPase inhibition. Unlike a traditional calcium sensor calbindin-D28k increases IMPase activity both in the calcium loaded and un-loaded states. Interestingly, the residues of Calbindin-D28k involved in the protein interaction are also involved in calcium binding (Berggard, Szczepankiewicz, *et al.,* 2002). The fusion proteins created here did not require addition of calcium in order to observe an increase in catalytic activity.

Several novel fusion proteins were produced using different linker lengths and directionality. Linker length exhibited an effect on the activity of the fusion protein, with the 11 amino acid linker (FP-11) displaying 50% less catalytic activity than the

other fusion proteins but possessing 2 times more catalytic activity than IMPase alone. The fusion proteins with linker lengths of 22 amino acids or more displayed the same catalytic activity, with no observable effect from the directionality of the proteins. None of the fusion proteins showed the same levels of catalytic activity that were observed when the two wild type proteins were mixed together. The most catalytically active fusion proteins displayed a relative activity of 4X in comparison to calbindin-D28k and IMPase together, with a relative activity of 6X when compared to IMPase alone. In the activity assay, a ratio of 1:33 IMPase to calbindin-D28k molecules was present as compared to the 1:1 ratio present in the fusion proteins assay. One hypothesis is that the flexible linker may cause some steric hindrance to the protein interaction or negatively affect the structural plasticity of the proteins compared to the wild type forms, thus explaining why the fusion proteins lacked the full catalytic activity of the wild type complex. However, the activity of the longer fusion proteins is closer to the activity displayed by the native complex than that of WT IMPase alone, rendering them a suitable model of the complex.

The SAXS data varies with varying linker length. The longest linker Cal-FP-66 displays the highest flexibility and possesses a structure distinct from the ideal globular system. It is possible that there may be increased polydispersity as domains from different fusion proteins form complexes. All of the proteins exhibit the expected multidomain topology in the Kratky and Distance distribution function plots. Both Rg and Dmax increase with linker length. *Ab-initio* envelope construction produced an identical structure for all of the fusion proteins irrespective of linker length or directionality. The envelopes retain a V-shape structure compared to the

in-silico model of the complex. The V-shape structure provides more internal space for the protein complex to occupy. Comparison of the SAXS data to the calculated scattering of the *in-silico* model (Levi *et al.,* 2013) reveals deviations at Low and High q regions. This is due to a difference in the overall shape of the molecules from the more linear *in silico* model to the V-shaped structure. There may also be structural changes present in the proteins that are not modelled in the docking simulations. However, only large conformational changes would be observable using the SAXS method as it is a low-resolution technique.

Conclusion

The production of fusion proteins using flexible linkers can be successfully employed to study the calbindin-IMPase interaction. The coupling of the two proteins via a flexible linker increases the catalytic activity of IMPase. Several fusion protein isoforms were analyzed by SAXS and all possess a V-shape confirmation, in contrast to a previous *in-silico* model that predicted a linear conformation. These fusion protein constructs provide a model that could be exploited for detailed analysis of the Calbindin-IMPase interaction in both crystallographic and mutagenic studies.

Chapter 4
Paper 3

Exploration of a Novel Fragment Binding Site at the Homodimer Interface of Inositol Monophosphatase.

Exploration of a Novel Fragment Binding Site at the Homodimer Interface of Inositol Monophosphatase.

James W. Noble, Iain J. Day, Mark Roe, Gary J. Tresadern and John R. Atack

Abstract

Inositol Monophosphatase (IMPase) is an enzyme involved in the recycling of inositol in the phosphatidylinositol signalling pathway. IMPase catalyses the final de-phosphorylation of inositol-1-phosphate, which is then used to re-synthesise phosphatidylinositol bisphosphate. IMPase has been proposed as a therapeutic target of lithium in bipolar disorder (Berridge, Downes, and Hanley, 1982). More recently, it has been shown that inhibition of IMPase can stimulate autophagy (Criollo *et al.*, 2007; Motoi *et al.*, 2014; Sarkar *et al.*, 2005). Despite the therapeutic potential of IMPase as a drug target, the discovery of specific inhibitors that are effective *in vivo* has remained elusive. Therefore, there is currently a lack of specific pharmacological tools to explore the inhibition of IMPase *in vivo*. Here we present a novel fragment binding site at the homodimer interface of IMPase. Furthermore, we have identified five chemical fragments that bind to this newly identified fragment binding site. The fragments themselves do not inhibit IMPase, however point mutations introduced at the dimer interface of the fragment-binding site have resulted in inhibition of the enzyme. This inhibition was noted despite the fragment-binding site being a distance of ~26Å away from the active site of IMPase. These results demonstrate that the dynamics of the homodimer interface are a critical feature for the catalytic activity of IMPase. The fragments were identified using a crystallographic soaking screen and binding was confirmed by NMR spectroscopy. This novel binding site is the first fragment binding site identified for

IMPase and may be useful starting point for the development of potent inhibitors. IMPase exists as a constitutive homodimer and here we have shown that changes in the properties of the homodimer interface inhibit IMPase activity. Therefore, disruption of the homodimer could be a useful pharmacological strategy to inhibit the enzyme.

Introduction

IMPase is a metallophosphodiesterase enzyme. It is a highly conserved homodimeric protein consisting of 277 amino acids per polypeptide chain. The IMPase structure is comprised of alternate layers of α-helices and β-sheets, forming a single globular tertiary structure that is thermally stable to temperatures in excess of 75°C (Kraft *et al.,* 2018; Bone, Springer, and Atack, 1992; McAllister *et al.,* 1992). IMPase requires magnesium for its activity and is inhibited by other ions, such as calcium, that can replace the magnesium in its active site (Atack *et al.,* 1995b). IMPase is involved in the phosphatidylinositol signalling cascade that is a central part of the biology of cell signalling. The IP signalling cascade is initiated by the activation of a G-protein coupled receptor that activates PLC. PLC produces IP3 by the hydrolysis of PIP2 in the inner leaflet of the cell membrane. IP3 then defuses through the cytosol and binds to receptors on the endoplasmic/sarcoplasmic reticulum and induces the release of calcium (Streb *et al.,* 1983, Furuichi *et al.,* 1989, Berridge, 1993). DAG remains in the inner leaflet of the cell membrane and binds to and actives PKC (Newton, 1995). Subsequently, IP3 is recycled back to inositol by a series of enzymes, of which IMPase catalyzes the last step.

Lithium is employed in the treatment of bipolar disorder and inhibits IMPase by preventing the release of the phosphate after the hydrolysis of myo-inositol-1-phosphate (IP1) (Lu *et al.,* 2012). It was demonstrated that lithium decreases inositol levels *in vivo* (Allison & Stewart, 1971) and these data later resulted in the formation of the inositol depletion hypothesis of lithium's efficacy in the treatment of bipolar disorder (Berridge, Downes, and Hanley, 1982). Recently, it has been shown that the inhibition of IMPase can induce autophagy and the subsequent clearance of peptides involved in the pathogenesis of neurodegenerative diseases *in vitro* (Motoi *et al.,* 2014; Sarkar *et al.,* 2005). These studies inhibited IMPase pharmacologically using the compounds lithium and L-690,330 and generated significant interest. This is the second method identified to induce autophagy pharmacologically, the first being with the use of rapamycin that induces autophagy via the inhibition of mTOR (Criollo *et al.,* 2007).

Despite IMPase being of therapeutic interest since the 1970s, no specific inhibitors have been discovered that are effective *in vivo.* In the 1990s, efforts were made by the pharmaceutical company Merck to design an inhibitor based on the IP1 substrate. They synthesized methylenebisphosphonic acid derivatives of IP1 that were non-hydrolysable (Baker *et al.,* 1990). These inhibitors possessed high affinity. L690-330 (IC_{50} 0.2 μM) was the most promising and later co-crystallized with IMPase (Atack *et al.,* 1993, Kraft *et al.,* 2018). As IMPase has an extremely hydrophilic active site in order to bind to its hydrophilic substrate IP1 and ion co-factors (Ferruz *et al.,* 2016), the L690-330 inhibitor also contains hydrophilic phosphate groups. Highly hydrophilic inhibitors lack cell and central nervous

system (CNS) penetration. Attempts were made to produce a tetrapivaloyloxymethyl ester prodrug that would be less charged however, these later failed *in vivo* due to solubility issues (Atack *et al.,* 1994). More recently, a compound known as Ebselen, that binds covalently to cysteine residues, was identified as an inhibitor of IMPase (Singh *et al.,* 2013). Although less potent (Ebselen IC_{50} 1.5 μM) than L690-330, it was more hydrophobic than the previously identified substrate mimetic. However, its small molecular weight (Mr = 274) and intrinsic reactivity make it prone to polypharmacology. The selenium-containing ring in Ebselen is similar to an isothiazolone and molecules with this group are known as a Pan-Assay Interference Compound (PAINS). These compounds are often avoided by medicinal chemists due to the challenges of engineering specificity into intrinsically reactive molecules (Baell and Nissink, 2018).

Here we aim to identify novel binding sites and chemical matter that could be employed to develop a new class of IMPase inhibitors. To achieve this a crystallographic fragment screen was performed. This allowed the detection of very weakly binding fragments that may not directly inhibit IMPase and therefore may not be identified by the use of other techniques. The discovery that IMPase can be allosterically modulated by protein-protein interaction with calbindin-D28K (Berggard *et al.,* 2002) has increased the interest in this approach. This finding indicates that there may be significant structural plasticity within IMPase that could be exploited pharmacologically.

Methods

Protein expression and Purification

IMPase was produced as described by Kraft *et al.,* 2018. During purification of the mutant IMPase enzymes the heat purification step was omitted.

Apo-IMPase Crystallisation

Crystallographic screens were performed using an IMPase concentration of 40 mg/mL, at a temperature of 293K, in a buffer composed of 20 mM Tris (pH 7.8), 150 mM NaCl and 1 mM MgCl. Crystallization was performed in MRC 2-well crystallization plates (Swissci), using a reservoir volume of 50 µl and a drop volume of 0.4 µl consisting of a 1:1 ratio of precipitant solution and protein solution. The Crystal Phoenix crystallography dispenser (Art Robbins Instruments) was used to prepare crystal plates. IMPase binds phosphate and sulphate, therefore buffer components that contain those groups, such as HEPES, were avoided. The precipitant screen Structural Screen 1 & 2 (Molecular Dimensions) yielded Apo crystals with conditions of 0.2 M Sodium acetate trihydrate, 0.1 M sodium cacodylate (pH 6.5) and 30 % w/v PEG 8000. The crystal condition and protein concentration were further empirically optimised to 0.19 M Sodium acetate trihydrate, 0.1 M sodium cacodylate (pH 6.5), 28.5 % w/v PEG 8000, 3.5 mM MgCl and incubation at 277K using 9.4 mg/mL IMPase.

Fragment Screen

Crystals were soaked with the addition of a fragment precipitant solution with either 3 fragments at a concentration of 13.3 mM or with one fragment at a

concentration of 4 mM and a final DMSO concentration of 40%. Crystals were incubated for 1 hour at 293K prior to the addition of 1.2 µl of the fragment precipitant solution mix. The crystals were incubated for a further hour and then picked and plunge cryo-cooled in liquid nitrogen. Around 400 fragments were screened successfully. The data were processed using the fast_dp data possessing pipeline followed by the difference map pipeline DIMPLE. Fragments were identified using Pan-Dataset Density Analysis (PanDDA) (Pearce *et al.,* 2017). Five fragments of interest were identified and those hits in "cocktail" were confirmed individually.

Activity Assay

The assay was performed in 384 clear flat-bottomed plates (BRAND), 30 nM IMPase was incubated with 0.125 mM Myo-inositol 1-monophosphate (Enzo) for 45 min at 37 °C and 80 % humidity to prevent evaporation. The assay was performed in a buffer of 20 mM Tris-HCL (pH 7.8), 150 mM NaCl, 4 mM MgCl and 1 mM EGTA in a total reaction volume of 15 µl. The assay was stopped by the addition of 30 µl of BIOMOL Green reagent (Enzo) and was incubated at room temperature for a further 30 min. The absorbance at 630 nm was analysed on a PHERAstar BMG plate reader.

NMR STD

Concentrations of 50 µm of IMPase and 5 mM of fragments were used for all STD NMR experiments and these were performed in a solution of 150 mM NaCl, 20 mM Tris (pH 7.8-HCL), 10 % DMSO and 10 % D2O. STD experiments were recorded with a saturation time of 0.5 s, with on and off-resonance irradiation applied at -0.5 and 30 ppm respectively (Mayer and Meyer, 2001) .

Mutant IMPase Crystallisation

Crystallisation of both IMPase mutant proteins was performed in MRC 2-well crystallisation plates (Swissci) using a reservoir volume of 50 µl and a drop volume of 0.4 µl, consisting of a 1:1 ratio of the precipitant solution and protein solution. The crystallisation of the methionine 179 mutant was performed at a concentration of 12 mg/ml in a buffer of 20 mM Tris (pH 7.8), 150 mM NaCl, 5 mM MgCl, and a precipitant solution of 0.19 M Sodium acetate trihydrate, 0.1 M sodium cacodylate (pH 6.5), 28.5 % w/v PEG 8000, 3.5 mM MgCl and with incubation at 293K. Crystallographic screens of the leucine 176 mutant IMPase were performed in a buffer of 20 mM Tris (pH 7.8), 150 mM NaCl, 5 mM MgCl using a 60 mg/ml protein concentration. The best diffracting crystals were identified from BCS high throughput percipient Screen (molecular dimensions, MD1-105) well C3 containing 0.15 M NaCl and 28 % v/v PEG smear medium.

Mutant Crystal Data Collection and Analysis

Data were collected at 100 K using 30 % glycerol as a cryoprotectant, on the I03 beamline (Diamond Light Source) as set up on the 03/05/2018 for mutant L176W. 1200 images were collected with a ω oscillation of 0.15 and an exposure time of 0.020 s per image at a wavelength of 0.976 Å, Beam size of 50 µm by 20 µm and transmission of 72.12 %. Diffraction- intensity data were indexed, integrated and scaled using the autoPROC toolbox (Vonrhein *et al.,* 2011). Molecular replacement was performed with Phaser (McCoy *et al.,* 2007), with initial refinement in refmac5 (Murshudov *et al.,* 2011) and Coot in the CCP4 suite of programs. The final model was completed in Coot (Emsley *et al.,* 2010) and the model was refined with BUSTER

v.2.10.2. Data were collected at 100 K with 30 % glycerol as a cryoprotectant, on Rigaku copper rotating anode X-ray generator and a CCD detector, at a wavelength of 1.54 Å and a detector distance of 58.8 mm for mutant M179W.

Results

Apo-IMPase Crystallisation

The crystals obtained using the initial crystallisation conditions formed shards. These were very thin, fragile and not suitable for high throughput picking of crystals. The crystals diffracted well, to a resolution of 1.5 Å. The optimisation screen yielded rod-shaped crystals and these improved when grown at a lower temperature of 277K (Figure 17).

Figure 11. Crystal optimisation experiment. The far-left image depicts the crystals obtained from the initial crystal screen. The center image depicts the crystals formed in the optimisation matrix. The image on the far right depicts the crystals formed in the optimised crystal conditions at a lower temperature.

Crystallographic Fragment Screen

Five fragments were identified that bound to IMPase (Figure 18) (Crystallographic

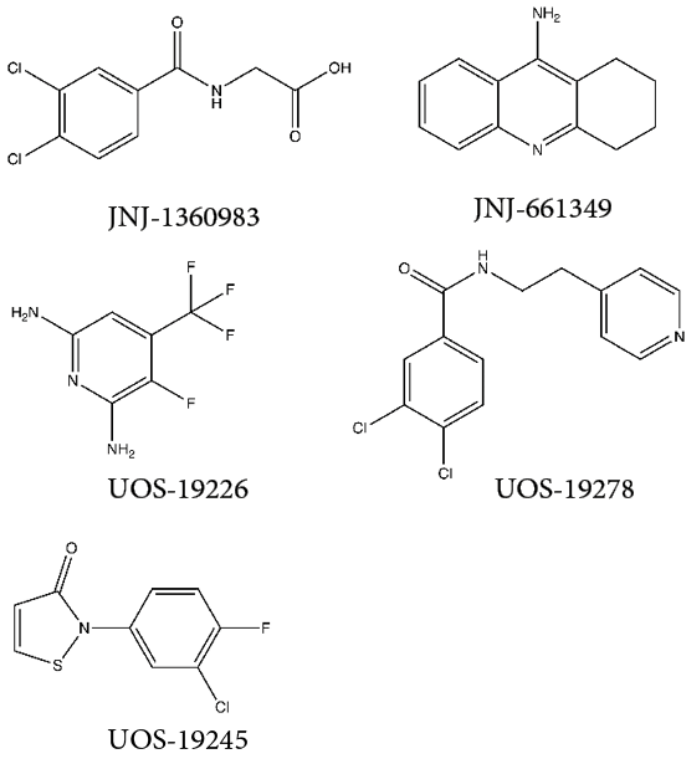

Figure 18. Structures of the five molecules identified in the fragment screen. UOS-19245 contains the reactive isothiazolone ring that binds non-specifically to the cysteine residues in IMPase.

Table 3 Crystallographic statistics for all crystals presented here. Values in parentheses are for the highest shell.

Data set	JNJ-1360983	JNJ-661349	UOS-19226	UOS-19278	UOS-19245	L176W	M179W
Beamline	IO4-1 (DLS)	IO4-1 (DLS)	IO3 (DLS)	IO3 (DLS)	IO4-1 (DLS)	IO3 (DLS)	RIGAKU
Unit-cell parameters							
A (Å)	55.29	51.76	51.81	58.63	56.20	54.91	84.99
B (Å)	76.37	75.76	76.10	74.87	77.09	75.95	84.99
C (Å)	57.42	71.76	71.95	58.93	57.91	57.03	152.16
A (°)	90	90	90	90	90	90	90
B (°)	95.03	105.98	105.98	99.12	95.08	94.46	90
γ (°)	90	90	90	90	90	90	120
Space group	P 1 21 1	P 1 21 1	P 1 21 1	P 1 21 1	P 1 21 1	P1 21 1	P 31 2 1
Wavelength	0.9159	0.9159	0.9762	0.9762	0.9282	0.9762	1.54056
Resolution range	22.31-1.53 (1.53-1.56)	51.01-1.62 (1.62 – 1.65)	69-.17 – 1.61 (1.61 – 1.64)	46.23 – 1.59 (1.59-1.62)	31.75 – 1.95 (1.95-1.98)	44.41 – 1.58(1.58-1.73)	28.12-2.20 (2.20-2.27)
No. of observations	361733 (18338)	336084 (16400)	440015 (16442)	445449 (21047)	153364 (7790)	113103 (5796)	304132 (21292)
No. of unique observations	71599 (3566)	66934 (3213)	69596 (3265)	68641 (3199)	35807 (1762)	34094 (1705)	33010 (2804)
Completeness	99.9 (99.9)	98.7 (95.6)	99.7 (94.3)	99.8 (94.8)	99.6 (98.8)	92.4 (72.7)	99.9 (99.8)
Multiplicity	5.1 (5.1)	5.0 (5.1)	6.3 (5.0)	6.5 (6.6)	4.3 (4.4)	3.3 (3.4)	9.2 (7.6)
Anomalous completeness	96.9 (97.5)	96.5 (93.8)	99.5 (94.5)	99.6 (94.7)	95.3 (95.7)	86.5 (70.2)	99.6 (95.6)
Anomalous multiplicity	2.6 (2.6)	2.6 (2.6)	3.2 (2.6)	3.3 (3.3)	2.2 (2.3)	1.7 (1.8)	4.7 (3.8)
R_{meas}	0.072 (1.752)	0.111 (1.753)	0.116 (1.988)	0.102 (1.789)	0.082 (1.132)	0.096 (0.876)	0.186 (0.684)
$CC_{1/2}$	1.00 (0.5)	1.0 (0.5)	1.0 (0.5)	1.0 (0.7)	1.0 (0.7)	1.0 (0.5)	0.99 (0.942)
I/σ(i)	11.8 (1.1)	9.3 (1.1)	8.4 (1.0)	8.2 (1.0)	12.6 (1.5)	9.3 (1.6)	10.2 (3.8)
Refinement	BUSTER v.2.10.3	BUSTER v.2.10.3	BUSTER v.2.10.3	BUSTER v.2.10.3	BUSTER v.2.10.3	BUSTER v.2.10.3	BUSTER v.2.10.3
Resolution range (Å)	22.34-1.53	51.01-1.62	1.80 – 47.02	23.24-1.59	26.62-1.95	21.14-1.58	28.12-2.20
R_{cryst}	0.195	0.187	0.183	0.192	0.194	0.190	0.231
Rfree	0.217	0.213	0.221	0.203	0.23	0.237	0.265
No. of protein atoms	4308	4132	4178	4311	3998	3915	4071
No. of ligand atoms	14	18	18	27	42	0	31
No. of solvent atoms	269	423	501	354	224	113	263
Mean B factor ($Å^2$)	34.15	21.03	21.70	32.15	41.22	27.19	26.05
R.m.s.d., bond lengths (Å)	0.01	0.01	0.01	0.01	0.01	0.01	0.009
R.m.s.d., bond angles (°)	1.12	1.12	1.09	1.09	1.06	1.12	1.20

statistics for all crystals are shown in Table 3).

Fragment UOS-19245 bound to multiple sites on IMPase by the covalent binding to cysteine residues. The isothiazolinone ring opens and forms a disulfide bond with cysteine residues in an unspecific manner (Supplementary Figure 3). Fragments UOS-19226, UOS-19278, JNJ-661349 and JNJ-1360983 bound to IMPase at the homodimer interface of the protein. These fragments are bound by cation π-stacking interactions to arginine 173 of IMPase (Figure 19).

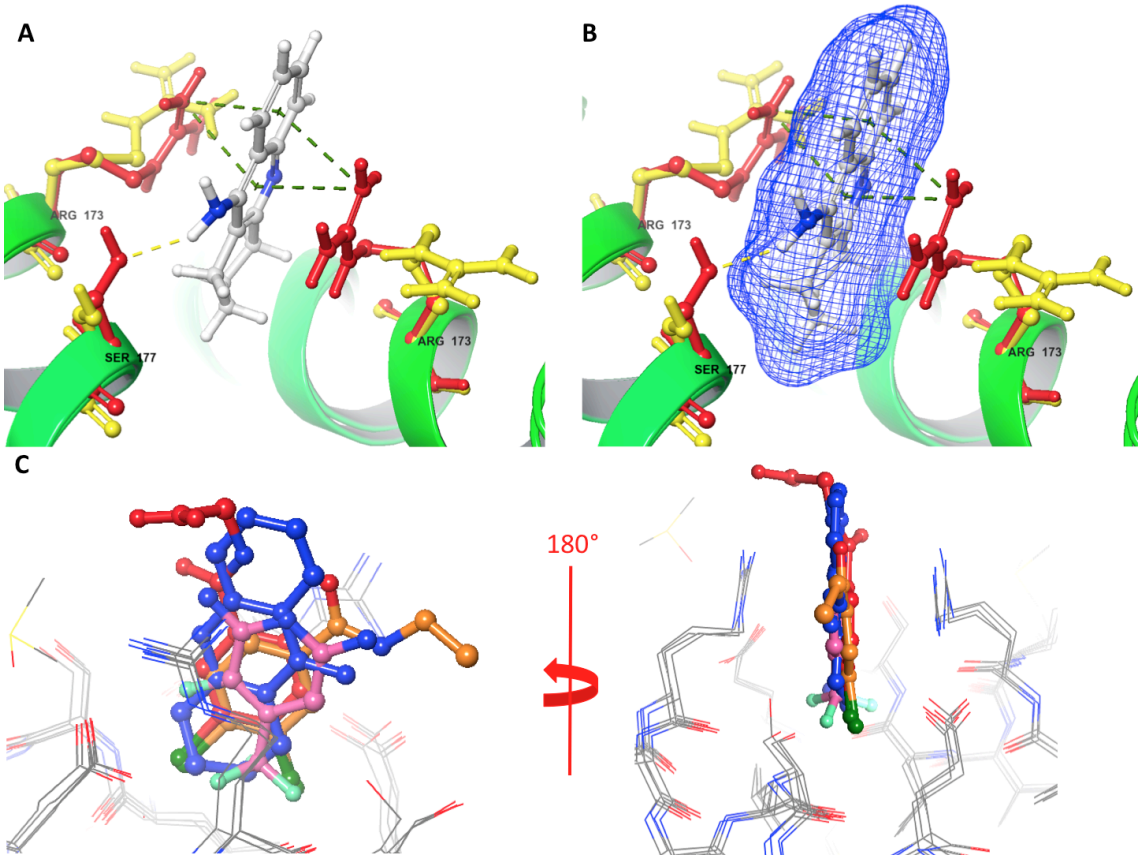

Figure 12. A) Fragment JNJ-661349 bound to the homodimer interface of IMPase, with the cation- π-stacking interaction denoted by a green dotted line and a hydrogen bind denoted by a yellow dotted line. B) The same as (A) with the addition of the surface of the fragment shown by a blue mesh, the aliphatic ring of JNJ-661349 buried in the homodimer interface. C) The superimposition of all the crystal structures. All of the halogen containing fragments have the halogen buried in the homodimer interface.

Saturation Transfer Difference (STD) NMR

Fragments that were commercially available (UOS-19226, UOS-19278 and JNJ-1360983) were assessed for IMPase binding using STD NMR. Negative peaks were observed for all fragments that were identified in the crystallography screen confirming binding to IMPase (Figure 20).

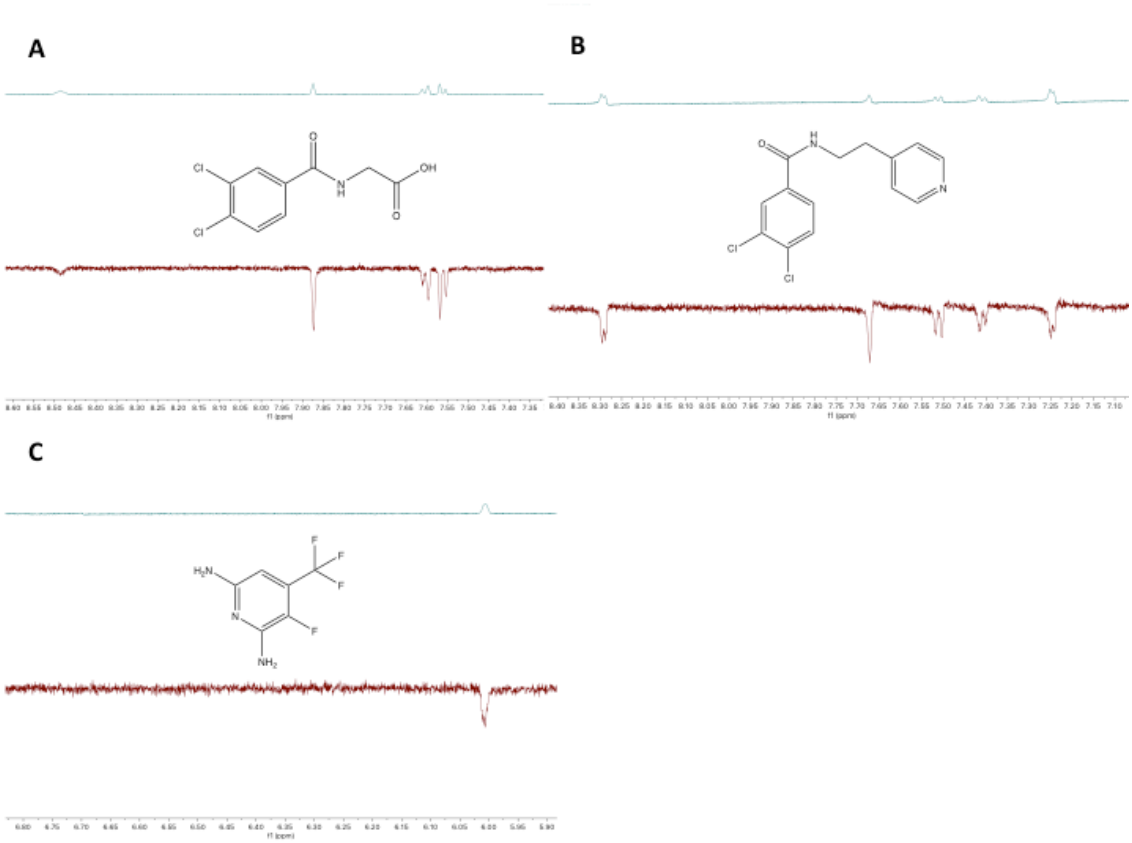

Figure 13. The STD NMR spectra for JNJ-1360983 (A), UOS-19278 (B) and UOS-19226 (C). The top blue spectra are the off-resonance spectra and the bottom burgundy spectra are the STD-spectra. The negative peaks indicate a positive result of fragment binding.

IMPase Mutants

IMPase exists as a constitutive homodimer, therefore, disruption of the homodimer interface by a drug molecule could be a strategy to identify novel inhibitors. In order test if disruption of this dimer interface at the fragment-binding site would lead to inhibition, mutants were developed in an attempt to simulate a hydrophobic drug

molecule penetrating the homodimer interface. Tryptophan is a hydrophobic residue that is close to the size of a small drug molecule. Tryptophan mutants were produces and exhibited a decrease in catalytic activity compared to the wild type IMPase. The methionine to tryptophan mutant had a relative activity of 48 % and the leucine to tryptophan mutant had a relative activity of 27 % compared to WT IMPase. Crystallisation and structural analysis revealed no significant structural change in the protein structure of these mutants compared to wild type IMPase (Figure 21).

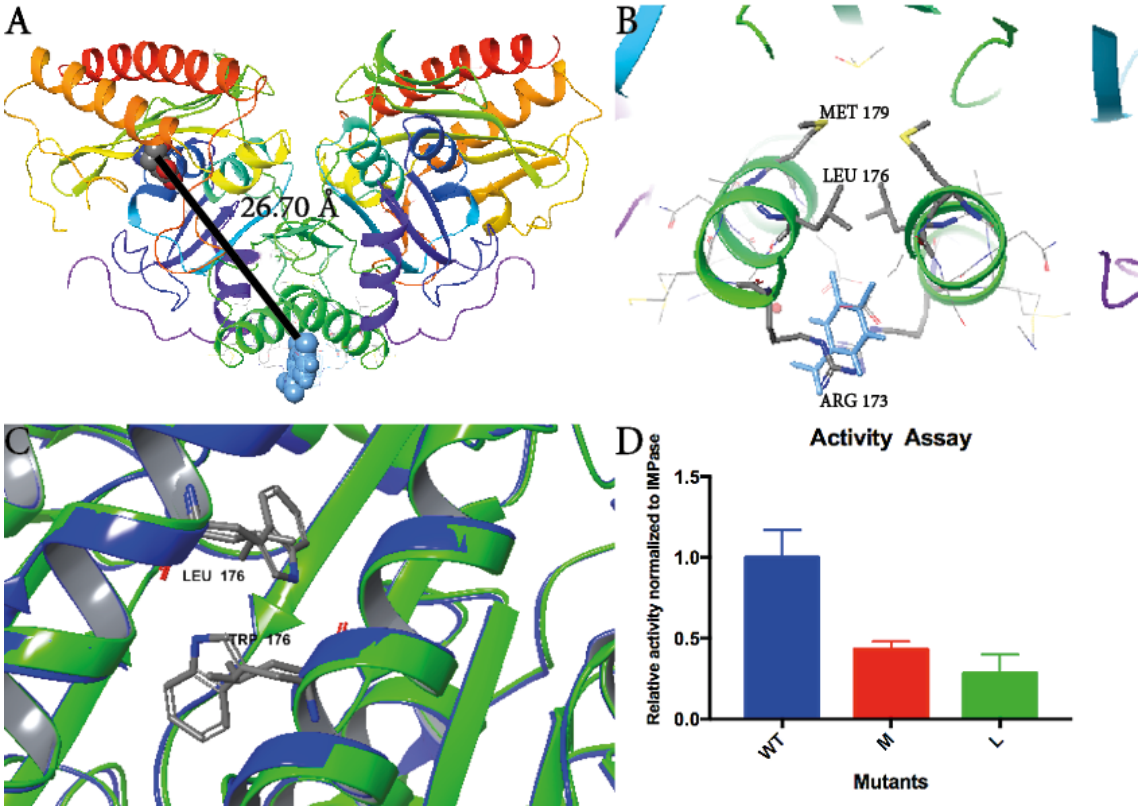

Figure 14. (A) shows a measure of the distance from a fragment bound to the homodimer interface to an active site residue of IMPase. (B) the residues mutated (176 and 179) to tryptophan. These residues are directly under the fragment binding site. (C) The crystal structures of the lysine to tryptophan mutant (GREEN) superimposed on to the wild type IMPase (BLUE). (D) The relative activities the IMPase mutants normalized to wild type IMPase.

Discussion

IMPase is a phosphodiesterase enzyme that is involved in the IP signalling cascade. IP3 is produced by the hydrolysis of phosphatidylinositol 4,5-bisphosphate. IP3 then defuses through the cytosol to channels on the ER or SR inducing the release of calcium (Majerus, 1992; Harwood, 2005). This cascade is involved in a myriad of physiological functions and is one of the key-signalling cascades in cell biology. IMPase is involved in the homeostasis of this pathway, catalysing the final dephosphorylation of the inositol 1-phosphate (ref).

IMPase has been of therapeutic interest since the formation of the inositol depletion hypothesis of lithium's therapeutic efficacy in the treatment of bipolar disorder and more recently due to the induction of autophagy by its inhibition (Berridge, Downes, and Hanley, 1982; Sarkar *et al.,* 2005). Despite repeated attempts to find drug candidates, effective inhibitors of IMPase have remained allusive. The inhibitory molecules that have been discovered to date have possessed undesirable physicochemical properties, such as being reactive or too hydrophilic or hydrophobic (Atack *et al.,* 1993; Atack *et al.*, 1994; Singh *et al.,* 2013). Here a crystallographic soaking screen was employed to identify novel binding sites and chemical matter. This method allows for the detection of the binding of fragments with low affinity, that may not be identified by the use of other techniques. Five binding fragments were identified yielding a hit rate of around 1-2 %. A reactive isothiazolinone fragment (UOS-19245) was identified; this chemical group is identical to that found in Ebselen, with a sulphur substituted for selenium in Ebselen (Singh *et al.,* 2013).

We have produced the first crystal structure of an isothiazolinone bound to IMPase. Electron density of the fragment can be observed around the majority of the cytosine residues in the IMPase crystal structure, demonstrating that there is not a specific binding site for this fragment. Four fragments were found to bind to the homodimer interface at the same binding site. This was the only specific fragment binding site identified in the screen, suggesting this is the most tractable fragment binding site on IMPase. The interaction at this binding site is produced by a cation π clamping mechanism, with arginine 173 from both polypeptide chains clamping around both sides of the aromatic rings in the fragments. These arginine residues change conformation and stabilize around the fragments. This fragment binding site is 26 Å away from the active site of IMPase, therefore, inhibition conferred from this site would likely be allosteric as opposed to competitive inhibition with the substrate. IP1 is a hydrophilic substrate and an inhibitor that binds to the active site would likely mimic these properties and would result in poor cell penetration. Therefore, inhibition via an allosteric site may enable compounds with improved physicochemical properties to be developed. There are two options when undertaking drug discovery at sites that are distant from the active site of an enzyme; firstly, to explore any potential allosteric activity of the site, or the development of a high affinity compound that can be developed into a PROTAC leading to *in situ* degradation of the target (Toure and Crews, 2016).

In order to test the hypothesis that disruption of the homodimer interface of IMPase would result in loss of catalytic activity, two mutants were developed that attempted to simulate a drug molecule penetrating the homodimer interface. L176W and M179W aimed to simulate hydrophobic drug molecules by either shallowly or

deeply penetrating the homodimer interface under the fragment banding site. Both mutants reduced the activity of IMPase, with the L176W (shallow) mutant having the largest reduction in activity at 73% compared to the 52% reduction in activity for the deeply penetrating M179W (deep) mutant (figure 21D). Interestingly the crystal structures of both mutants revealed no difference in the secondary, tertiary and quaternary protein structure of the mutants when compared to wild type IMPase. This indicates that the dynamics of this homodimer interface are important for the catalytic cycle of IMPase, as small changes in the properties of the interface can reduce and inhibit IMPase activity. This can be achieved without a full disruption of the homodimer interface, which would be challenging for a small molecule inhibitor.

Proteins forming inside a crystal lattice are in a very different environment from being in solution. Crystallographic contacts may act as a binding site or influence fragment binding. Therefore, it is necessary to confirm the binding of fragments to protein in solution. This was performed using STD NMR, a technique where the protein is in its native form in solution. All commercially available fragments were tested, and binding was detected providing confirmation of binding of the fragments to IMPase in solution.

Conclusion

In this paper, we describe identification of a novel fragment-binding site at the homodimer interface of IMPase. This is the first example shown of non-covalent binding of drug-like molecules to IMPase, outside of its active site. Four non-covalently binding fragments were identified using a combination of NMR and

crystallographic screening. Using site-directed mutagenesis, we have shown that the properties of the homodimer interface directly under the fragment binding are important for catalytic activity of the enzyme, despite the fragment binding site being located approximately 26 Å away from the active site. The introduction of mutated residues did not disrupt the structure of IMPase, or the homodimer interface, suggesting that the physiochemical properties of the interface are important in the catalytic cycle of IMPase.

Chapter 5
Paper4

Isothiazolinone Inhibition of Inositol Monophosphatase

Isothiazolinone Inhibition of Inositol Monophosphatase

James W. Noble, Gary J. Tresadern and John R. Atack

Abstract

Inositol monophosphates (IMPase) is an enzyme of significant therapeutic interest both in the treatment of bipolar disorder and the induction of autophagy. In 2013, Singh *et al.,* reported the discovery of a novel safe IMPase inhibitor. The inhibitor they identified, named Ebselen, is a covalent inhibitor. Ebselen possesses a selenium-nitrogen single bond that breaks open and covalently bonds to cysteine residues in proteins. Here we aim to explore this group of reactive compounds by screening 67 isothiazolinone containing compounds for inhibitory activity against IMPase. From this screen, we identified 4 compounds as inhibitors of IMPase. These inhibitors exhibit IC_{50} values in the low micromolar range similar to that reported for ebselen (1.5 μM). The compounds were identified using an enzymatic colorimetric phosphate quantification assay and binding was confirmed by thermal denaturation assay. The identified compounds displayed the biochemical properties of irreversible inhibitors as inhibition was time-dependent, and dilution of the compounds does not decrease level of inhibition. The compounds identified from this screen all possess similar chemical structures. Here we present a new class of irreversible IMPase inhibitors that are significantly chemically different from ebselen. This novel group of inhibitors could be further developed to create potent IMPase inhibitors.

Introduction

IMPase has been of therapeutic interest since the formation of the inositol depletion hypothesis of the efficacy of lithium in the treatment of bipolar disorder (Berridge, Downes, and Hanley, 1982). IMPase is a homodimeric enzyme that is involved in the homeostasis of the IP3 signalling cascade. IMPase catalyses the final dephosphorylation of the inositol sugar from Inositol 1-Phosphate (ref). The inositol depletion hypothesis was initially based on the discovery that lithium treatment in rats causes a 30 % reduction in the inositol concentration in the cerebral cortex. This was later combined with the discovery that lithium treatment increases the concentration of Inositol 1-Phosphate in the cerebral cortex (Allison *et al.,* 1976, Allison & Stewart, 1971). Furthermore, IMPase purified from rats and bovine sources was shown to be sensitive to lithium (Naccarato *et al.,* 1974, Hallcher & Sherman, 1980, Harwood, 2005). Lithium is a small ion and exhibits polypharmacology. Therefore, identifying exactly how lithium exerts its therapeutic efficacy is challenging, due to the wide range of enzymes lithium inhibits. As lithium exhibits polypharmacology, it also possesses significant toxicity with a small therapeutic window that requires continual monitoring of lithium plasma concentration (Timmer & Sands, 1999).

It has recently been shown that inhibition of IMPase can induce autophagy and that this effect can be reversed by the addition of free inositol *in vitro* (Sarkar *et al.,* 2005). Subsequent studies have described the clearance of peptides induced by lithium and more specific IMPase inhibitors (L-690,330). Studies have described the clearance of mutated Huntington in Huntington's disease, α-synuclein in

Parkinson's disease and phosphorylated tau in Alzheimer's disease (Criollo *et al.,* 2007; Motoi *et al.,* 2014).

The development of specific inhibitors of IMPase would facilitate an evaluation of the inositol depletion hypothesis and enable evaluation of the role of IMPase inhibition in autophagy *in vivo.* Attempts at developing specific IMPase inhibitors have ended in varying degrees of success and failure. In the 1990s, the pharmaceutical company Merck developed an array of inhibitors based on the Inositol 1-Phosphate substrates of IMPase. Merck developed a non-hydrolysable substrate mimetic by synthesising methylenebisphosphonic acid derivatives (Baker *et al.,* 1990). The compounds developed had a high potency and of these L-690,330 was the most promising, with an IC_{50} of 0.2 μM *in vitro* (Atack *et al*., 1993). L-690,330 possesses two negatively charged phosphate groups which results in poor cell and central nervous system penetration. Attempts to create a prodrug that would be metabolised in the cells to form the active L-690,330 molecule failed as the prodrug precipitated at the site of administration *in vivo* (Atack *et al.,* 1994). Despite the failure of L-690,330 as an effective treatment, it is still useful *in vitro* as a specific IMPase inhibitor.

A screen of the US National Institutes of Health Clinical Compound Collection (NCC) of bioactive compounds (450 compounds) identified the compound Ebselen as an inhibitor of IMPase (Singh *et al.,* 2013). Ebselen contains a pan assay interference (PAINS) group known as an isoselenazolone. This chemical group contains a Selenium-Nitrogen single bond that can break open and form covalent bonds with cysteine residues in proteins (Baell & Nissink, 2018). Here we explore this reactive

chemical group further by screening 67 isothiazolinone containing compounds from the Janssen Pharmaceutical library for the inhibition of IMPase. We have substituted the selenium for sulphur as this is an element found more commonly in commercial drugs (Feng *et al.,* 2016). The aim is to discover potential new inhibitors and to evaluate if the isothiazolinone chemical group has the potential to be engineered into a high-affinity specific inhibitor.

Methods

Colorimetric Phosphate Quantitation Assay

67 unique compounds and fragments were tested for inhibitory activity with respect to IMPase. Each compound was screened in triplicate at a concentration of 266.4 μM with an enzyme concentration of 0.8 μg/μL in an assay buffer of 20 mM Tris (pH 7.8) 150 mM NaCl 3 mM MgCl and 5% DMSO and a final Myo-inositol 1-monophosphate (Enzo) concentration of 0.125 mM. Compounds were added to the reaction 10 min before the substrate. The biochemical assay for phosphate detection was performed in Clear 384 well BRANDplates® pureGrade™ F-bottom plates (BRAND). Plates were incubated at 37 °C and 80 % humidity (to inhibit evaporation) for 40 min. Post incubation 30 μl of BIOMOL® green (Enzo)reagent was added and plates were incubated at room temperature for 30 min to allow the colour to develop. Measurement of absorbance at λ= 630 nm was performed in a PHERAstar FS plate reader from BMG Labtech. The screen was performed in triplicate and hits were defined as showing inhibition of IMPase > 30 %. To determine the IC_{50} values of the compounds, a dilution series for each compound series was prepared. 40 nM of IMPase was incubated with the compound for 20 min before the addition of 3 μl substrate. The assay was then performed as stated above.

Thermal Denaturation assay

Thermal Denaturation studies of IMPase were performed with inhibitors using a LightCycler 480 II (Roche) in Multiwell 96 well white plates (Roche). A 10 x concentration of SYPRO® Orange Protein Gel Stain (Sigma S5692) was used as the detection reagent. 6 μM of IMPase was diluted in a buffer of 0.5 % DMSO, Tris 20 mM (pH 7.8), 150 mM NaCl and 3 mM MgCl with varying compound concentrations. Thermal Denaturation was monitored through a temperature range of 20-95°C with an integration time set to 1 sec and fluorescence measured with excitation at 465 nm and emission at 580 nm.

Biochemical Inhibitor Mechanistic Assays

Inhibition Time Course

40 nM IMPase was incubated with a dilution series of JNJ-6157935 in a buffer of 20 mM Tris (pH 7.8), 150 mM NaCl, 3 mM MgCl and 5% DMSO. The incubation was performed at room temperature at time points of 10, 20 and 30 min. The assay was performed as described in Colorimetric Phosphate Quantitation Assay method section.

Inhibition Dilution Assay

1.35 mg/mL IMPase was incubated with 500 μM JNJ-6157935 in a buffer of 20 mM Tris (pH 7.8), 150 mM NaCl, 3 mM MgCl and 5 % DMSO. Incubation was performed at room temperature for 30 min and the sample was then diluted to 44.7 nM IMPase (giving a final compound concentration on 500nM). 3 μl of Myo-inositol 1-

monophosphate (Enzo) substrate was then added resulting in a final concentration of 0.125 mM. IMPase alone and IMPase with 100 µM or 500 µM JNJ-6157935 were treated identically to the dilution sample. The assay was then performed as stated in the Colorimetric Phosphate Quantitation Assay method.

Results

Compound Screen

The compound screen yielded a skewed distribution of the activity of IMPase, with most compounds registering an increase in activity. Four wells produced inhibitory results identifying three novel compounds. These compounds were distinct from the normal distribution of IMPase activity and separated from the skewed distribution of the screen (Figure 22A). IC_{50} curves were then determined for all three "HIT" compounds. The IC_{50} values recorded for JNJ6150704, JNJ6157935 and JNJ6170374 were 2.4, 7.9 and 18.1 µM respectively (Figure 22B).

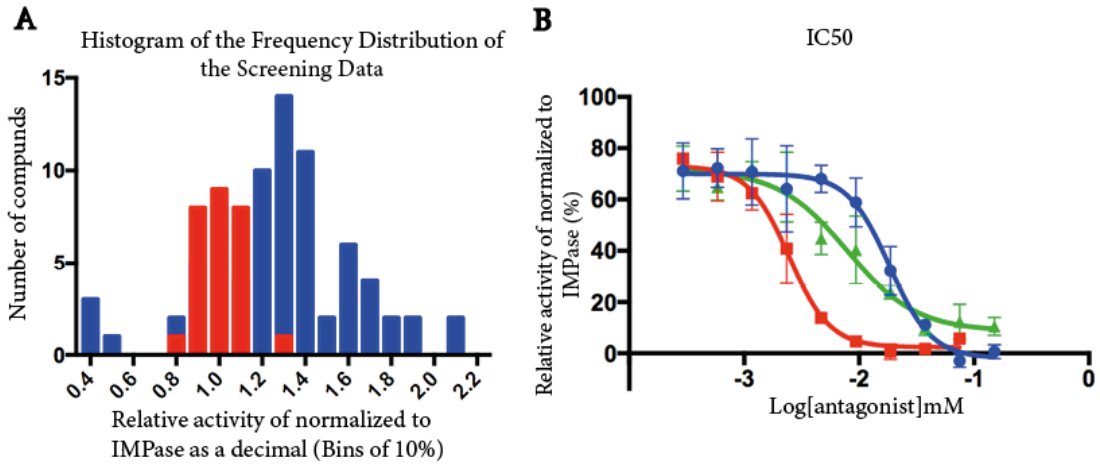

Figure 15. A) A histogram of the screening data. Red is IMPase without compound, blue is IMPase with compound. The screen was performed in single point with the mean average of three replicates used in the histogram. B) IC_{50} curves with the mean and standard deviation for each data point plotted (n=3). Red is JNJ6150704 with an IC_{50} of 2.4µM, Green is JNJ6157935 with an IC_{50} of 7.9 µM, Blue is JNJ6170374 with an IC_{50} of 18.1 µM.

Compounds and SAR

The three hit compounds came from the same sub-group of compounds within the screen as these compounds all have a similar chemical structure (Figure 23).

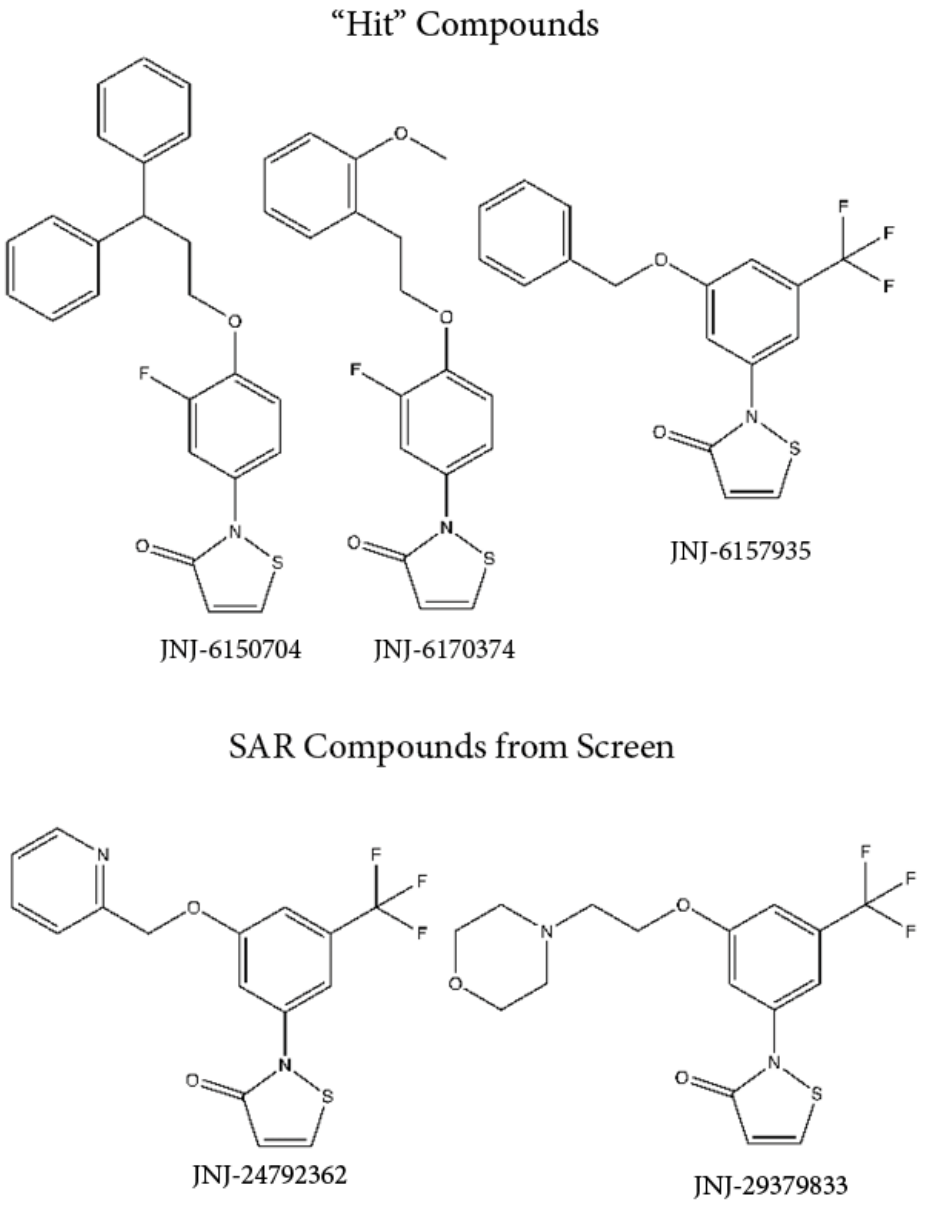

Figure 16. The chemical structure of the group of the compounds that exhibited inhibition of IMPase. The top three compounds were identified in the initial screen as IMPase inhibitors. The bottom two compounds were from the same class and were not identified in the initial screen as inhibitors. The reactive isothiazolone ring of the molecule is placed at the bottom of the molecules.

There were two compounds (JNJ-24792362 and JNJ-29379833) present in the compound library that came from the same class of compounds as the identified hits,

however they did not demonstrate inhibitory properties in the initial screen. IC_{50} curves were performed with the compounds of similar structure to assess any potential activity. Compound JNJ-24792362 demonstrated limited activity with only one atom substituted when compared to JNJ-6157935, identified from the initial screen. A pyridyl group replaced the phenyl causing a significant reduction in activity. Replacing the phenyl ring for a morpholine group (JNJ-29379833) eliminated all activity of the compounds (Figure 24).

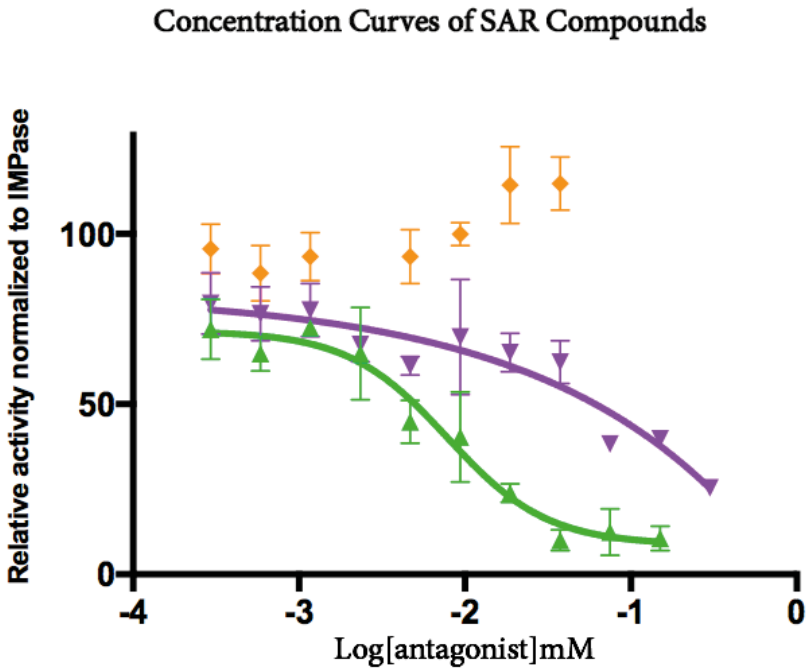

Figure 17. IC_{50} curves with the mean and standard deviation for each data point plotted (n=3). JNJ6157935 (green) with an IC50 of 7.9 µM, the SAR compound JNJ24792362 (lilac) and JNJ29379833 (yellow). Compound JNJ24792362 did exhibit some inhibitory activity but no inhibitory activity was observed for JNJ29379833.

Thermal Denaturation Orthogonal testing

Shifts were observed in the thermal denaturation curves of IMPase in the presence of all of the compounds that demonstrated inhibitory activity in the Colorimetric Phosphate Quantitation Assay. Shifts were concentration dependent and

demonstrated a similar morphology to the previously described inhibitor Ebselen. Due to the additional hydrophobic aromatic ring, at high concentrations compound JNJ-6150704 induced the fluorescence of the dye in the assay (Figure 25).

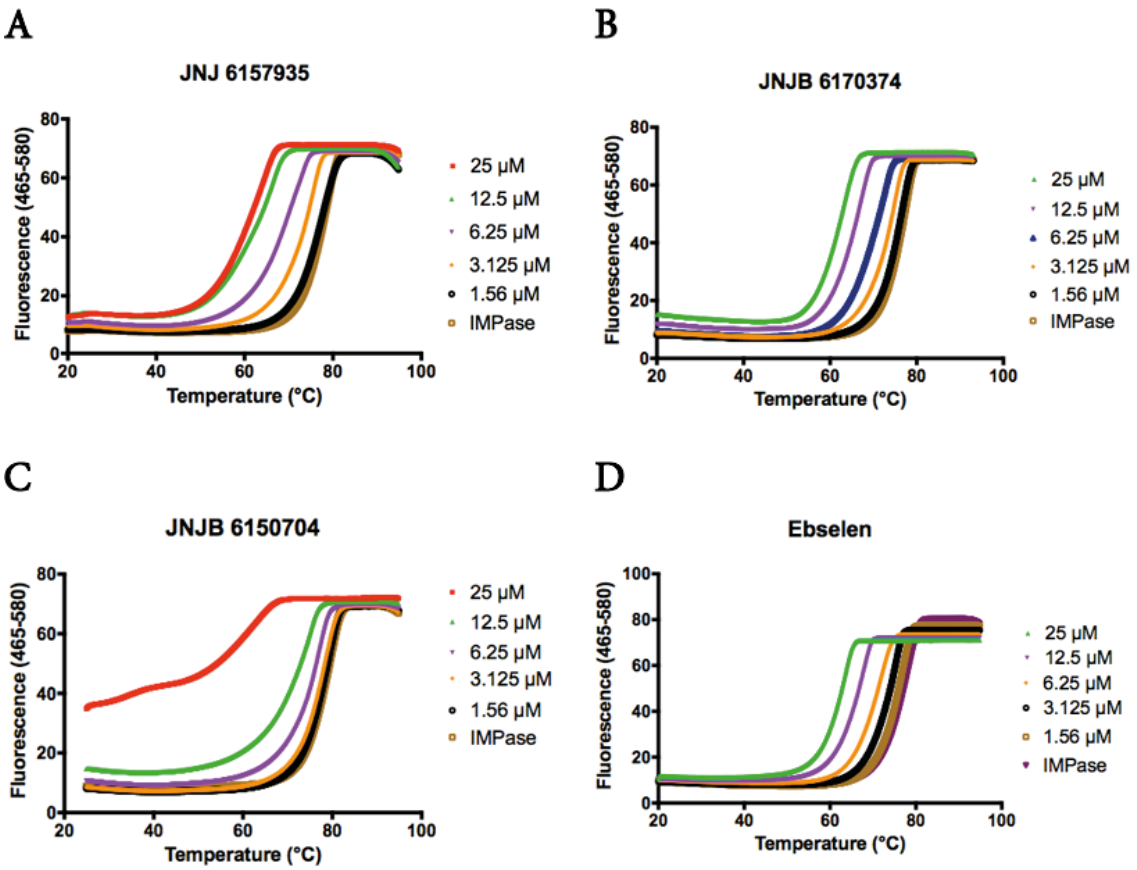

Figure 18. Thermal denaturation curves of IMPase with different concentrations of compound. D) is the positive control compound ebselen. Three replicate thermal denaturation curves were performed, with one representative curve shown here.

Mechanism of action

A dilution and a time-course assay were used to determine if the class of compounds were covalent non-reversible inhibitors. The activity of IMPase was not restored when JNJ6157935 was diluted to below its maximum inhibitory concentration to 500 nM. This is indicative of non-reversible inhibition. The activity of this compound was both time and concentration dependent. At the 10 min time point, full inhibition

of IMPase was not reached. At 20 and 30 min, full inhibition of IMPase was reached with no statistical difference in the IC_{50} value of these respective curves (Figure 26).

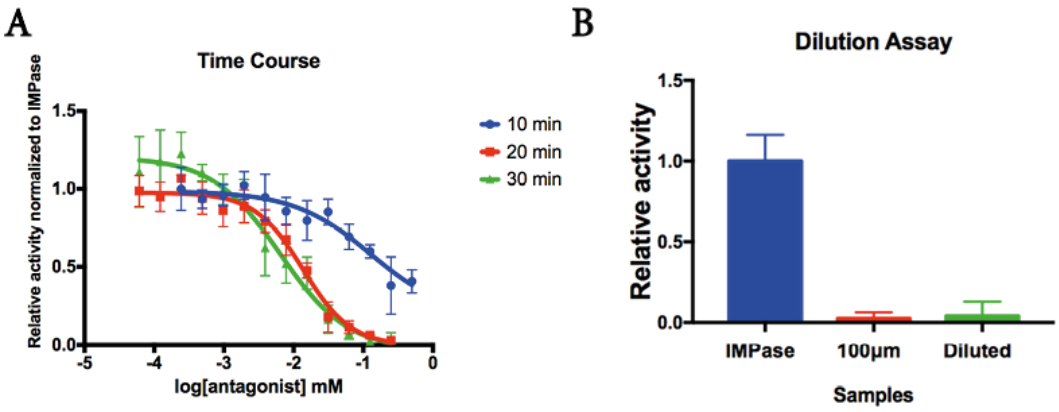

Figure 19. A) IC_{50} dilution series of JNJ6157935 incubated for different amounts of time with IMPase before the addition of the substrate. Green 30mins (n=3), red 20mins (n=3), blue 10mins (n=2). The mean and standard deviation for each data point is plotted. B) A bar graph of relative activity normalized to IMPase activity. The mean and standard deviation for each data bar is plotted.

Discussion

IMPase is a protein that is of significant therapeutic interest both with regards to Bipolar disorder and more recently the induction of autophagy induced by IMPase inhibition (Berridge, Downes, and Hanley, 1982; Sarkar *et al.,* 2005). Despite this interest, specific inhibitors that are effective *in vivo* have remained elusive. Ebselen was found to inhibit IMPase from a screen of the National Institutes of Health Clinical Collection. This is a chemical library of small molecules that have a history of use in clinical trials and therefore a proven track record for safety (Singh *et al.,* 2013). Ebselen has an isoselenazolone ring. The Selenium-Nitrogen single bond breaks open and covalently modifies IMPase giving rise to ebselen's inhibitory efficacy. Here for the first time, we employ a specifically curated isothiazolone screen of 67 unique compounds to explore this chemical group, substituting the

isoselenazolone of ebselen has for an isothiazolone ring. This replaces the selenium for sulphur and has two benefits. Firstly, although selenium is an essential trace element it has known toxicity issues, can cause selenosis and therefore should be avoided in drug molecules (Olson, 1986). Secondly, sulphur is a more common element in drugs and therefore allows the screening of a wider selection of compounds (Feng *et al.,* 2016). Both isoselenazolone and isothiazolone possess the same ability to break open and form bonds with cysteine residues in proteins (King *et al.,* 2009; Pacula *et al.,* 2017).

Four compounds were identified in the preliminary screen as exhibiting inhibitory activity. The compounds identified all belonged to the same structural subset of the compound library. Examination of the identified molecules reveals that the long tail region, on the opposite side of the molecule from the isothiazolone ring, is particularly important for determining the activity of the compound. Exploring this region with medicinal chemistry could be a strategy for further optimisation of the activity of the compounds.

Shifts in thermal denaturation curves of IMPase were used as an orthogonal assay to confirm binding of the hit molecules. Thermal denaturation was selected as an orthogonal assay as unlike the Colorimetric Phosphate Quantitation Assay that measures catalytic activity, the thermal denaturation assay measures the change in the stability of IMPase due to the molecules binding to the target. Both assays use the protein in its native state and do not require any protein modifications. The shifts observed in the thermal denaturation curve of IMPase upon treatment with each of the four hit compounds were large and concentration dependent. The shifts

were similar in morphology to that obtained by the compound ebselen, which was used as a positive control.

The novel molecules described in this paper are irreversible binders, as inhibition is observed after dilution of the compounds from maximal inhibitory range. The compounds also require longer incubation times in order to inhibit IMPase, a trait often observed with irreversible covalent binders. This result suggests that the reactivity of the isothiazolone ring is required for the inhibition of IMPase and inhibition is not achieved solely via binding of the compound on its own.

After the identification of ebselen as an inhibitor of IMPase, no further exploration in order to discover further covalent inhibitors has been performed. By performing a limited screen of 67 molecules, we have identified three IMPase inhibitors with a potency range of between 2.4-18 μM, similar to that of ebselen (ebselen 1.5 μM (Singh *et al,*. 2013). Reactive groups on potential drug molecules imparts an intrinsic polypharmacology. Therefore, compounds with these groups must possess very high affinity to the protein target, in order to counteract this property. From this study, we have observed that a range of chemical matter other than ebselen that can inhibit IMPase with the use of isothiazolone reactive groups. However, only 3 compounds from the isothiazolone compound library were potent enough to be detected in the initial screen, equating to a hit rate of 4.5 %. This demonstrates that the reactive isothiazolone group alone is not responsible for the inhibitory activity observed in these compounds, and opens up the possibility of engineering potency and specificity through medical chemistry efforts.

Conclusion

We have identified a new group of IMPase inhibitors by screening compounds that share a similar chemical group to the previously identified inhibitor ebselen. The inhibitors described were identified using a biochemical enzymatic primary assay and a biophysical orthogonal assay. 67 isothiazolone compounds were selected for screening, based on the known mechanism for activity of the isoselenazolone ring in ebselen . Although, this group is known to be reactive, only a small subset of molecules screened (4.5 %) displayed inhibitory activity at the screening concentration tested, suggesting that potency could be engineered into the reactive chemical backbone. The compounds identified exhibit IC_{50} values in the low micromolar range. As these compounds possess reactive chemical groups they are likely to possess innate polypharmacology. Therefore, significant medicinal chemistry efforts must be undertaken in order to optimise the affinity of these compounds.

Chapter 6

FINAL DISCUSSION

Final Discussion

The primary aims of this thesis were to gain new insights into the calbindin-IMPase interaction and to develop novel pharmacology of IMPase. The project was split into two branches: The biological allosteric modulation of IMPase and the pharmacological allosteric modulation of IMPase. The approach for the biological branch was to first obtain a crystal structure of the IMPase binding partner calbindin-D28k and to subsequently develop a series of calbindin-IMPase fusion proteins in order to stabilize and study the protein complex. The approach for the pharmacological branch was to firstly discover new fragment binding sites of IMPase by performing a crystallographic fragment screen, and secondly to identify new covalent inhibitors of IMPase based on the ebselen reactive group.

Calbindin-D28k is a highly expressed calcium binding protein with expression reaching up to 1.5 % of total protein content in certain sections of the brain (Christakos, Gabrielides, and Rhoten, 1989). In this thesis, the focus centred on calbindin-D28k due to its ability to increase the activity of IMPase, by as much as 250 fold (Berggard, Szczepankiewicz, *et al.,* 2002). This finding indicates that there may be significant structural plasticity in IMPase that could be exploited pharmacologically. However, few studies have been published that study the protein interaction *in vitro,* aside from simple biochemical analysis and *in silico* modelling (Levi *et al.,* 2013). Despite the involvement of calbindin-D28k in many physiological processes and the interest in its therapeutic potential, an X-ray crystal structure of the protein has remained elusive. Past attempts to obtain a structure have failed to yield results (Zhang *et al.,* 2008). Calcium buffering proteins have

historically remained a challenge for structural analysis by crystallography, due to their composition of small flexible domains, resulting in intrinsic flexibility that can inhibit crystallisation. Due to the flexible nature of calcium binding protein, NMR is often the method of choice to obtain structural models of proteins of this type. The calbindin-D28k NMR model was reported in 2006. At the time, calbindin-D28k (30 kDa) was one of the largest protein structures resolved by this technique (Kojetin *et al., 2006)*. NMR is often employed to explore the structure of smaller proteins <35 kDa and there are two main reasons for this. Firstly, larger molecules tumble more slowly in solution and exhibit shorter NMR signal relaxation times. Secondly, larger proteins result in more complex spectra and the signals from nuclei overlap, which makes analysis increasingly difficult with increasing size (Yu, 1999).

After purification of human calbindin-D28k, the SAXS data obtained in this thesis was distinct from that predicted by the NMR model. Therefore, we attempted to obtain a crystal structure of calbindin-D28k. Production of a X-ray crystal structure allowed the direct visualisation of the calcium ions bound by calbindin-D28k, thus providing new insights compared to the existing NMR spectroscopy data. The crystal structure obtained exhibited significant variations from that of the NMR model. The crystal structure was less condensed compared to the NMR model. Furthermore, the SAXS data was more aligned to the crystal structure than the NMR model, indicating that the crystal structure is a better model of calbindin-D28k in solution. Both of these findings are somewhat counterintuitive as it has been argued that NMR models are more biologically relevant (ref), as proteins are in solution when NMR spectra are obtained. Packing proteins into a crystal lattice can cause

structural deviations from the protein structure in solution (Garbuzynskiy *et al,*. 2005).

The proposed new model of the structure of calbindin-D28k at high resolution (1.51 A) provides an improved understanding of calbindin-D28k structure and suggests mechanisms by which calbindin-D28k may bind to IMPase. Thus, these additional structural insights of calbindin-D28k have revealed that the N-terminal region of the protein is particularly flexible. This is the region of calbindin-D28k that is implicated in the protein-protein interactions of the protein (ref). Mutagenesis of aspartate residues 24 and 26 to alanine inhibit the potentiation of IMPase activity by calbindin-D28k and a peptide fragment of Ran-binding protein M has also been shown to interact with this region of the protein (Lutz *et al,*. 2003). This intrinsic flexibility most likely frustrated the attempts to obtain a crystal structure of calbindin-D28k in the past. However, this flexibility could be an important property of calbindin-D28k that enables it to make protein interactions. Disorder-to-order transitions upon binding is a well-documented property of specific protein-protein interactions (Mendoza-Espinosa *et al.,* 2009). The flexibility of the N-terminal should be considered in any future modelling of the Calbindin-IMPase interaction.

To gain further insight into the calbindin-IMPase interaction, the creation of fusion proteins using a flexible amino acid linker was explored. This technique of fusing protein binding partners together has previously been used to obtain structures of protein complexes and to study protein complexes (Reddy Chichili, Kumar, and Sivaraman, 2013). Here, I successfully designed fusion protein constructs that demonstrate improved catalytic activity compared to IMPase alone. This is the first

time that the activating effect of calbindin-D28k on IMPase has been confirmed. SAXS data collected from the fusion protein constructs predict a flexible multi-domain protein. *Ab initio* reconstruction of the proteins from the SAXS data revealed a V-shaped protein complex that differed from the structure predicted by a published docking model of the interaction (ref). The low-resolution structures of the fusion protein are longer than those predicted by the *in-silico* docking model. All four fusion proteins possess the same globular structure, irrespective of differences in the activity due to the fusion protein linker directionality and linker length. Attempts to crystallise the fusion proteins to obtain a high-resolution structure of the protein complex have failed to yield positive results. As the fusion proteins are larger than 130 kDa they are at the lower limit of resolution by cryo-EM, and therefore it may be possible to obtain a structure using this method in the future. A high-resolution structure of these fusion proteins may enable an understanding of how calbindin-D28k exhibits its activating effect on IMPase. An understanding of the structural plasticity of IMPase may then be informative in the design of novel therapeutics. In summary, regarding the biological allosteric modulation of IMPase, we have demonstrated that IMPase binds to a flexible region of calbindin-D28k. We have reported a high resolution model of calbindin-D28k and shown that the Calbindin-IMPase interaction forms a V-shaped complex that deviates from previous predictions. We have developed a set of fusion proteins that can be employed to obtain high resolution structures of the complex.

IMPase has been of significant therapeutic interest since the development of the inositol depletion hypothesis in the 1970/80s and more recently in the induction of autophagy (Berridge, Downes, and Hanley, 1982; Sarkar *et al.,* 2005). Despite this,

the identification of novel inhibitors and chemical matter have been frustratingly sparse. In this thesis, I aimed to increase the chemical space in which to explore IMPase pharmacology. Prior to this work, non-covalent binding sites outside of the active site had not been identified. IMPase has recently been shown to have allosteric properties in relation to its interaction with calbindin-D28k (ref or refer to your work), indicating that binding sites outside of the active sites can modulate IMPase activity. Therefore, I aimed to identify novel fragment binding sites of IMPase. To achieve this, I elected to perform a crystallographic fragment screen. Screening by the use of crystallography techniques is sensitive and may identify fragments that bind with low affinity that are otherwise missed by less sensitive techniques. Here I identified a novel, non-covalent binding site 26Å outside of the active site of IMPase. The fragment screen identified four novel fragments that bind at the homodimer interface of IMPase. IMPase is a constitutive homodimer in solution. Therefore, disruption of the homodimer interface may present a possible pharmacological mechanism for the inhibition of IMPase.

To test this hypothesis, I generated mutant proteins harbouring mutations sited directly below the fragment binding site of IMPase. These mutations aimed to simulate hydrophobic compounds penetrating the homodimer interface. These mutations resulted in a significant reduction of IMPase activity. Crystallographic analysis of the mutant proteins revealed that the mutations did not disrupt the structure of IMPase. This suggests that a change in dynamics of the protein interface is responsible for the inhibitory effect of these mutations. The fragment binding site could be exploited further by the development of a PROTAC. If medicinal chemistry efforts can design higher affinity fragments and link to a E3 ligase substrate, the

resulting compound would trigger the *in situ* degradation of IMPase via the proteasomal degradation pathway. The absence of IMPase is predicted to result in the same biological effect as the direct inhibition of IMPase.

In 2013 it was reported that the molecule ebselen could inhibit IMPase (Singh *et al.,* 2013). Ebselen possesses a reactive chemical group termed isoselenazolone. Here we aimed to screen compounds with a similar reactive group termed isothiazolone due to substitution of a selenium atom for sulphur. Selenium possesses intrinsic toxicity which can cause selenosis, and therefore should be avoided in drug molecules (Olson, 1986). Secondly, sulphur is a more common element in medicinal chemistry and therefore would facilitate screening of a wider selection of compounds (Feng *et al.*, 2016). The compounds identified in this screen were all of a similar structure and inhibited IMPase via an irreversible mechanism. These novel IMPase inhibitors exhibit similar activity to that reported for ebselen but have a significantly different chemical structure. They represent a novel group of inhibitors however, they likely inhibit IMPase via the same mechanism as ebselen. I have significantly expanded the number of known compounds that irreversibly inhibit IMPase. This provides a larger group of compounds to be studied and may lead to the production of potent specific covalent inhibitors.

Conclusion

I have significantly added to the understanding of the Calbindin-IMPase interaction by obtaining the first crystal structure of calbindin-D28K and by the development of novel Calbindin-IMPase fusion proteins. The crystal structure of calbindin-D28k revealed a flexible N-terminus and provided the first direct visualization of the calcium binding sites.

The Calbindin-IMPase fusion proteins demonstrated increased activity and possess a V-shaped confirmation. These fusion proteins may be used to study the protein complex further. In structural studies the use of cryo-EM may yield the best results as the flexible linkers may inhibit crystallisation. The fusion proteins are considered too large to be useful for NMR studies. Further mutagenesis or kinetic studies of the fusion proteins may also provide more insight into the mechanism by which Calbindin-D28K increases the activity of IMPase.

I have significantly expanded the known chemical matter that both binds to and inhibits IMPase. A novel fragment binding site at the homodimer interface of IMPase was identified and single mutations at the site inhibit protein activity by over 50%. However, more work is required to identity the properties of the homodimer interface that are critical for IMPase activity. This data would enable effective design of IMPase inhibitors at the homodimer interface. The fragments identified here would need further development before they would be of therapeutic interest. This could be achieved either by the creation of a PROTAC that would induce the *in situ* degradation of IMPase or by development of the fragments into a homodimer penetrating compound.

Four novel irreversible inhibitors of IMPase were identified. These compounds possess a similar reactive group to the previously identified inhibitor ebselen and likely inhibit via a similar mechanism. All of these compounds inhibited IMPase at IC_{50} concentrations close to that of ebselen. As these new compounds were identified from a small, targeted screen of 67 compounds, this indicates that medicinal chemistry efforts around this reactive group may enable the development of a high affinity and specific inhibitor.

Bibliography

Ackermann, K. E., B. G. Gish, M. P. Honchar, and W. R. Sherman. 1987. 'Evidence that inositol 1-phosphate in brain of lithium-treated rats results mainly from phosphatidylinositol metabolism', *Biochem J*, 242: 517-24.

Akerfeldt, K. S., A. N. Coyne, R. R. Wilk, E. Thulin, and S. Linse. 1996. 'Ca2+-binding stoichiometry of calbindin D28k as assessed by spectroscopic analyses of synthetic peptide fragments', *Biochemistry*, 35: 3662-9.

Allison, J. H., and M. A. Stewart. 1971. 'Reduced brain inositol in lithium-treated rats', *Nat New Biol*, 233: 267-8.

Allison, James H., Marie E. Blisner, William H. Holland, Paul P. Hipps, and William R. Sherman. 1976. 'Increased brain myo-inositol 1-phosphate in lithium-treated rats', *Biochemical and Biophysical Research Communications*, 71: 664-70.

American Psychiatric Association (2013) Diagnostic and Statistical Manual of Mental Disorders, 5

Arai, R., K. Ito, T. Ohnishi, H. Ohba, R. Akasaka, Y. Bessho, K. Hanawa-Suetsugu, T. Yoshikawa, M. Shirouzu, and S. Yokoyama. 2007. 'Crystal structure of human myo-inositol monophosphatase 2, the product of the putative susceptibility gene for bipolar disorder, schizophrenia, and febrile seizures', *Proteins*, 67: 732-42.

Arnold, D. B., and N. Heintz. 1997. 'A calcium responsive element that regulates expression of two calcium binding proteins in Purkinje cells', *Proceedings of the National Academy of Sciences*, 94: 8842-47.

Atack, J. R., S. M. Cook, A. P. Watt, S. R. Fletcher, and C. I. Ragan. 1993. 'In vitro and in vivo inhibition of inositol monophosphatase by the bisphosphonate L-690,330', *J Neurochem*, 60: 652-8.

Atack, J. R., A. M. Prior, S. R. Fletcher, K. Quirk, R. McKernan, and C. I. Ragan. 1994. 'Effects of L-690,488, a prodrug of the bisphosphonate inositol monophosphatase inhibitor L-690,330, on phosphatidylinositol cycle markers', *J Pharmacol Exp Ther*, 270: 70-6.

Baell, J. B., and J. W. M. Nissink. 2018. 'Seven Year Itch: Pan-Assay Interference Compounds (PAINS) in 2017-Utility and Limitations', *ACS Chem Biol*, 13: 36-44.

Baker, Raymond, Paul D. Leeson, Nigel J. Liverton, and Janusz J. Kulagowski. 1990. 'Identification of (1S)-phosphoryloxy-(2R,4S)-dihydroxycyclohexane as a potent inhibitor of inositol monophosphatase', *Journal of the Chemical Society, Chemical Communications*: 462.

Barkai, A. I. 1981. 'Myo-inositol turnover in the intact rat brain: increased production after d-amphetamine', *J Neurochem*, 36: 1485-91.

Bellido, T., M. Huening, M. Raval-Pandya, S. C. Manolagas, and S. Christakos. 2000. 'Calbindin-D28k is expressed in osteoblastic cells and suppresses their apoptosis by inhibiting caspase-3 activity', *J Biol Chem*, 275: 26328-32.

Bergfors, T. M. 1999. *Protein Crystallization: Techniques, Strategies, and Tips : a Laboratory Manual*.

Berggard, T., S. Miron, P. Onnerfjord, E. Thulin, K. S. Akerfeldt, J. J. Enghild, M. Akke, and S. Linse. 2002. 'Calbindin D28k exhibits properties characteristic of a Ca2+ sensor', *J Biol Chem*, 277: 16662-72.

Berggard, T., O. Szczepankiewicz, E. Thulin, and S. Linse. 2002. 'Myo-inositol monophosphatase is an activated target of calbindin D28k', *J Biol Chem*, 277: 41954-9.

Berggård, Tord, Maria Silow, Eva Thulin, and Sara Linse. 2000. 'Ca2+- and H+-Dependent Conformational Changes of Calbindin D28k†', *Biochemistry*, 39: 6864-73.

Berridge, M J. 1997. 'Elementary and global aspects of calcium signalling.', *The Journal of Physiology*, 499: 291–306.

Berridge, M. J. 1993. 'Inositol trisphosphate and calcium signalling', *Nature*, 361: 315-25.

Berridge, M. J., C. P. Downes, and M. R. Hanley. 1982. 'Lithium amplifies agonist-dependent phosphatidylinositol responses in brain and salivary glands', *Biochem J*, 206: 587-95.

Bobay, B. G., A. L. Stewart, A. T. Tucker, R. J. Thompson, K. M. Varney, and J. Cavanagh. 2012. 'Structural insights into the calcium-dependent interaction between calbindin-D28K and caspase-3', *FEBS Lett*, 586: 3582-9.

Bojarski, L., J. Herms, and J. Kuznicki. 2008. 'Calcium dysregulation in Alzheimer's disease', *Neurochem Int*, 52: 621-33.

Bone, R., J. P. Springer, and J. R. Atack. 1992. 'Structure of inositol monophosphatase, the putative target of lithium therapy', *Proc Natl Acad Sci U S A*, 89: 10031-5.

Bragg, W. H., and W. L. Bragg. 1913. 'The Reflection of X-rays by Crystals', *Proceedings of the Royal Society A: Mathematical, Physical and Engineering Sciences*, 88: 428-38.

Cade, J. F. 1949. 'Lithium salts in the treatment of psychotic excitement', *Med J Aust*, 2: 349-52.

Calker, Dietrich van, and Robert H. Belmaker. 2000. 'The high affinity inositol transport system - implications for the pathophysiology and treatment of bipolar disorder', *Bipolar Disorders*, 2: 102-07.

Chernov, Alexander A. 2003. 'Protein crystals and their growth', *Journal of Structural Biology*, 142: 3-21.

Christakos, S., C. Gabrielides, and W. B. Rhoten. 1989. 'Vitamin D-dependent calcium binding proteins: chemistry, distribution, functional considerations, and molecular biology', *Endocr Rev*, 10: 3-26.

Clemens, T. L., S. A. McGlade, K. P. Garrett, G. L. Craviso, and G. N. Hendy. 1989. 'Extracellular calcium modulates vitamin D-dependent calbindin-D28K gene expression in chick kidney cells', *Endocrinology*, 124: 1582-4.

Cole, Andrew G., and David Gani. 1994. '‘Active’ conformation of the inositol monophosphatase substrates adenosine 2′-phosphate and inositol phosphate: role of the ribofuranosyl O-atom and inositol O-atoms in chelating a second magnesium ion', *J. Chem. Soc., Chem. Commun.*: 1139-41.

Cowtan, K. 2012. 'Completion of autobuilt protein models using a database of protein fragments', *Acta Crystallogr D Biol Crystallogr*, 68: 328-35.

Criollo, A., M. C. Maiuri, E. Tasdemir, I. Vitale, A. A. Fiebig, D. Andrews, J. Molgo, J. Diaz, S. Lavandero, F. Harper, G. Pierron, D. di Stefano, R. Rizzuto, G. Szabadkai, and G. Kroemer. 2007. 'Regulation of autophagy by the inositol trisphosphate receptor', *Cell Death Differ*, 14: 1029-39.

D'Angelo, E., J. Crutchfield, and M. Vandiviere. 2001. 'Rapid, sensitive, microscale determination of phosphate in water and soil', *J Environ Qual*, 30: 2206-9.

DiMasi, Joseph A., Ronald W. Hansen, and Henry G. Grabowski. 2003. 'The price of innovation: new estimates of drug development costs', *Journal of Health Economics*, 22: 151-85.

Emsley, P., B. Lohkamp, W. G. Scott, and K. Cowtan. 2010. 'Features and development of Coot', *Acta Crystallogr D Biol Crystallogr*, 66: 486-501.

Evans, P. R., and G. N. Murshudov. 2013. 'How good are my data and what is the resolution?', *Acta Crystallogr D Biol Crystallogr*, 69: 1204-14.

Fauroux, Christine M. J., and Sally Freeman. 2009. 'Inhibitors of Inositol Monophosphatase', *Journal of Enzyme Inhibition*, 14: 97-108.

Feng, M., B. Tang, S. H. Liang, and X. Jiang. 2016. 'Sulfur Containing Scaffolds in Drugs: Synthesis and Application in Medicinal Chemistry', *Curr Top Med Chem*, 16: 1200-16.

Ferruz, N., G. Tresadern, A. Pineda-Lucena, and G. De Fabritiis. 2016. 'Multibody cofactor and substrate molecular recognition in the myo-inositol monophosphatase enzyme', *Sci Rep*, 6: 30275.

Fleming, A., T. Noda, T. Yoshimori, and D. C. Rubinsztein. 2011. 'Chemical modulators of autophagy as biological probes and potential therapeutics', *Nat Chem Biol*, 7: 9-17.

Franke, D., M. V. Petoukhov, P. V. Konarev, A. Panjkovich, A. Tuukkanen, H. D. T. Mertens, A. G. Kikhney, N. R. Hajizadeh, J. M. Franklin, C. M. Jeffries, and D. I. Svergun. 2017. 'ATSAS 2.8: a comprehensive data analysis suite for small-angle scattering from macromolecular solutions', *J Appl Crystallogr*, 50: 1212-25.

Franke, D., and D. I. Svergun. 2009. 'DAMMIF, a program for rapid ab-initio shape determination in small-angle scattering', *J Appl Crystallogr*, 42: 342-46.

Furuichi, T., S. Yoshikawa, A. Miyawaki, K. Wada, N. Maeda, and K. Mikoshiba. 1989. 'Primary structure and functional expression of the inositol 1,4,5-trisphosphate-binding protein P400', *Nature*, 342: 32-8.

Gani, David, C. Peter Downes, Ian Batty, and Janice Bramham. 1993. 'Lithium and myo-inositol homeostasis', *Biochimica et Biophysica Acta (BBA) - Molecular Cell Research*, 1177: 253-69.

Ganzhorn, A. J., and M. C. Chanal. 1990. 'Kinetic studies with myo-inositol monophosphatase from bovine brain', *Biochemistry*, 29: 6065-71.

Garbuzynskiy, S. O., B. S. Melnik, M. Y. Lobanov, A. V. Finkelstein, and O. V. Galzitskaya. 2005. 'Comparison of X-ray and NMR structures: is there a systematic difference in residue contacts between X-ray- and NMR-resolved protein structures?', *Proteins*, 60: 139-47.

Gill, R., F. Mohammed, R. Badyal, L. Coates, P. Erskine, D. Thompson, J. Cooper, M. Gore, and S. Wood. 2005. 'High-resolution structure of myo-inositol monophosphatase, the putative target of lithium therapy', *Acta Crystallogr D Biol Crystallogr*, 61: 545-55.

Hallcher, L. M., and W. R. Sherman. 1980. 'The effects of lithium ion and other agents on the activity of myo-inositol-1-phosphatase from bovine brain', *J Biol Chem*, 255: 10896-901.

Hammond, W. A. 1871. *A Treatise on diseases of the nervous system* (Appleton).

Harwood, A. J. 2005. 'Lithium and bipolar mood disorder: the inositol-depletion hypothesis revisited', *Mol Psychiatry*, 10: 117-26.

Hassell, A. M., G. An, R. K. Bledsoe, J. M. Bynum, H. L. Carter, 3rd, S. J. Deng, R. T. Gampe, T. E. Grisard, K. P. Madauss, R. T. Nolte, W. J. Rocque, L. Wang, K. L. Weaver, S. P. Williams, G. B. Wisely, R. Xu, and L. M. Shewchuk. 2007. 'Crystallization of protein-ligand complexes', *Acta Crystallogr D Biol Crystallogr*, 63: 72-9.

Hennecke, J., and D. C. Wiley. 2002. 'Structure of a complex of the human alpha/beta T cell receptor (TCR) HA1.7, influenza hemagglutinin peptide, and major histocompatibility complex class II molecule, HLA-DR4 (DRA*0101 and DRB1*0401): insight into TCR cross-restriction and alloreactivity', *J Exp Med*, 195: 571-81.

Hirschfeld, Robert M. A., Lydia Lewis, and Lana A. Vornik. 2003. 'Perceptions and Impact of Bipolar Disorder: How far have we really come? Results of the National Depressive and Manic-Depressive Association 2000 survey of individuals with bipolar disorder.', *The Journal of Clinical Psychiatry*, 64: 161-74.

Itaya, Koichi, and Michio Ui. 1966. 'A new micromethod for the colorimetric determination of inorganic phosphate', *Clinica Chimica Acta*, 14: 361-66.

Johnson, K. A., L. Chen, H. Yang, M. F. Roberts, and B. Stec. 2001. 'Crystal structure and catalytic mechanism of the MJ0109 gene product: a bifunctional enzyme with inositol monophosphatase and fructose 1,6-bisphosphatase activities', *Biochemistry*, 40: 618-30.

King, A. R., A. Lodola, C. Carmi, J. Fu, M. Mor, and D. Piomelli. 2009. 'A critical cysteine residue in monoacylglycerol lipase is targeted by a new class of isothiazolinone-based enzyme inhibitors', *Br J Pharmacol*, 157: 974-83.

Klionsky, D. J., and S. D. Emr. 2000. 'Autophagy as a regulated pathway of cellular degradation', *Science*, 290: 1717-21.

Kojetin, D. J., R. A. Venters, D. R. Kordys, R. J. Thompson, R. Kumar, and J. Cavanagh. 2006. 'Structure, binding interface and hydrophobic transitions of Ca2+-loaded calbindin-D(28K)', *Nat Struct Mol Biol*, 13: 641-7.

Kook, S. Y., H. Jeong, M. J. Kang, R. Park, H. J. Shin, S. H. Han, S. M. Son, H. Song, S. H. Baik, M. Moon, E. C. Yi, D. Hwang, and I. Mook-Jung. 2014. 'Crucial role of calbindin-D28k in the pathogenesis of Alzheimer's disease mouse model', *Cell Death Differ*, 21: 1575-87.

Kozin, M. B., and D. I. Svergun. 2001. 'Automated matching of high- and low-resolution structural models', *Journal of Applied Crystallography*, 34: 33-41.

Kraft, L., S. M. Roe, R. Gill, and J. R. Atack. 2018. 'Co-crystallization of human inositol monophosphatase with the lithium mimetic L-690,330', *Acta Crystallogr D Struct Biol*, 74: 973-78.

Lambers, T. T., F. Mahieu, E. Oancea, L. Hoofd, F. de Lange, A. R. Mensenkamp, T. Voets, B. Nilius, D. E. Clapham, J. G. Hoenderop, and R. J. Bindels. 2006. 'Calbindin-D28K dynamically controls TRPV5-mediated Ca2+ transport', *EMBO J*, 25: 2978-88.

Leech, A. P., G. R. Baker, J. K. Shute, M. A. Cohen, and D. Gani. 1993. 'Chemical and kinetic mechanism of the inositol monophosphatase reaction and its inhibition by Li+', *Eur J Biochem*, 212: 693-704.

Levi, I., Y. Eskira, M. Eisenstein, C. Gilon, A. Hoffman, Y. Tal-Gan, J. Fanous, Y. Bersudsky, R. H. Belmaker, G. Agam, and O. Almog. 2013. 'Inhibition of inositol monophosphatase (IMPase) at the calbindin-D28k binding site: molecular and behavioral aspects', *Eur Neuropsychopharmacol*, 23: 1806-15.

Lewitzka, U., E. Severus, R. Bauer, P. Ritter, B. Muller-Oerlinghausen, and M. Bauer. 2015. 'The suicide prevention effect of lithium: more than 20 years of evidence-a narrative review', *Int J Bipolar Disord*, 3: 32.

Lu, S., W. Huang, X. Li, Z. Huang, X. Liu, Y. Chen, T. Shi, and J. Zhang. 2012. 'Insights into the role of magnesium triad in myo-inositol monophosphatase: metal mechanism, substrate binding, and lithium therapy', *J Chem Inf Model*, 52: 2398-409.

Lutz, Ward, Elena M. Frank, Theodore A. Craig, Richele Thompson, Ronald A. Venters, Doug Kojetin, John Cavanagh, and Rajiv Kumar. 2003. 'Calbindin D28K interacts with Ran-binding protein M: identification of interacting domains by NMR spectroscopy', *Biochemical and Biophysical Research Communications*, 303: 1186-92.

Majerus, P. W. 1992. 'Inositol phosphate biochemistry', *Annu Rev Biochem*, 61: 225-50.

Mayer, Moriz, and Bernd Meyer. 2001. 'Group Epitope Mapping by Saturation Transfer Difference NMR To Identify Segments of a Ligand in Direct Contact with a Protein Receptor', *Journal of the American Chemical Society*, 123: 6108-17.

McAllister, G., P. Whiting, E. A. Hammond, M. R. Knowles, J. R. Atack, F. J. Bailey, R. Maigetter, and C. I. Ragan. 1992. 'cDNA cloning of human and rat brain myo-inositol monophosphatase. Expression and characterization of the human recombinant enzyme', *Biochem J*, 284 (Pt 3): 749-54.

McCoy, A. J., R. W. Grosse-Kunstleve, P. D. Adams, M. D. Winn, L. C. Storoni, and R. J. Read. 2007. 'Phaser crystallographic software', *J Appl Crystallogr*, 40: 658-74.

McPherson, A., and J. A. Gavira. 2014. 'Introduction to protein crystallization', *Acta Crystallogr F Struct Biol Commun*, 70: 2-20.

Mendoza-Espinosa, P., V. Garcia-Gonzalez, A. Moreno, R. Castillo, and J. Mas-Oliva. 2009. 'Disorder-to-order conformational transitions in protein structure and its relationship to disease', *Mol Cell Biochem*, 330: 105-20.

Motoi, Y., K. Shimada, K. Ishiguro, and N. Hattori. 2014. 'Lithium and autophagy', *ACS Chem Neurosci*, 5: 434-42.

Murshudov, G. N., P. Skubak, A. A. Lebedev, N. S. Pannu, R. A. Steiner, R. A. Nicholls, M. D. Winn, F. Long, and A. A. Vagin. 2011. 'REFMAC5 for the refinement of macromolecular crystal structures', *Acta Crystallogr D Biol Crystallogr*, 67: 355-67.

Newman, J., D. Egan, T. S. Walter, R. Meged, I. Berry, M. Ben Jelloul, J. L. Sussman, D. I. Stuart, and A. Perrakis. 2005. 'Towards rationalization of crystallization screening for small- to medium-sized academic laboratories: the PACT/JCSG+ strategy', *Acta Crystallogr D Biol Crystallogr*, 61: 1426-31.

Newton, A. C. 1995. 'Protein Kinase C: Structure, Function, and Regulation', *Journal of Biological Chemistry*, 270: 28495-98.

Noble, J. W., R. Almalki, S. M. Roe, A. Wagner, R. Duman, and J. R. Atack. 2018. 'The X-ray structure of human calbindin-D28K: an improved model', *Acta Crystallogr D Struct Biol*, 74: 1008-14.

O'Toole, M., K. T. Lau, R. Shepherd, C. Slater, and D. Diamond. 2007. 'Determination of phosphate using a highly sensitive paired emitter-detector diode photometric flow detector', *Anal Chim Acta*, 597: 290-4.

Ohnishi, T., T. Murata, A. Watanabe, A. Hida, H. Ohba, Y. Iwayama, K. Mishima, Y. Gondo, and T. Yoshikawa. 2014. 'Defective craniofacial development and brain function in a mouse model for depletion of intracellular inositol synthesis', *J Biol Chem*, 289: 10785-96.

Ohnishi, T., H. Ohba, K. C. Seo, J. Im, Y. Sato, Y. Iwayama, T. Furuichi, S. K. Chung, and T. Yoshikawa. 2007. 'Spatial expression patterns and biochemical properties distinguish a second myo-inositol monophosphatase IMPA2 from IMPA1', *J Biol Chem*, 282: 637-46.

Olson, O. E. 1986. 'Selenium Toxicity in Animals with Emphasis on Man', *Journal of the American College of Toxicology*, 5: 45-70.

Ottis, P., and C. M. Crews. 2017. 'Proteolysis-Targeting Chimeras: Induced Protein Degradation as a Therapeutic Strategy', *ACS Chem Biol*, 12: 892-98.

Pacula, A. J., K. B. Kaczor, A. Wojtowicz, J. Antosiewicz, A. Janecka, A. Dlugosz, T. Janecki, and J. Scianowski. 2017. 'New glutathione peroxidase mimetics-Insights into antioxidant and cytotoxic activity', *Bioorg Med Chem*, 25: 126-31.

Pantoliano, M. W., E. C. Petrella, J. D. Kwasnoski, V. S. Lobanov, J. Myslik, E. Graf, T. Carver, E. Asel, B. A. Springer, P. Lane, and F. R. Salemme. 2001. 'High-density miniaturized thermal shift assays as a general strategy for drug discovery', *J Biomol Screen*, 6: 429-40.

Pollack, S. J., J. R. Atack, M. R. Knowles, G. McAllister, C. I. Ragan, R. Baker, S. R. Fletcher, L. L. Iversen, and H. B. Broughton. 1994. 'Mechanism of inositol monophosphatase, the putative target of lithium therapy', *Proc Natl Acad Sci U S A*, 91: 5766-70.

Reddy Chichili, V. P., V. Kumar, and J. Sivaraman. 2013. 'Linkers in the structural biology of protein-protein interactions', *Protein Sci*, 22: 153-67.

Ross, C. A., and M. A. Poirier. 2004. 'Protein aggregation and neurodegenerative disease', *Nat Med*, 10 Suppl: S10-7.

Sarkar, S., R. A. Floto, Z. Berger, S. Imarisio, A. Cordenier, M. Pasco, L. J. Cook, and D. C. Rubinsztein. 2005. 'Lithium induces autophagy by inhibiting inositol monophosphatase', *J Cell Biol*, 170: 1101-11.

Schewe, Tankred. 1995. 'Molecular actions of Ebselen—an antiinflammatory antioxidant', *General Pharmacology: The Vascular System*, 26: 1153-69.

Schmidt, H. 2012. 'Three functional facets of calbindin D-28k', *Front Mol Neurosci*, 5: 25.

Schmidt, H., B. Schwaller, and J. Eilers. 2005. 'Calbindin D28k targets myo-inositol monophosphatase in spines and dendrites of cerebellar Purkinje neurons', *Proc Natl Acad Sci U S A*, 102: 5850-5.

Schneidman-Duhovny, D., M. Hammel, J. A. Tainer, and A. Sali. 2013. 'Accurate SAXS profile computation and its assessment by contrast variation experiments', *Biophys J*, 105: 962-74.

———. 2016. 'FoXS, FoXSDock and MultiFoXS: Single-state and multi-state structural modeling of proteins and their complexes based on SAXS profiles', *Nucleic Acids Res*, 44: W424-9.

Shamir, A., N. Elhadad, R. H. Belmaker, and G. Agam. 2005. 'Interaction of calbindin D28k and inositol monophosphatase in human postmortem cortex: possible implications for bipolar disorder', *Bipolar Disord*, 7: 42-8.

Sheldrick, G. M. 2008. 'A short history of SHELX', *Acta Crystallogr A*, 64: 112-22.

Sherman, W. R., L. Y. Munsell, B. G. Gish, and M. P. Honchar. 1985. 'Effects of systemically administered lithium on phosphoinositide metabolism in rat brain, kidney, and testis', *J Neurochem*, 44: 798-807.

Shintani, T., and D. J. Klionsky. 2004. 'Autophagy in health and disease: a double-edged sword', *Science*, 306: 990-5.

Shorter, E. 2009. 'The history of lithium therapy', *Bipolar Disord*, 11 Suppl 2: 4-9.

Singh, N., A. C. Halliday, M. Knight, N. A. Lack, E. Lowe, and G. C. Churchill. 2012. 'Cloning, expression, purification, crystallization and X-ray analysis of inositol monophosphatase from Mus musculus and Homo sapiens', *Acta Crystallogr Sect F Struct Biol Cryst Commun*, 68: 1149-52.

Singh, N., A. C. Halliday, J. M. Thomas, O. V. Kuznetsova, R. Baldwin, E. C. Woon, P. K. Aley, I. Antoniadou, T. Sharp, S. R. Vasudevan, and G. C. Churchill. 2013. 'A safe lithium mimetic for bipolar disorder', *Nat Commun*, 4: 1332.

Sooy, Karen, Thomas Schermerhorn, Mitsuhiko Noda, Manju Surana, William B. Rhoten, Michael Meyer, Norman Fleischer, Geoffrey W. G. Sharp, and Sylvia Christakos. 1999. 'Calbindin-D28kControls [Ca2+]iand Insulin Release', *Journal of Biological Chemistry*, 274: 34343-49.

Streb, H., R.F. Irvine, MJ Berridge, and I Schulz. 1983. 'Release ofCa2+from a nonmitochondrial intracellular store in pancreaticacinar cells by inositol-1,4,5-trisphosphate', *Nature*, 306: 67-69.

Sun, S., F. Li, X. Gao, Y. Zhu, J. Chen, X. Zhu, H. Yuan, and D. Gao. 2011. 'Calbindin-D28K inhibits apoptosis in dopaminergic neurons by activation of the PI3-kinase-Akt signaling pathway', *Neuroscience*, 199: 359-67.

Svergun, Dmitri I., and Michel H. J. Koch. 2003. 'Small-angle scattering studies of biological macromolecules in solution', *Reports on Progress in Physics*, 66: 1735-82.

Taylor, G. 2003. 'The phase problem', *Acta Crystallogr D Biol Crystallogr*, 59: 1881-90.

Toure, M., and C. M. Crews. 2016. 'Small-Molecule PROTACS: New Approaches to Protein Degradation', *Angew Chem Int Ed Engl*, 55: 1966-73.

Valentini, E., A. G. Kikhney, G. Previtali, C. M. Jeffries, and D. I. Svergun. 2015. 'SASBDB, a repository for biological small-angle scattering data', *Nucleic Acids Res*, 43: D357-63.

Venters, Ronald A., Linda M. Benson, Theodore A. Craig, Keriann H. Paul, David R. Kordys, Richele Thompson, Stephen Naylor, Rajiv Kumar, and John Cavanagh. 2003. 'The effects of Ca2+ binding on the conformation of calbindin D28K: A nuclear magnetic resonance and microelectrospray mass spectrometry study', *Analytical Biochemistry*, 317: 59-66.

Viegas, Aldino, João Manso, Franklin L. Nobrega, and Eurico J. Cabrita. 2011. 'Saturation-Transfer Difference (STD) NMR: A Simple and Fast Method for Ligand Screening and Characterization of Protein Binding', *Journal of Chemical Education*, 88: 990-94.

Vonrhein, C., C. Flensburg, P. Keller, A. Sharff, O. Smart, W. Paciorek, T. Womack, and G. Bricogne. 2011. 'Data processing and analysis with the autoPROC toolbox', *Acta Crystallogr D Biol Crystallogr*, 67: 293-302.

Wagner, A., R. Duman, K. Henderson, and V. Mykhaylyk. 2016. 'In-vacuum long-wavelength macromolecular crystallography', *Acta Crystallogr D Struct Biol*, 72: 430-9.

Wasserman, R. H., R. A. Corradino, and A. N. Taylor. 1969. 'Binding Proteins from Animals with Possible Transport Function', *J Gen Physiol*, 54: 114-37.

Williams, R. S., L. Cheng, A. W. Mudge, and A. J. Harwood. 2002. 'A common mechanism of action for three mood-stabilizing drugs', *Nature*, 417: 292-5.

Winter, G., D. G. Waterman, J. M. Parkhurst, A. S. Brewster, R. J. Gildea, M. Gerstel, L. Fuentes-Montero, M. Vollmar, T. Michels-Clark, I. D. Young, N. K. Sauter, and G. Evans. 2018. 'DIALS: implementation and evaluation of a new integration package', *Acta Crystallogr D Struct Biol*, 74: 85-97.

Yamaguchi, T., K. Sano, K. Takakura, I. Saito, Y. Shinohara, T. Asano, and H. Yasuhara. 1998. 'Ebselen in acute ischemic stroke: a placebo-controlled, double-blind clinical trial. Ebselen Study Group', *Stroke*, 29: 12-7.

Ye, Y., and A. Godzik. 2003. 'Flexible structure alignment by chaining aligned fragment pairs allowing twists', *Bioinformatics*, 19 Suppl 2: ii246-55.

Yenari, M. A., M. Minami, G. H. Sun, T. J. Meier, D. M. Kunis, J. R. McLaughlin, D. Y. Ho, R. M. Sapolsky, and G. K. Steinberg. 2001. 'Calbindin D28K Overexpression Protects Striatal Neurons From Transient Focal Cerebral Ischemia', *Stroke*, 32: 1028-35.

Yin, Y., Y. Li, M. C. Kerzic, R. Martin, and R. A. Mariuzza. 2011. 'Structure of a TCR with high affinity for self-antigen reveals basis for escape from negative selection', *EMBO J*, 30: 1137-48.

Yu, H. 1999. 'Extending the size limit of protein nuclear magnetic resonance', *Proc Natl Acad Sci U S A*, 96: 332-4.

Yuan, H. H., R. J. Chen, Y. H. Zhu, C. L. Peng, and X. R. Zhu. 2013. 'The neuroprotective effect of overexpression of calbindin-D(28k) in an animal model of Parkinson's disease', *Mol Neurobiol*, 47: 117-22.

Zhang, C., Y. Sun, W. Wang, Y. Zhang, M. Ma, and Z. Lou. 2008. 'Crystallization and preliminary crystallographic analysis of human Ca 2+-loaded calbindin-D28k', *Acta Crystallogr Sect F Struct Biol Cryst Commun*, 64: 133-6.

Appendix

Supplementary Figure 1

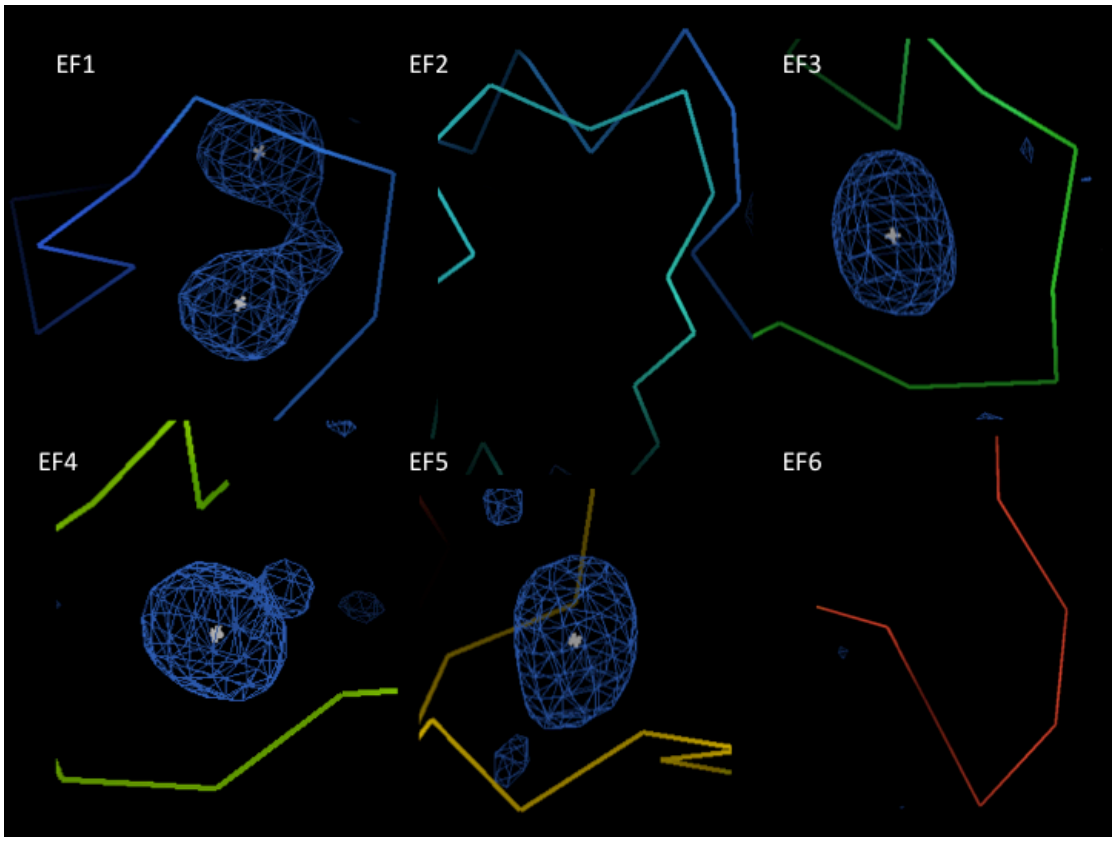

Figure S1 Anomalous Fourier map and heavy atoms computed with ANODE (Thorn & Sheldrick, 2011). Only the calcium binding EF hands contain strong peaks in the Fourier synthesis, allowing the direct visualization of the calcium atoms from crystal condition 1. EF hand 1, 3, 4 and 5 contain calcium with EF1 having two strong peaks indicating it binding calcium in two different conformations.

Supplementary Figure 2

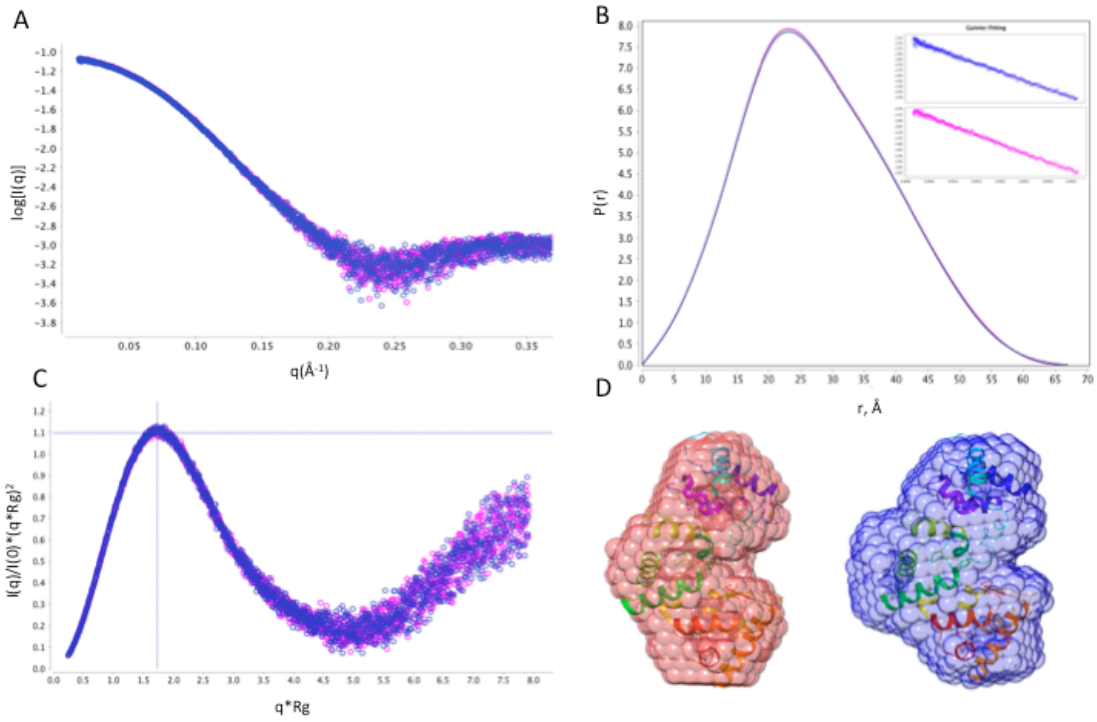

Figure S2 This figure is colour coded, blue APO and pink for calcium bound Calbindin- D28K A. Log10 SAXS intensity versus scattering vector, q. Plotted range represents the positive only data within the specified q-range. B. Pair-distance, P(r), distribution function. Maximum dimension, dmax, is the largest non-negative value that supports a smooth distribution function. The Guinier fitting for both data sets are also shown. C. Dimensionless Kratky plot. Cross-hair marks the Guinier-Kratky point (1.732, 1.1), the main peak position for globular particles. D. Ab initio envelopes with 6FIE superimposed.

Supplementary Figure 3

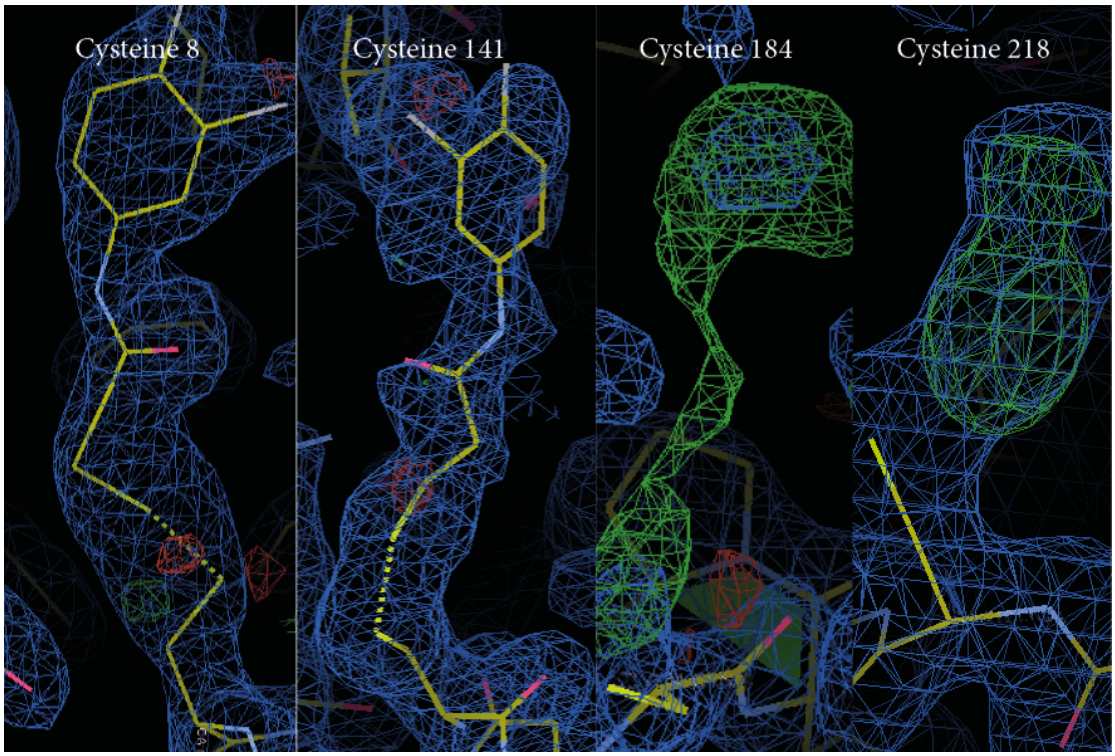

Figure S3 shown here is the electron density of a IMPase crystal soaked with the reactive fragment UOS-19245, 4 different cysteine residues have additional electron density that suggested the presents of the fragment. It can be sheen from the electron density that the fragment is only partially visible with cysteine 184 and 218, and bound close to full occupancy with cysteine 8 and 14